uOttawa

L'Université canadienne
Canada's university

FACULTÉ DES ÉTUDES SUPÉRIEURES ET POSTOCTORALES

uOttawa

L'Université canadienne
Canada's university

FACULTY OF GRADUATE AND POSDOCTORAL STUDIES

Tolga Kurt
AUTEUR DE LA THÈSE / AUTHOR OF THESIS

Ph.D. (Electrical Engineering)
GRADE / DEGREE

School of Information Technology and Engineering
FACULTÉ, ÉCOLE, DÉPARTEMENT / FACULTY, SCHOOL, DEPARTMENT

Signal Shapes for Multi-carrier Communication Systems

TITRE DE LA THÈSE / TITLE OF THESIS

Abbas Yongacoglu
DIRECTEUR (DIRECTRICE) DE LA THÈSE / THESIS SUPERVISOR

Jean-Yves Chouinard
CO-DIRECTEUR (CO-DIRECTRICE) DE LA THÈSE / THESIS CO-SUPERVISOR

EXAMINATEURS (EXAMINATRICES) DE LA THÈSE / THESIS EXAMINERS

T. Aboulnasr

A. Miri

F. Danillo-Lemoine

A. Khandani (absent)

Gary W. Slater
Le Doyen de la Faculté des études supérieures et postdoctorales / Dean of the Faculty of Graduate and Postdoctoral Studies

Ph. D. Thesis

Signal Shapes for Multi-Carrier Communication Systems

Tolga Kurt

For fulfillment of Doctor of Philosophy degree in Electrical Engineering

Ottawa-Carleton Institute for Electrical and Computer Engineering

School of Information Technology and Engineering

Faculty of Engineering

University of Ottawa

15.12.2006

Your file Votre référence
ISBN: 978-0-494-32408-0
Our file Notre référence
ISBN: 978-0-494-32408-0

Abstract

Signals transmitted over the wireless channels are affected by dispersion. In order to combat the dispersion, the signal shapes employed must decay very rapidly both in time and frequency. In this work, we introduce a novel method for orthonormalizing any given function by employing a two dimensional Fourier transform for any given integer lattice density. Then, by using this method, we propose pulse shapes that increase the capacity of multi-carrier pulse shapes significantly.

In the literature, it is assumed that the best localized orthogonal signal, isotropic orthogonal transfer algorithm (IOTA) can be achieved by orthogonalizing the best localized nonorthogonal signal, namely the Gaussian signal. We show that by combining Hermite functions and orthogonalizing them, an orthogonal signal with better localization than the IOTA signal can be achieved.

Multi-carrier schemes employing offset-quadrature-amplitude modulation employ lattice densities of 0.5 due to the Wilson expansions that are employed. In this dissertation, we extend the analysis to other density levels providing a trade-off between localization and capacity. We also provide a localized pulse shape for unit density lattices.

By employing more than one Weyl-Heisenberg frames that are orthonormal both within the frame and in between the frames, the capacity of multi-carrier systems are increased. Different lattice diversity scenarios are investigated for capacity enhancement. It is shown that by employing this methodology, the capacity of a multi-carrier system can be doubled. Additionally, a system level comparison as well as the inter-operability of the novel pulse shapes are presented.

Acknowledgments

First of all I would like to thank to Dr. Abbas Yongaçoğlu for guidance throughout this work as well as my co-advisor Dr. Jean-Yves Chouinard.

I also would like to extend my thanks to Dr. Amir Khandani, Dr. Tyseer Abdulnasr, Dr. Florance Danilo-Lemoine, and Dr. Ali Miri for accepting to be in my defence committee and for providing valuable comments. In addition, I would like to thank Dr. Hakan Deliç, who was my advisor in my Master of Science studies and encouraged me to this field of study.

I would like to thank my father Çetin Kurt for teaching me to be strong enough to stand up regardless of anything that happens and my mother Vesile Kurt, for teaching me to be compassionate enough to reach down to help the fallen when I stand strong.

Finally, my wife Güneş, your joy is the sole reason of my sanity and thanks for all your help, without you this would be an MBA.

L'absence affile l'amour, mais la présence le renforce.

Tolga Kurt
Ottawa, 2006.

TO THE MEMORY OF MY UNCLE DR. AHMET KURT,

WHO WAS ABLE TO HEAL THOUSANDS, BUT HIMSELF...

Contents

List of Figures

List of Tables

Notation

$\|x\|$	Norm of x
$A(t,f)$	Ambiguity function
$A_c(t,f)$	Cross ambiguity function
$C_{\mathbf{H}}$	Channel dispersion function
D_i	i^{th} Hermite function weight in the pulse shape
$e_\alpha(z)$	Monomial as a function of z
E_i	Linear space i
f_D	Doppler spread
F	Frequency separation between subcarriers
$\|F\|_F^2$	Bargmann-Fock norm
$G(g,\alpha,\beta)$	Gabor system
H_i	i^{th} Hermite function
$h_{mn}(x)$	Modified window function for wavelets
$Im\{A\}$	Image of map A
$ker\{A\}$	Kernel of map A
j	$\sqrt{-1}$
K	Lower frame bound
l	Maximum delay spread of the channel
L	Integer time-frequency multiplication

M	Upper frame bound
N	Length of the transmitted data sequence
P	Length of the cyclic prefix
R	Autocorrelation
$S_H(\tau)$	Delay spectrum
T	Time separation between OFDM symbols
T_l	Localization in time domain
T_n	Translation operator
M_m	Modulation operator
$\mathbf{X}(n)$	Inverse discrete Fourier transform of the transmitted data sequence
$\mathbf{x}(n)$	Transmitted data sequence
x^*	Complex conjugate of x
$\mathbf{X_{CP}}(n)$	Transmitted data sequence with cyclic prefix
V_g	Short time frequency transform
W_l	Localization in frequency domain
$Z_x(u, \theta)$	Discrete Zak transform of a pulse shape
$Z_y(u, \theta)$	Orthonormalized discrete Zak transform of a pulse shape
Δ	Density of the lattice
δ	Dirac delta function
$\chi(\nu, \tau)$	Arbitrary complex unit module function
$\phi(t), \Psi(t)$	Pulse shape
$\Psi_R(t)$	Rectangular pulse shape
Λ	Lattice
σ_τ^2	Delay spread
$\varphi(t)$	Base function for OFDM pulse shapes
$\varphi_{mn}(t)$	Frequency and time shifts of $\varphi(t)$

Acronyms

3GPP	Third Generation Partnership Project
AMC	Adaptive Modulation and Coding
AWGN	Additive White Gaussian Noise
BER	Bit Error Rate
BPSK	Binary Phase Shift Keying
BT	Bargmann Transform
BWA	Broadband Wireless Access
CDMA	Code Division Multiple Access
COFDM	Coded Orthogonal Frequency Division Multiplexing
CP	Cyclic Prefix
CQI	Channel Quality Indicator
CRC	Communication Research Center
DFT	Discrete Fourier Transform
DSCH	Downlink Shared Channel
DSL	Digital Subscriber Line
DZT	Discrete Zak Transform
EDGE	Enhanced Data Rates for GSM Evolution
ETSI	European Telecommunications Standards Institute
FFT	Fast Fourier Transform

GSM	Global System for Mobile Communications
HARQ	Hybrid Automatic Repeat Request
HiperMAN	High Performance Radio Metropolitan Area Network
HSDPA	High Speed Downlink Packet Access
HS-DSCH	High Speed Downlink Shared Channel
HSUPA	High Speed Uplink Packet Access
ICI	Inter-channel Interference
IDFT	Inverse Discrete Fourier Transform
IFFT	Inverse Fast Fourier Transform
IEEE	Institute of Electrical and Electronics Engineers
ISCI	Inter Sub-Channel Interference
ISI	Inter-symbol Interference
IOTA	Isotropic Orthogonal Transfer Algorithm
LDPC	Low Density Parity Check Codes
MC	Multi Carrier
NLOS	Non-Line of Sight
NMA	Nelder-Mead Algorithm
OFDM	Orthogonal Frequency Division Multiplexing
OFDMA	Orthogonal Frequency Division Multiple Access
OQAM	Offset Quadrature Amplitude Modulation
PAPR	Peak to Average Power Ratio
PS	Prolate Spheroidal
QAM	Quadrature Amplitude Modulation
QoS	Quality of Service
ROF	Radio over Fiber
SNR	Signal to Noise Ratio
STFT	Short Time Fourier Transform
TDMA	Time Division Multiple Access

TTI	Transmission Time Interval
UDALOP	Unit Density Axial-Localized Pulse
UE	User Equipment
UWB	Ultra Wide Band
VoIP	Voice over IP
WiFi	Wireless Fidelity
WiMAX	Worldwide Interoperability for Microwave Access
WLAN	Wireless Local Area Network

Chapter 1

Introduction and Motivations

Multi-carrier (MC) transmission, in particular orthogonal frequency division multiplexing (OFDM), is employed recently in various systems mainly due to its robustness against channel distortions [1]. These systems are lattice structures formed by time-frequency shifts of a prototype function such as rectangular pulse or raised cosine pulse. MC systems divide the frequency selective wideband channel into narrow flat fading subchannels [2]. Hence, very large bandwidths can be employed easily due to the reduced effect of channel dispersions.

There are two types of dispersions in wireless systems. These are the frequency dispersion and the time dispersion. Frequency dispersion appears due to the Doppler spread and the time dispersion is due to multi-path propagation. In OFDM systems, it is straightforward to combat time dispersion by adding a cyclic prefix or suffix to the symbols. However under frequency dispersion, OFDM performs poorly due to bad frequency localization properties of the pulse shapes used in the system.

In order to get a good localization property, the signal shapes employed in the carriers must decay very rapidly both in time and frequency. The localization problem in the

OFDM systems is due to the slow decaying property of the raised cosine pulse or the square pulse that is employed. Hence other signal shapes have been considered [3, 4].

Although the Gaussian pulse has the best localization property in both time and frequency, it does not match the orthogonality criteria required by the OFDM systems. The time-frequency shifts of the signals must be orthogonal for the detection process of the OFDM signals. Transforming the Gaussian pulse into an orthogonal pulse with a slightly worse localization was proposed in [3] and named as the Isotropic Orthogonal Transfer Algorithm (IOTA) approach. IOTA has very close localization to Gaussian signal, yet it is orthogonalized in time and frequency.

Another approach was to orthogonalize the Gaussian signal by combining it with Hermitian signals [4]. In [4], five Hermitian signals including the Gaussian signal were combined in order to acquire an orthogonal signal. However the results were limited to symmetric Hermitian signals and orthogonality is not guaranteed for an arbitrary lattice structure.

From frame theory it is well known that for unit density structures, a well localized orthogonal set cannot be achieved due to Balian-Low theorem [5, 6]. Hence in the literature many structures employing half lattice density, so called OFDM/QAM approaches were proposed [7, 8].

In this work, a novel method for orthonormalizing any given function by employing a two dimensional Fourier transform for any given integer lattice density is proposed. If mother function is defined as the function to be orthonormalized, it is shown that by employing a Gaussian pulse as the mother function, the IOTA function can be achieved and hence the method shown in [3] is only a special case of the method proposed here. It is also shown analytically that the orthonormalization in lattices with a density less than one is easier to achieve. In this work, we also show that deviation from optimality increases significantly for lattice density values higher than 0.5.

Other orthonormalization methods such as [7] also exist in the literature. However the proposed methods in [7] employ a matrix inversion, which is not guaranteed to exist for any given lattice structure. In this thesis, we propose a more general orthonormalization procedure, and present much simpler orthonormalization methods for well known lattices.

All of the above mentioned approaches assume that the best localized orthogonal signal can be achieved by orthogonalizing the best localized nonorthogonal signal, namely the Gaussian signal. In this work, we prove that this is incorrect. It is shown that by combining Hermite functions and orthogonalizing them, an orthogonal signal which is better localized than the IOTA signal can be achieved. The proposed method is a general case, since the first Hermite function is the Gaussian signal, and the set of Hermite functions is an orthogonal set which includes the most localized signals which are orthogonal to the Gaussian signal [9] and forms a set of basis functions for $L^2(\mathbb{R}^d)$.

On the other hand, due to the Balian-Low theorem, Wilson frames of half densities are employed. However Balian-Low states well localization as exponentially decaying pulses for all frequency band and time durations. On the other hand, for practical engineering purposes, the localization is not important after the pulse is decayed to very low amplitude values. By using this argument, we propose a novel and centrally well localized pulse shape for multi-carrier systems with unit density.

We also propose using multiple Weyl-Heisenberg frames at the time. By doing this, we increase the capacity of the multi-carrier systems significantly. We propose multiple pulse shapes that are orthonormal to the time-frequency shifts of themselves and shifts of others in the group. Therefore, they can be used at the same time without introducing interference to one another. We investigate the both half density and unit density cases for capacity enhancement. With the introduction of multiple lattice densities, the effective capacity of multi-carrier systems is doubled.

The proposed pulse shapes are supported by simulation results quantifying the performance gains. We also provide the effects of imperfections such as phase jitter and peak to average power ratio to the system performance. The system-level coverage and quality analysis for OFDM systems with different pulse shapes are presented.

In addition to those, compatibility of multiple pulse shapes are investigated. Since most of the equipment installed will be using rectangular pulse shapes, the transceivers with novel pulse shapes are shown to be compatible with the rectangular pulse.

1.1 Outline

This thesis is organized as follows. In Chapter 2, mathematical background and literature review is presented. Hilbert spaces and other useful definitions in Hilbert spaces are given. Various time-frequency representations are presented. Frame theory including Gabor frames is briefly reviewed. Existing orthonormalization methods in the literature are given. Also, an introduction to non-orthogonal pulse shapes and offset-QAM systems is made.

In Chapter 3, a novel orthonormalization method is derived. In this chapter, an orthonormality criteria and a method for orthogonalizing any signal using this criteria is given. Ambiguity function is defined according to the given definition. Special lattice density cases are investigated.

In Chapter 4, multi carrier systems and different pulse shapes are investigated. Also the lattice density and its effect on pulse shapes are investigated. With the application of the proposed orthogonalization method, the choice of mother functions and ambiguity functions are presented. Some unsuccessful alternatives are reviewed and the effect of lattice density is given.

In Chapter 5, simulation results are presented. The effect of inter-carrier interference and inter-symbol interference are given. OFDM based imperfections and compatibility issues are reviewed. Effect of inter-carrier interference for different number of subbands is simulated. The sensitivity to jitter and peak to average power ratio with employed pulse shapes are given.

In Chapter 6, a system level simulation of a WiMAX system employing different pulse shapes is presented. Different system level scenarios including HSDPA and WiMAX at different frequencies are considered. The effect of multiple access techniques and smart antennae are given. The effect of user velocity under different pulse shaping methods is simulated.

In Chapter 7, capacity enhancing pulse shaping is investigated. Multiple frames overlapping in both time and frequency are considered. Results are given for different lattice densities giving way to significant capacity increases in multi-carrier systems. Performance in Gaussian and fading channels are simulated. A system level capacity calculation is presented.

In Chapter 8, conclusions and possibilities for future work are given.

1.2 Contributions

- **A novel orthonormalization method for multi-carrier systems:** In this thesis, we propose a novel orthonormalization algorithm which converts any given function to another function whose time-frequency shifts are orthogonal to each other and resembles the localization properties of the original function. This novel method is very fast to apply therefore suitable for computer based optimization algorithms for finding a suitable original function to serve purposes such as good localization.

- **A novel very well localized pulse shape:** In this thesis, we show that the conjecture that states IOTA as the best localized pulse shape is incorrect. The IOTA pulse shape approach used only the first Hermite pulse, namely the Gaussian pulse, as a mother function and orthonormalized it. However, we show that by using a weighted of combination of Gaussian pulse and other pulse shapes, an orthonormal pulse set with better localization can be achieved.

- **Pulse shape for unit density lattices:** Until this study, all the well localized pulse shaping work in the literature concentrated on the half density lattices. This is due to the Balian-Low theorem stating that well localized pulses does not exist for unit density frames. However, for practical purposes, it is sufficient that the pulse shape is localized only for the regions that has considerable amplitude. By using this idea, we propose a novel pulse shape for unit lattice density, namely UDALOP. This novel pulse shape is both much better localized than the raised cosine pulse shape, and it does not require the offset-QAM structure, which divides the constellations as imaginary and real.

- **Analysis on the applicability of the Hermite pulse shapes:** We quantify the performance gains for the novel pulse shapes under different channel conditions. We present the effect of the new pulse shapes to peak-to-average power ratio for the first time. Also, we show that, if a rectangular pulse is utilized at one end of the communication channel, where as an Hermite pulse on the other end, the system still works better than the system that utilizes a rectangular pulse at both ends. This result shows that inter-operability would not be a problem with the possible new devices using the proposed pulse shapes.

- **System level performance gains for the novel pulse shapes:** We use the proposed pulse shapes in system level simulations using real geographical data and base station information. We show that the Hermite pulse shape provides robustness to a high velocity mobile system.

- **Capacity enhancement using superpositioned lattices:** Finally, we utilize more than one Weyl-Heisenberg frame at the same time such that the all the time-frequency shifts in one frame overlap with the time-shifts in the other frame, yet do not produce significant interference. By utilizing these superpositioned frames, we have shown that the capacity of a multi-carrier system can be doubled.

Chapter 2

Literature Review

We start by stating mathematical definitions which are used throughout the dissertation. In this chapter, definition of Hilbert spaces and the relations within these spaces are reviewed. Uncertainty principle is presented. Various time-frequency representations and definition for ambiguity function are given. Frame theory, in particular Gabor frames is reviewed.

Multi-carrier systems and different orthogonalization methods in these systems are investigated. An introduction to non-orthogonal signal shapes and offset-QAM systems is made.

2.1 Hilbert Spaces

In order to present the theory of signal shaping in multi-carrier systems, we first present the mathematical background of the frame theory behind it, following the notation of [10].

A map:

$A : E_1 \mapsto E_2$

between two linear spaces E_1 and E_2 is called linear if and only if for every $x, y \in E_1$ and for any two scalars a, b the equation:

$$A(ax + by) = aA(x) + bA(y) \tag{2.1}$$

is satisfied.

Kernel and Image sets associated with the linear map A are defined as:

$$\begin{aligned} ker\{A\} &= \{x \in E_1 : Ax = 0\}, & (2.2) \\ Im\{A\} &= \{Ax : x \in E_1\}, & (2.3) \end{aligned}$$

which are also linear spaces.

Definition 1 *The norm $\|x\|$ for $x \in E$ is a function from E to $\mathbb{R}$ with the following properties:*

1. $\|x\| \geq 0$ *and* $\|x\| = 0$ *if and only if* $x = 0$
2. $\|\lambda x\| = |\lambda| \|x\|$ *for a scalar* λ
3. $\|x + y\| \leq \|x\| + \|y\|$.

Definition 2 *A normed linear space X can be defined as a linear space E with a norm $\| \cdot \| : X = (E, \| \cdot \|)$.*

Definition 3 *A sequence (x_k) in X is called a Cauchy sequence if and only if $\forall \epsilon > 0$, there exists a natural number $N \in \mathbb{N}$ such that $\|x_k - x_m\| < \epsilon \; \forall k, m > N$.*

Next, by using the definition of Cauchy sequence, we define the complete spaces and Banach spaces.

Definition 4 *A normed space X is a complete space, if and only if every Cauchy sequence (x_k) in X converges to an element x of the space X.*

Definition 5 *A complete normed space $(X, \|\cdot\|)$ is called a Banach space.*

If a normed space is not complete, a linear mapping can be defined for completion.

Theorem 1 *[10] Let X be a normed linear space, a complete normed space $\hat{X}$ and a linear operator $Y : X \mapsto \hat{X}$ exist such that:*
(i) $\|Yx\| = \|x\|$ $\forall x \in X$ and
(ii) $YX^* = \hat{X}$ or in other words, ImY is a dense set in $\hat{X}$.

$\hat{X}$ is called the completion of X. Prior to defining an Hilbert space, we first need to define the inner product.

Let $\mathbb{H}$ be a linear space over $\mathbb{C}$ with a complex valued function of two variables $\langle m, n\rangle : \mathbb{H} \times \mathbb{H} \mapsto \mathbb{C}$ with the properties:

1. Linearity with respect to first argument:

$$\langle am_1 + bm_2, n\rangle = a\langle m_1, n\rangle + b\langle m_2, n\rangle,$$

   for scalars $a, b \in \mathbb{C}$.

2. $\langle m, n\rangle^* = \langle n, m\rangle$

3. $\langle m, n\rangle \geq 0$, and $\langle m, m\rangle = 0$ if and only if $m = 0$.

Such a function is called an inner product or a scalar product. If we consider the function $u(x) = \langle x, x\rangle^{1/2}$, it can be shown that it is a norm [10] and is be referred to as $u(x) = \|x\|$ throughout this dissertation.

Definition 6 $\mathbb{H}$ *is called a Hilbert space, if* $\mathbb{H}$ *is a complete normed space with the norm defined by* $\|x\|$.

Hilbert spaces will be utilized in defining the Weyl-Heisenberg frames that constitutes an important aspect of multi-carrier lattice structures that will be used throughout the thesis. In the following section, these definitions are applied to time-frequency representation problems.

2.2 Time-Frequency Representation

In order to represent a signal completely, neither the time representation nor the frequency representation of the signal alone is sufficient. Both must be investigated at the same time. For this reason, time-frequency representations have been an active research area [11].

Due to the inherent nature of the very same problem, the joint representation in time and frequency has a few dilemmas. One of these dilemmas is very well presented in the important paper by D. Slepian in 1976 [12]. In [12], the definitions of the bandwidth and the band-limited signals are discussed in the frequency representation of a signal. Consider a copper wire; due to its structure, signals with frequencies that are higher than a certain frequency cannot propagate through the wire. If we consider a signal transmitted through that copper wire between time t_1 and time t_2, it certainly is time limited. However, if we follow the definition of finite Fourier transform, any bandlimited signal must be infinite in time. This paradox, like many other is a result from the difference between the real world and the modeled world of science.

In particular, this one is due to the granularity in real world: i.e, in theory such power as 10^{-1000} W may exist, however we have no way of making such observation and approximate that to 0. Therefore the definition of band-limited signals is subject to a granularity.

One of the first examples of time-frequency representations can be found in the musical notes. As shown in Fig. 2.1, the musical notes consists of signs that represent the frequency components on certain time intervals.

Figure 2.1: Turkish March by W.A. Mozart: Notes in time and frequency.

The problem in a 2D frame representation such as a time-frequency plane is to acquire as localized information as possible in one dimension, without broadening the information in the other. The naturally rising question is, can we decrease the time intervals such that we define those notes indefinitely? In other words, can we increase the density of the frequencies (notes) indefinitely in a certain time interval? The questions are addressed in the following section.

2.2.1 Uncertainty Principle

The same problem appears in both engineering and physics. The classical uncertainty principle, which is known as Heisenberg-Pauli-Weyl inequality can be stated as follows [11]:

Theorem 2 *If $u \in L^2(\mathbb{R})$ and any $m, n \in \mathbb{R}$, then:*
$\left(\int_{-\infty}^{\infty}(x-m)^2|u(x)|^2dx\right)^{1/2}\left(\int_{-\infty}^{\infty}(w-n)^2|\hat{u}(w)|^2dw\right)^{1/2} \geq \frac{1}{4\pi}\|u\|^2,$
where $\hat{u}$ is the Fourier transform of u.

Theorem 2 can be followed by the lemma:

Lemma 1 *Let M and N be operators on a Hilbert space $\mathbb{H}$. Then for all $m, n \in \mathbb{R}$:*
$\|(M-m)u\|\|(N-n)u\| \geq \frac{1}{2}|\langle[M,N]u,u\rangle|.$

Equality exists if and only if u is a multiple of $T_n M_m \varphi_l(x) = e^{j2\pi m(x-n)}e^{-j\pi(x-n)^2/l}$ for $m, n \in \mathbb{R}$ and $l > 0$, where $j = \sqrt{-1}$. By employing Lemma 1, it can be proven that translation and modulation doesn't change the uncertainty. In order words, for the equality to hold, u must be multiple of time-frequency shift of a Gaussian pulse. T_n and M_m are the translation and modulation operators that are defined as follows.

Definition 7 *(Translation) $T_n u(t) = u(t-n)$.*

Definition 8 *(Modulation)* $M_m u(t) = e^{j2\pi mt}u(t)$.

The concept of uncertainty can also be examined in a time-frequency lattice structure. We can define a lattice Λ as:

Definition 9 *A lattice $\Lambda \subseteq \mathbb{R}^d$ is a discrete subgroup of $\mathbb{R}^d$ such that $\Lambda = \mathbf{A}\mathbb{Z}^{\mathbf{d}}$ where $\mathbf{A}$ is defined as an invertible $d \times d$ matrix over $\mathbb{R}$. We can also define the volume of a lattice as $|det\mathbf{A}|$, the lattice density as $1/volume$ and we can also define the dual lattice as $\Lambda^{\perp} = (\mathbf{A}^{-1})^{\mathbf{T}}\mathbb{Z}^{\mathbf{d}}$, where det. represents the determinant of a matrix.*

Hence, if we consider a 2-D lattice $\Lambda \subseteq \mathbb{R}^2$, with time and frequency as dimensions, the problem is to represent any given signal in this lattice. However, due to the uncertainty principle, as we increase the resolution in time, we lose resolution in frequency or vice-versa. For example, a cosine signal composed of a single frequency is infinitely long in time. In other words the localization in time and frequency cannot be increased independently from each other indefinitely.

The localization of a function $\psi(t)$ and its Fourier transform $\Psi(f)$ can be defined as the multiplication of its localization in time, T_l, and localization in frequency, W_l, which are given by:

$$T_l = \sqrt{\int_{-\infty}^{+\infty} t^2|\psi(t)|^2 dt}, \tag{2.4}$$

$$W_l = \sqrt{\int_{-\infty}^{+\infty} f^2|\Psi(f)|^2 df}, \tag{2.5}$$

where $\Psi(f)$ represents the Fourier transform of $\psi(t)$. For any signal $\psi(t)$ with unit variance such that $||\psi(t)|| = 1$, uncertainty principle implies that:

$$T_l W_l \geq \frac{1}{4\pi}. \tag{2.6}$$

The equality is again satisfied by the translations and modulations of the Gaussian pulse.

A very crude example explaining how time and frequency observations relate to one another can be given as follows. Suppose that a coin gets flipped with a frequency of 2 flips per second. If we observe the coin for 0.1 seconds, we may as well miss the flip and never observe the desired frequency. Even if we see a flip, in order to determine the flip rate, we need to see a second one, which is impossible in duration of 0.1 seconds. We must observe at least for duration of 0.5 seconds. The term 4π comes from the definition of the Fourier transform.

2.2.2 Short-Time Fourier Transform and Bargmann Transform

Even though the uncertainty principle states that the exact time and frequency response of a signal cannot be given jointly, still there are useful representations for specific applications that do not require extremely high resolution as in the case of Fig. 2.1. Such an example is the short-time Fourier transform, which concentrates to a certain time interval with the help of a window function.

The short-time Fourier transform (STFT), V_g, of a function $u(x, w)$ can be given as:

$$V_g u(x, w) = \int_{\mathbb{R}^d} u(t)\varphi^*(t - x)e^{-j2\pi tw}dt, \qquad x, w \in \mathbb{R}^d. \tag{2.7}$$

Depending on the characteristics of the window function $\varphi(t)$ and its complex conjugate $\varphi^*(t)$, the STFT can concentrate on different properties of the signal. A signal can be represented by using translations and modulations on a window function and employing STFT for every window function.

A special case of STFT is called the Bargmann transform (BT) [13]. BT utilizes the Gaussian function as a window. Due to its unique localization, the BT with time-frequency shifts is very important in physics and referred to as coherent states [14].

Considering the Gaussian function in $\mathbb{R}^d$, $\varphi(x) = 2^{d/4}e^{-\pi x^2}$, the Bargmann transform can be written as:

Definition 10 *The BT of u in* $\mathbb{R}^d$*:* $\{Bu : \mathbb{R}^s \mapsto \mathbb{C}^d\}$ *such that:*

$$Bu(z) = 2^{d/4}\int_{\mathbb{R}^d} u(t)e^{2\pi tz - \pi t^2 - \frac{\pi}{2}z^2}\,dt, \tag{2.8}$$

where $z = x + jy$

Definition 11 *The Bargmann-Fock space* $F^2(\mathbb{C}^d)$ *is defined as the Hilbert space of all functions such that the norm defined below is finite:*

$$\|F\|_F^2 = \int_{\mathbb{C}^d} |F(z)|^2 e^{-\pi|z|^2}\,dz. \tag{2.9}$$

Next a theorem that forms the basis for the usage of Hermite functions in this thesis is defined [11].

Theorem 3 *The collection of all monomials of the form:*

$$e_\alpha(z) = \left(\frac{\pi^{|\alpha|}}{\alpha!}\right)^{\frac{1}{2}} z^\alpha, \tag{2.10}$$

where α *is a vector of dimension d with non-zero elements, is an orthonormal basis for the Bargmann-Fock space.*

Since the BT is a unitary operator [11] and is an entire function on $\mathbb{C}^d$, the pre-image of the orthonormal basis $e_\alpha : H_\alpha = B^{-1}e_\alpha$ is an orthonormal basis for $L^2(\mathbb{R}^d)$. The functions $H_\alpha \in L^2(\mathbb{R}^d)$ are referred to as Hermite functions and they are a very critical set of functions throughout this dissertation with their localization properties and the fact that due to their orthonormal basis property, any function in $L^2(\mathbb{R}^d)$ can be written as a linear combination of Hermite functions.

Hermite functions have been utilized in various communication systems including ultra-wideband systems (UWB) [15, 16] and optical systems [17–19]. In UWB systems they are proposed as multiple access methodology for single carrier systems. In this dissertation, we extend this analysis to multi-carrier systems in the following chapters. In optical systems, they are employed in order to analytically describe the transmitted pulse shapes from the lasers. Since they form a basis, any pulse shape in $L^2(\mathbb{R}^d)$ transmitted from the laser can be expressed as a Hermite series [17–19].

2.2.3 Ambiguity Function and Wigner Distribution

In signal density analysis, it is crucial to investigate how the energy of a signal is concentrated in specific locations of the time-frequency plane. A very common measure is the ambiguity function, which is defined as :

Definition 12 *Ambiguity function $A_\phi(t,f) of \phi \in L^2(\mathbb{R}^d)$ is defined as:*

$$A_\phi(t,f) = \int_{\mathbb{R}^d} \phi(u+t/2)\phi^*(u-t/2)\exp(j2\pi fu)du. \tag{2.11}$$

The ambiguity function is sometimes referred to as Wigner distribution and employed widely for signal investigation as an alternative to STFT [20–22].

One important property of the ambiguity function is symmetry [11]:

$$A_\phi^*(t,f) = (A_\phi(-t,-f))^* = A_\phi(t,f). \tag{2.12}$$

Also, the ambiguity function is not a one-to-one function and A_ϕ determines ϕ only up to a phase factor. The inverse transform is given by:

$$\phi(t) = \frac{1}{\phi(0)} \int_{\mathbb{R}^d} A_\phi(t, f) e^{j\pi t f}. \tag{2.13}$$

2.3 Frame Theory

In representations over $L^2(\mathbb{R}^d)$, transforms such as STFT or Wigner distribution provide signal representations for infinitely many window function translation and modulations $(T_n M_m g)$. On the other hand, $L^2(\mathbb{R}^d)$ is a separable Hilbert space, and a lattice structure with finite time-frequency shifts suffice for representation of any $u \in L^2(\mathbb{R}^d)$.

In this dissertation, it is shown that the discretization of the continuous time-frequency plane corresponds to having multi-carrier system instead of a single carrier system. In order to demonstrate this, we start by defining a frame which will be the time-frequency shifted version of the pulses in the multi-carrier system.

Definition 13 *The sequence $\{e_i : i \in \mathbb{Z}\}$ in a Hilbert space is called a frame if for all $u \in \mathbb{H}$, there exists some constants $K, N > 0$ such that:*

$$K\|u\|^2 \leq \sum_i |\langle u, e_i \rangle|^2 \leq N\|u\|^2. \tag{2.14}$$

The two constants K, N are called frame bounds and $\{e_i : i \in \mathbb{Z}\}$ is called a tight frame if $K = N$. The value $K = N$ is a measure of the amount of redundancy in the tight frame. If $\{e_i\}$ is an orthogonal basis then it is a tight frame, and if it is orthonormal, then $K = N = 1$. Next we define the operators for frames.

Definition 14 *For any subset $\{e_i\}$ in a Hilbert space $\mathbb{H}$, the coefficient (analysis) oper-*

ator C is defined as:

$$Cu = \{\langle u, e_i \rangle\}. \tag{2.15}$$

The synthesis (reconstruction) operator D is defined as:

$$Dc = \sum_i c_i e_i \in \mathbb{H}, \tag{2.16}$$

and the frame operator S on $\mathbb{H}$ is defined as:

$$Su = \sum_i \langle u, e_i \rangle e_i. \tag{2.17}$$

It is important to note that C and D are adjoint to each other, i.e. $C = D^*$ [11].

Corollary 1 *If $\{e_i\}$ is a frame with bounds K, N, then $\{S^{-1}e_i\}$ is called the dual frame with bounds N^{-1}, K^{-1}.*

2.3.1 Gabor Frames

A frame structure that is of particular interest to this dissertation is the Gabor frames [23]. Gabor frames reflect a discrete system built by translation and modulations of a window function. We start by defining a Gabor system.

Definition 15 *Let $\varphi \in L^2(\mathbb{R}^d)$ be a non-zero window function, and $\alpha, \beta > 0$ be lattice constants, the set of time frequency shifts:*

$$G(g, \alpha, \beta) = \{T_{\alpha n} M_{\beta m} g : m, n \in \mathbb{Z}^d\} \tag{2.18}$$

is called a Gabor system.

Definition 16 *If the Gabor system G is a frame for $L^2(\mathbb{R}^d)$, it is called a Gabor frame or a Weyl-Heisenberg frame.*

The frame operator for a Gabor frame is:

$$Su = \sum_m \sum_n \langle u, T_{\alpha m} M_{\beta m} g \rangle T_{\alpha n} M_{\beta m} g. \tag{2.19}$$

One important property for the Gabor frame operator is that the order of modulation and translation doesn't play a major role. Furthermore, there exists a dual window of g, ξ such that $G(\xi, \alpha, \beta)$ is the dual frame for $G(g, \alpha, \beta)$. Hence the reconstruction of a function in a Hilbert space can be achieved by the dual frames defined as:

$$\begin{aligned} u &= \sum_m \sum_n \langle u, T_{\alpha n} M_{\beta m} g \rangle T_{\alpha n} M_{\beta m} \xi \\ &= \sum_m \sum_n \langle u, T_{\alpha n} M_{\beta m} \xi \rangle T_{\alpha n} M_{\beta m} g. \end{aligned} \tag{2.20}$$

It is important to note that if the frame is a tight frame formed by an orthonormal basis vector (i.e the limits $M = N = 1$), then the reconstruction is achieved with the same window since $\xi = g$. Further details and some other useful properties of Weyl-Heisenberg frames can be found in [24].

It is also important to note that, in signal analysis, the traditional understanding for the lattice constants is that, $\alpha\beta < 1$ corresponds to oversampling, $\alpha\beta = 1$ corresponds to critical sampling, and $\alpha\beta > 1$ corresponds to undersampling.

2.3.2 Balian-Low Theorem and Wilson Expansions

In time-frequency processing, it is almost always required that the window functions converting the Hilbert space to a frame (Gabor frame in particular) must have good localization properties in time and frequency. For example when signal properties around a point in time-frequency plane are to be investigated, we wish to localize at the desired point and avoid all possible interference from points that are far apart from the investigation area. Similarly, if those time-frequency shifts in a Gabor frame constitute different information, it is desired that the information is localized and do not interfere with other information carrying points. This property is important in particular when trying to achieve pulses that localizes in time and frequency at the same time.

The uncertainty principle requires that a Gabor system $G(g, \alpha, \beta)$ is a frame if and only if $\alpha\beta \leq 1$. If $\alpha\beta = 1$, then $G(g, \alpha, \beta)$ is an orthonormal basis. However for the case of $\alpha\beta = 1$, the Balian-Low theorem states that, there exists no window function g, which is well localized in both time and frequency [5].

Theorem 4 *(Balian-Low)*
If $G(g, \alpha, \frac{1}{\alpha})$ is a frame for $L^2(\mathbb{R})$, then $(\int_{-\infty}^{\infty} |tg(t)|^2 dt)(\int_{-\infty}^{\infty} |\gamma\hat{g}(\gamma)|^2 d\gamma) = +\infty$.

It can be concluded from the theorem above that the density of the lattice must be sacrificed and increased in order to have a frame with good localization properties. In [25], it is shown that by introducing a window function g with double peak values instead of a single peak value [26], well localized, exponentially decaying window functions can be achieved.

Definition 17 *Given a Gabor system $G(g, 1, \frac{1}{2})$ in $L^2(\mathbb{R})$ with redundancy of $\frac{1}{\alpha\beta} = 2$, the associated Wilson system $W(g)$ can be defined with the functions:*

$$\psi_{n,0} = T_n g, \qquad n \in \mathbb{Z}, \tag{2.21}$$

$$\psi_{m,n} = \frac{1}{\sqrt{2}} T_{n/2} \left(M_m + (-1)^{m+n} M_{-m} \right) g, \qquad \{m, n\} \in \mathbb{Z} \times N. \tag{2.22}$$

Equivalently, with the help of trigonometric functions, the Wilson functions can be equivalently represented as:

$$\psi_{m,n}(x) = \begin{cases} \sqrt{2} \cos(2\pi n x) g(x - \frac{m}{2}) & \text{if } m + n \text{ is even} \\ \sqrt{2} \sin(2\pi n x) g(x - \frac{m}{2}) & \text{if } m + n \text{ is odd.} \end{cases} \tag{2.23}$$

With the introduction of the orthogonal trigonometric functions, all the redundancy in the Gabor system has been eliminated [26].

In wireless multi-carrier communications, the Wilson bases have led to the introduction of Off-set quadrature amplitude modulation (OQAM)-OFDM systems. However, until now, no orthogonal Wilson basis functions have been known to exist [27] with lattice densities higher than 0.5. In this dissertation, we also investigate the effect of increased density on the orthogonal basis while α and β takes on values in the range $0.5 \leq \alpha\beta \leq 1$.

2.4 Multi-carrier Systems

With the success of wireless local area networks (WLANs), especially with the implementation of IEEE 802.11 standards [28], wireless last mile technology is becoming a promising candidate for replacing high-cost wired broadband solutions. Wireless systems provide a more rapidly scalable infrastructure development, cost-effective growth and quality of service (QoS) support with respect to wired systems.

Already deployed systems such as EDGE, and IS-95 provide nominal bit rates up to 384 kbps. However integration of wireless data services over diverse platforms such as indoor, micro and macro cellular systems, as well as high spectrum efficiency requirement motivates the demand for a multiple access and modulation scheme other than time division multiple access (TDMA) and code division multiple access (CDMA).

With its frequency-flat spectrum characteristics and high spectrum efficiency, multi carrier systems, specifically OFDM systems have drawn much attention as a possible candidate for next generation wireless access systems, commonly referred to as 4G.

Both WLANs, and recently, fixed broadband wireless access systems employ multi-carrier options in corresponding ETSI and IEEE standards including ETSI-HiperMAN [29], IEEE 802.11 [28], IEEE 802.16-2004 [30], regarding fixed broadband wireless applications. There are two modes of OFDM operation in physical layer requirements of IEEE 802.16-2004. Also within the WiMAX [31] framework whose aim is to standardize broadband wireless products in the industry, OFDM is the main modulation and multiple-access method that is considered.

In terms of mobile applications, OFDM plays a major role in the mobile extension of IEEE 802.16-2004, as the amendment IEEE 802.16*e* [32]. The mobile broadband networks in South Asia with the WiBro standard employ OFDM as well [33].

Although the idea of sending data from multiple frequencies in parallel has been around for a while [2], with the application to the broadband wireless applications, OFDM systems became subject to countless research activities. The main advantage of OFDM systems is the fact that it divides the frequency selective fading broadband spectrum into small frequency flat subbands. With the help of this division, frequency selective fading effects of the wide band channels are overcome.

A general OFDM system architecture can be represented as shown in Fig. 2.2. The modulation of the subbands can be easily achieved by applying inverse discrete Fourier transform (IDFT). First the N data symbols are converted from serial to parallel as:

$$\mathbf{x}(n) = [x_0(n), x_1(n) \ \cdots \ x_{N-1}(n)]^T. \tag{2.24}$$

Next N-point inverse discrete Fourier transform (IDFT) is applied to these symbols, so that the subcarriers are modulated as:

$$X(n) = \frac{1}{N}\sum_{k=1}^{N} x(k)\exp(j2\pi(k-1)(n-1)/N), \qquad 1 \leq n \leq N. \tag{2.25}$$

Following the IDFT, a cyclic prefix (CP) is appended to each block before transmission, where the last P elements of the OFDM symbol are added to the beginning of the

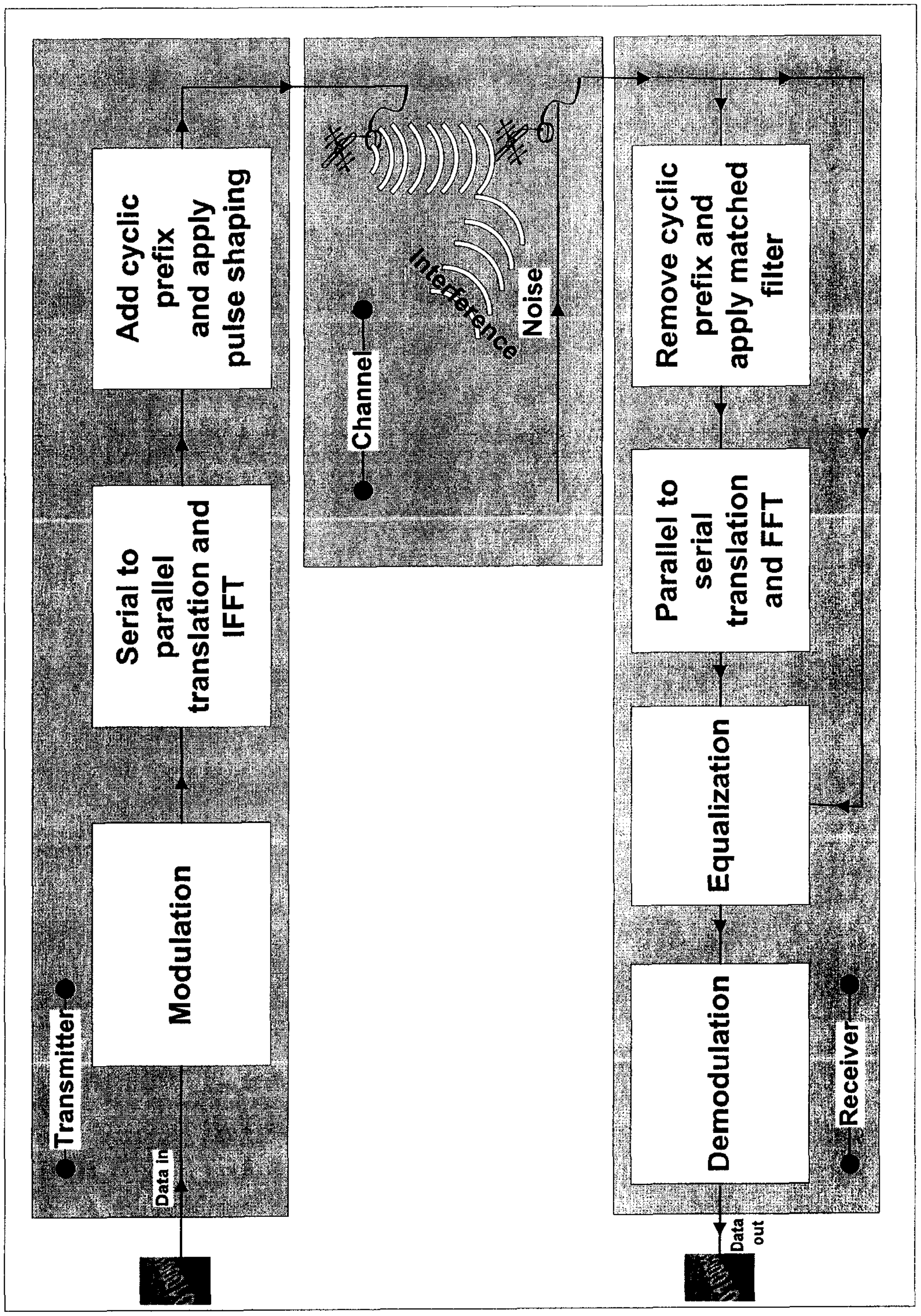

Figure 2.2: OFDM system architecture.

symbol in order to avoid intersymbol interference (ISI) among the blocks:

$$\mathbf{X}_{CP}(n) = [X_{N-P}(n) \ \cdots \ X_{N-1}(n) \ X_0(n) \ X_1(n) \ \cdots \ X_{N-1}(n)]^T. \tag{2.26}$$

The cyclic prefix is chosen such that $P > l$ where l is the maximum delay spread of the wireless channel. With the implementation of CP, even if there is multi-path delay spread in the channel, the orthogonality of the subcarriers are kept as long as the condition $P > l$ is satisfied. Transposing the signal from digital to analog domain, pulse shaping is employed. At the receiver, the equalization is accomplished in the frequency domain after discrete Fourier transform (DFT) is applied to the matched filtered signal.

Although CP provides the protection against multi-path delay spread or channel dispersion in time, OFDM systems are vulnerable to dispersion in frequency, namely the Doppler spread. Since the subbands of the OFDM systems are very densely packed, with the increasing speed of the receiver and transmitter with respect to each other, orthogonality between sub-carriers are disrupted and performance degradation is faced. This is one of the major challenges of OFDM systems that are meant for the mobile applications. This is also the reason behind the application of OFDM mainly to the fixed wireless systems. The mobility issue is also investigated under the frame work of the nomadic wireless broadband standard work groups; IEEE 802.16e [32] and IEEE 802.20 [34]. Both of these standards employ OFDM architecture; hence the increase in the mobility of OFDM systems is critical for the future development of 4G networks.

The poor performance of OFDM systems under severe frequency dispersion is mainly due to bad frequency localization properties of the raised cosine pulse shapes and rectangular pulse shapes used in the system. When the pulses are not well-localized, any shifts in the spectrum, resulting from imperfect channel conditions, scramble the subbands together. With a well-localized pulse, these shifts would only effect the immediate neighboring bands and with less interfering power.

In order to get a good localization property, the signal shapes employed in the carriers must decay very rapidly both in time and frequency. Although the Gaussian pulse has the best localization property in both time and frequency, it does not match the orthogonality criteria required by the OFDM systems. The time-frequency shifts of the signals must be orthogonal for the detection process of the OFDM signals. However finding such orthogonal pulses, which are very well localized, is not a straightforward process and intuitive solutions are hard to come up with. In the following section, we investigate the orthogonalization methods that are proposed in order to produce well localized orthogonal Weyl-Heisenberg frames.

2.5 Orthogonalization Methods

In order to represent the multi-carrier signal space in frequency and time, we consider the rectangular lattice structure in $L^2(\mathbb{R}^2)$ as shown in Fig. 2.3. The carriers are equally spaced in time and frequency. If the frequency spacing is given as F and time spacing is given by T, then we can define the density of the lattice as:

$$\Delta = 1/FT. \tag{2.27}$$

In this section, we show the criterion to be satisfied by a base (window) function $\varphi(t)$ in $L^2(\mathbb{R}^2)$ so that its time-frequency shifts in the form of:

$$\varphi_{mn}(t) = T_{nT}M_{mF}\varphi(t) = \varphi(t - nT)\exp(j2\pi mFt).$$

make up an orthonormal set such that these sets of functions form an OFDM system. We begin our discussion without making any assumptions on the lattice shape. The functions $\varphi_{mn}(t)$ are also called the coherent states since they are generated by time-frequency shifts from a single function $\varphi(t)$ [35].

For such a set of functions $\varphi(t)$, the orthonormality condition can be written as:

$$\int_{-\infty}^{\infty} \varphi_{kl}^*(t)\varphi_{mn}(t)dt = \delta_{km}\delta_{ln}, \tag{2.28}$$

where δ is the Kronecker Delta function. Due to lattice translation invariance, with respect to the central signal $\varphi_{00}(t)$ we can rewrite (2.28) as:

$$\int_{-\infty}^{\infty} \varphi_{00}^*(t)\varphi_{mn}(t)dt = \delta_m\delta_n. \tag{2.29}$$

Base functions must have two main properties in order to be used in an OFDM system [4]:

- The orthogonality of the base functions is required in order to have detection that is free of inter-symbol interference (ISI) and inter-carrier interference (ICI).

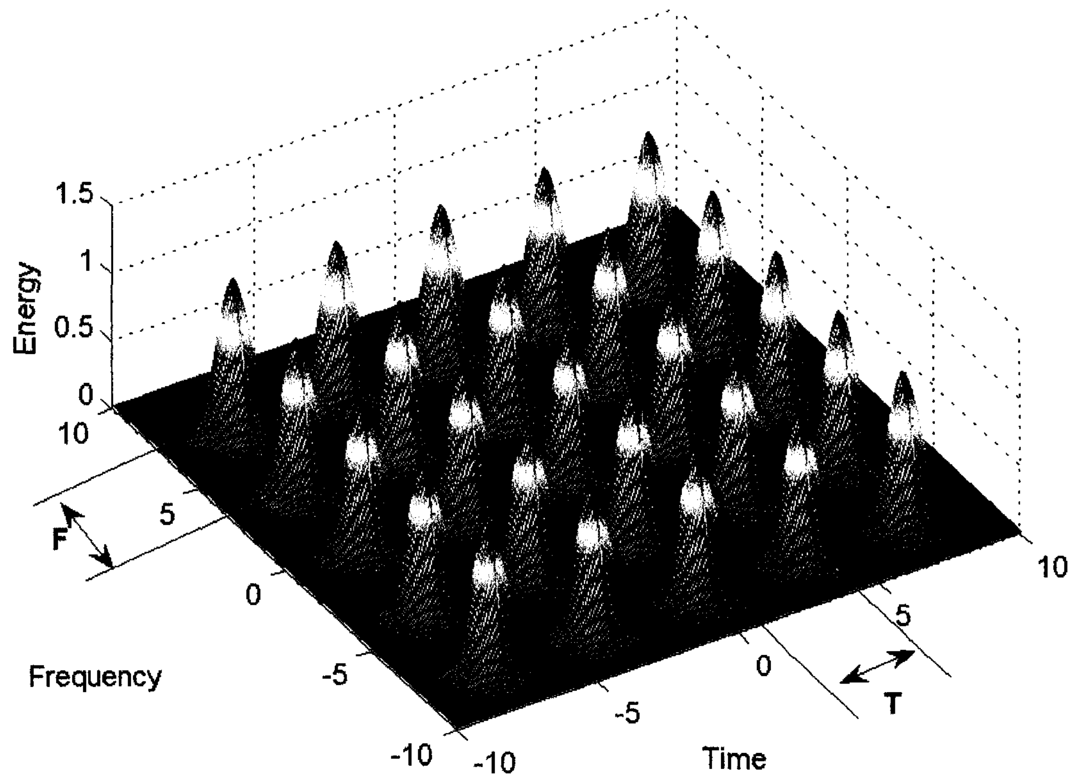

Figure 2.3: Distribution of orthonormal carriers in the time-frequency lattice for rectangular lattice structures.

- The base functions must have good localization properties, which is necessary to avoid interference by energy that leaks to neighboring symbols as a result of the dispersive channel.

With the definitions of time and frequency localizations in (2.5), we have stated that for any signal $\psi(t)$ with unit variance, uncertainty principle implies that:

$$T_l W_l \geq \frac{1}{4\pi}. \tag{2.30}$$

The Gaussian function is the most localized function in terms of both time localization and frequency localization and the localization is given by $1/4\pi$. The Gaussian function is represented by:

$$\psi(t) = e^{-\pi t^2}, \tag{2.31}$$

which has the same frequency response as its time response. In order to compare the localization of frequency domain Nyquist impulse functions with different raised cosine roll-off factors to Gaussian function, localization of the corresponding functions are summarized in Table 2.1. One must also note that, although the localization of the functions get better as the roll-off factor increases, so does the bandwidth requirement of the pulse.

Regardless of its good localization properties, the Gaussian function is not very useful for multi-carrier system purposes, since the Weyl-Heisenberg frame formed by the translations and modulations of the Gaussian function doesn't form an orthonormal basis set for $L^2(\mathbb{R}^2)$. Hence, in the literature several methods have been proposed in order to orthogonalize the Gaussian function.

Here we utilize the ambiguity functions defined in (2.11). The importance of the ambiguity function lies in the fact that it gives the correlation between time and the frequency shifts of $\phi(t)$. This is critical when designing a multi-carrier system where the carriers are actually the shifts of $\phi(t)$. For a multi-carrier system to work, the ambiguity

Table 2.1: Comparison of time and frequency localization values of Nyquist impulse functions with raised cosine roll-off factors to a Gaussian function.

roll-off factor	time localization (T_l)	frequency localization (W_l)	overall localization ($T_l W_l$)
0	0.8486	0.2884	0.2448
0.1	0.7493	0.2921	0.2188
0.5	0.35	0.3812	0.1334
1	0.2487	0.3615	0.0899
Gauss	0.2821	0.2821	0.0796

function is required to be zero at the integer multiples of time separation T and frequency separation F. In the following section, we investigate different orthogonalization methods, which in general make use of the ambiguity function.

2.5.1 Linear Combination of Hermite Functions

The method of orthogonalization by linear combination of Hermite functions was first proposed in [4]. For the procedure given by Haas and Belfiore [4], $\phi(t)$ has to be invariant when Fourier transform is applied. The following limitation exists for lattice density Δ: According to the Balian Low theorem [35], when the density $\Delta = 1$, $\phi(t)$ must be poorly localized either in time or frequency. Therefore Wilson functions defined in (2.23) are employed and for the orthogonalization, $\Delta = 0.5$ is assumed.

In order to establish the orthogonality, the following conditions are set for the ambiguity function:

$$
\begin{aligned}
A(0,0) &= 1 \\
A(\sqrt{2},0) &= 0 \\
A(\sqrt{2},\sqrt{2}) &= 0 \\
A(2\sqrt{2},0) &= 0 \\
A(2\sqrt{2},\sqrt{2}) &= 0.
\end{aligned}
\tag{2.32}
$$

Hence the lattice point at the center must have unit value and the values for the ambiguity function must be zero at four neighboring lattice points. Since the basis functions are symmetric with respect to the origin, these are necessary and sufficient conditions for the basis function to be zero in the closest neighbors. For the other carriers, orthogonality is satisfied by the fast decaying pulse shape. This concept can be seen in Fig. 2.4. The value of the ambiguity function at the positions which are not marked by either 1 or 0 become automatically 0.

In order to satisfy the conditions on the ambiguity function, first Q symmetric Hermite functions are linearly combined as:

$$\phi(t) = \sum_{k=0}^{Q-1} D_{4k} H_{4k}, \tag{2.33}$$

where D_{4k} and H_{4k} represent the weight and the actual $4k^{th}$ Hermite function respectively. The main motivation behind employing Hermite functions is that the first Hermite function is the Gaussian function and the k^{th} Hermite function is the k^{th} best localized function that is orthogonal to the Gaussian and other Hermite functions. Furthermore any $4k^{th}$ Hermite function has a Fourier transform exactly equal to itself. Hence, the

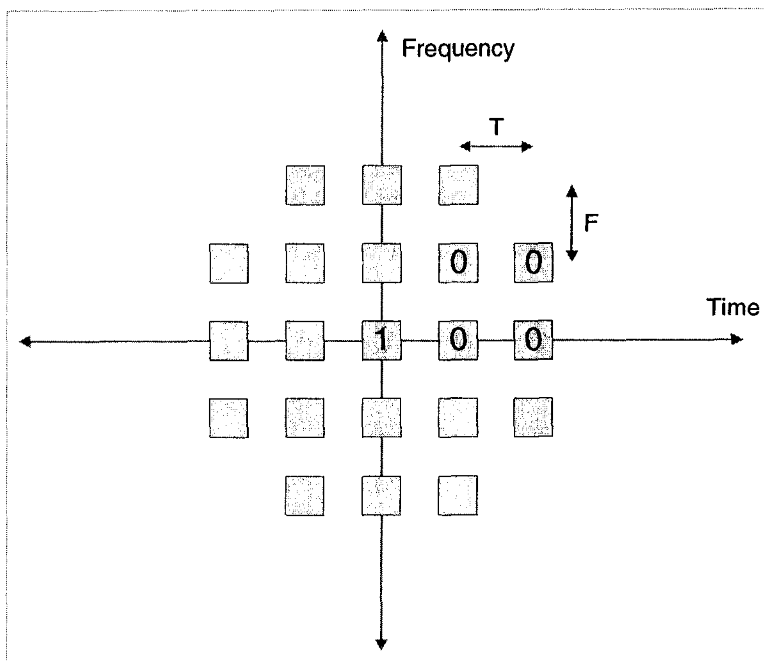

Figure 2.4: Time-frequency plane demonstration of conditions for orthogonality for linear combination of Hermite functions.

following Hermite functions are considered in [4],

$$
\begin{aligned}
H_0(t) &= \exp(-\pi t^2) \\
H_4(t) &= 16\exp(-\pi t^2)(4\pi^2 t^4 - 6\pi t^2 + 0.75) \\
H_8(t) &= 256\exp(-\pi t^2)(16\pi^4 t^8 - 112\pi^3 t^6 + 210\pi^2 t^4 \\
&\quad -105\pi t^2 + 11.67) \\
H_{12}(t) &= 4096\exp(-\pi t^2)(64\pi^6 t^{12} - 1056\pi^5 t^{10} + 5940\pi^4 t^8 \\
&\quad -13860\pi^3 t^6 + 12993.75\pi^2 t^4 - 3898\pi t^2 162.42 \\
H_{16}(t) &= 65536\exp(-\pi t^2).(256\pi^8 t^{16} - 7680\pi^7 t^{14} + 87360\pi^6 t^{12} \\
&\quad -480480\pi^5 t^{10} + 1351350\pi^4 t^8 - 1891890\pi^3 t^6 + 1182431.25\pi^2 t^4 - 253378.125\pi t^2 + 7918)
\end{aligned}
\tag{2.34}
$$

In order to find five unknown coefficients D_{4k}, the five ambiguity conditions are employed to form a system of five equations and five unknowns. The solution gives the parameter set:

$$
\begin{aligned}
D_0 &= 1.1850899 \\
D_4 &= -1.9324881 \cdot 10^{-3} \cdot D_0 \\
D_8 &= -7.3110588 \cdot 10^{-6} \cdot D_0 \\
D_{12} &= -3.1542096 \cdot 10^{-9} \cdot D_0 \\
D_{16} &= 9.6634138 \cdot 10^{-13} \cdot D_0.
\end{aligned}
\tag{2.35}
$$

By employing these coefficients in (2.33), the window function forming the Weyl-Heisenberg frame is defined.

2.5.2 Matrix Inversion Method

Matrix inversion method was proposed in [7]. If we consider the k^{th} frequency and l^{th} time shift of the non-orthogonal pulse $\psi(t)$ denoted by $\psi_{k,l}(t)$, we can form an auto-correlation matrix $\mathbf{R}$ such that:

$$\mathbf{R}_{k,l,k',l'} =< \psi_{k',l'}(t)\psi_{k,l}(t) > . \tag{2.36}$$

Then, by employing $\mathbf{R}$, the orthogonalized pulse $\phi(t)$ can be achieved by:

$$\phi(t) = \sum_{k,l} \mathbf{R}_{k,l,0,0}^{-1/2}\psi_{k,l}(t). \tag{2.37}$$

The weakness of this method is that $\mathbf{R}$ must be a full rank matrix.

2.5.3 IOTA

Isotropic Orthogonal Transform Algorithm (IOTA) pulse shape was first proposed in [3]. It is presented as the pulse shaping part of the coded orthogonal division multiplexing (COFDM) system given in [3].

In IOTA method, an orthogonalization operator O is defined to map any pulse shape $x(u)$, to an orthogonalized pulse shape $y(u)$ such that $x(u), y(u), u \in L^2(\mathbb{R}^d), O : x \mapsto y$:

$$y(u) = \frac{2^{\frac{1}{4}}x(u)}{\sqrt{\sum_k \|x(u - k/\sqrt{2})\|^2}}. \tag{2.38}$$

In [3], it has been shown that if $x(u)$ is chosen as the Gaussian pulse, the resulting pulse shape $y(u)$ has very good localization and it also forms an orthogonal Weyl-Heisenberg frame. Because of its nearly isotropic properties, the pulse shape formed by orthogonalizing the Gaussian pulse is named IOTA.

The main drawback of this method is that it is limited to time-frequency symmetric pulse shape $x(u)$ and square lattice structure, where time-frequency symmetry is defined as having the same value (amplitude and phase) for the same points in normalized time and normalized frequency plane. The main reason is that the method requires the condition that orthonormalization of one dimension must be sufficient for orthonormalization in both dimensions.

2.5.4 Discrete-Time Zak Transform

Zak transform first introduced in [36], has an important role in different fields of communication particularly in the analysis of Weyl-Heisenberg frames as a valuable tool in the calculation of dual frames and frame bounds [37].

The orthogonalization method proposed in [8], employs the discrete-time Zak transform (DZT). The DZT of a pulse $x(u)$ in $L^2(\mathbb{Z})$ for $u \in \mathbb{Z}$, is defined as:

$$Z_x(u,\theta) = \sum_{r=-\infty}^{+\infty} x\left[u + r\frac{L}{2}\right] e^{-j2\pi r\theta}, \tag{2.39}$$

where L relates to the sampling interval in this particular case. It is also the number of carriers, u is the time index and θ is the continuous normalized frequency variable.

In [8], the pulse shapes to be orthonormalized are first transformed by DZT. Then in the transformed space, the orthonormalization is defined by:

$$Z_y(u,\theta) = \frac{2Z_x(u,\theta)}{\sqrt{M|Z_x(u,\theta)|^2 + M|Z_x(u,\theta-\frac{1}{2})|^2}}. \tag{2.40}$$

Then inverse DZT is applied in order to achieve orthogonal pulse shapes. This method is actually the generalization of the method described in [3] that resulted in IOTA.

2.6 Non-Orthogonal Signal Shapes

The idea of using non-orthogonal signal shapes in OFDM systems was first proposed in [38]. The introduction of the notion of non-orthogonality arises from the three limitations of the orthogonal pulses presented in the literature.

- Most of the orthogonal signal shaping approaches assumes time-frequency symmetric pulses which are not optimal when time and frequency dispersion of the channel are different (which is true for most practical systems).
- The models are limited to the usage of same pulses at the transmitter and receiver.
- The proposed models suffer as pulse shapes are transferred from analog to digital domain, mainly in the cases of [4]. This is mainly due to the quantization errors in the digital devices.

In [38], non-orthogonal shapes with lattice density $\Delta = 0.5$ are investigated and compared with the method proposed in [4]. The channel is modeled as a doubly dispersive channel in both frequency and time. Time dispersion is modeled as exponential decaying with decay factor $\tau_d = 0.1$ and frequency dispersion is modeled as Jake spectrum with a Doppler spread of $f_D T = 0.1$. Channel characteristics are assumed to be perfectly known at the receiver.

Since there are different signal shapes employed in both receiver and transmitter, in [38], the cross-ambiguity is defined as:

$$A_c(t, f) = \int_{-\infty}^{+\infty} \phi_t^*(u)\phi_r(u-t)\exp(j2\pi f u)du, \tag{2.41}$$

where ϕ_t is the pulse shape at the transmitter (modulation) and ϕ_r is the pulse shape at the receiver (demodulation). The ambiguity definition is slightly different from the previous version given in Chapter 2. This is due to the difference in notation between engineering and mathematics.

Also a wide sense stationary channel dispersion function $C_{\mathbf{H}}(\tau, \nu)$ is considered in order to represent the dispersion in both time and frequency. The aim is to maximize the inner product $< C_{\mathbf{H}}, |A_c|^2 >$. The idea is equivalent to maximizing the cross-ambiguity function where considerable channel scattering occurs.

In this method, the transmitted pulse shape is built by maximizing $\langle C_{\mathbf{H}}, |A|^2 \rangle$ by keeping A normalized. This is accomplished in a nonlinear way by employing the methods described in [39].

Although the performance of the non-orthogonal pulse shapes in the fading channel was shown to be superior to the case in [4], the additive white Gaussian noise (AWGN) performance of the non-orthogonal pulse shapes was inferior to the orthogonal ones. The major drawbacks of the non-orthogonal work of [38] can be summarized as follows:

- A channel dependent non-orthogonal method has been compared to the channel independent model of [4]. However, there exist channel dependent orthogonal models [7], which must be taken into consideration.

- One of the limitations of the orthogonal methods that is pointed out is the time-frequency symmetry of the pulses, i.e. the frequency domain representation and the time domain representation of the pulse must be identical. This is not necessarily the case for this orthonormalization method, as shown in the next chapter.

- The effect on bit error rate is not elaborated, only pulse distortion effect was presented.

2.7 Offset-QAM/OFDM

As afore-mentioned, for lattice density of 1, there cannot be any well localized Weyl-Heisenberg frames. However, if we modulate real and imaginary parts of the symbols by using different carriers, a very densely packed lattice can be achieved with unit density. In order to achieve this, the orthogonal trigonometric Wilson functions in (2.23) are employed as real and imaginary signals. These systems are called Offset-QAM/OFDM systems [8,40–43]. The OQAM/OFDM system can be modeled as shown in Fig. 2.5.

As it can be seen in Fig. 2.5, although the closest neighboring subcarriers are densely packed, they do not affect each other as in the case of classical OFDM. This is due to $\pm\pi/2$ phase shifts between the data that modulates a carrier and its closest four neighbors on the time-frequency plane. Hence even if the carriers lose orthogonality, the symbols may not, resulting in a double robustness against dispersion. This phenomenon is presented in Fig. 2.5 by splitting the carriers into two groups; half of them are marked with j indicating the phase difference. The other half are unmarked.

The OQAM/OFDM architectures must employ real and even pulse shapes in their corresponding Weyl-Heisenberg frames [8]. The orthogonality conditions are also modified as given in [8].

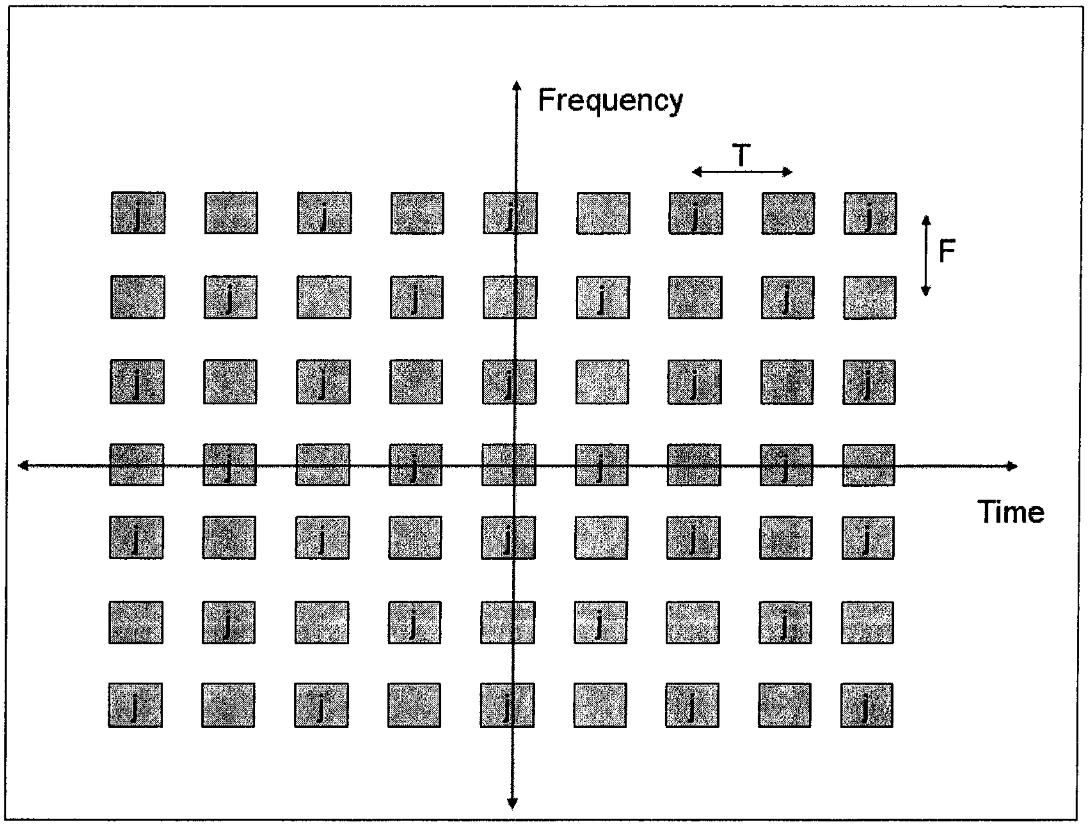

Figure 2.5: Offset QAM lattice structure.

2.8 Conclusions

In this chapter, mathematical definitions related to the thesis are reviewed including Hilbert spaces, time-frequency analysis and frame theory. In particular, we have investigated Gabor frames. Uncertainty principle and ambiguity functions are defined.

We have reviewed various methods employed for orthonormalization processes that exist in the literature. We have also given an overview of the OFDM system structure employed in this thesis. An introduction to non-orthogonal signal shapes and offset-QAM systems is made.

Also, the underlying analytic reasoning behind the employment of Hermite functions throughout the thesis is given.

Next, employing the models and methodology introduced in this chapter, we present a novel orthonormalization method.

Chapter 3

A Novel Orthonormalization Method

Existing orthonormalization methods in the literature have been reviewed in the previous chapter. Initially, we have acquired results on orthonormalization process and system performance using orthonormalized pulses. In this chapter, we introduce a novel orthonormalization technique. First, the orthonormality criteria followed by the orthonormalization process is detailed. Ambiguity function is also represented using the orthonormality definitions given in this chapter.

3.1 Orthonormality Criteria

As stated in the previous chapter in (2.29), the orthonormality criterion is given by:

$$\int_{-\infty}^{\infty} \varphi_{00}^{*}(t)\varphi_{mn}(t)dt = \delta_m \delta_n.$$

Applying the discrete two dimensional discrete Fourier transform to both sides of the equation, we obtain the equivalent expression:

$$\sum_m \sum_n \exp(-j2\pi nT\nu) \exp(-j2\pi mF\tau) \int_{-\infty}^{\infty} \varphi_{00}^*(t)\varphi_{mn}(t)dt = 1. \tag{3.1}$$

When the definition of $\varphi_{mn}(t)$ is placed in the above equation we get:

$$\sum_m \sum_n \exp(-j2\pi nT\nu) \exp(-j2\pi mF\tau) \int_{-\infty}^{\infty} \varphi^*(t)\varphi(t - nT) \exp(j2\pi mFt)dt = 1. \tag{3.2}$$

Using the relation

$$\sum_m \exp(j2\pi mFu) = \frac{1}{F} \sum_m \delta(u - m/F),$$

and computing the integral with respect to t gives the orthonormality condition:

$$\sum_m \sum_n \exp(-j2\pi nT\nu)\varphi^*(\tau + m/F)\varphi(\tau + m/F - nT) = F, \tag{3.3}$$

and by employing the lattice density $\Delta = 1/FT$, we obtain:

$$\sum_m (\varphi(\tau + m\Delta T) \exp(j2\pi m\Delta T\nu))^* \sum_n \varphi(\tau + (m\Delta - n)T) \exp(j2\pi(m\Delta - n)T\nu) = \frac{1}{\Delta T} \tag{3.4}$$

as the orthonormality criterion. The criterion of (3.4) is the most general case for equal time spacing and equal frequency spacing.

In general, we investigate the integer inverse densities, namely $\Delta = 1/L$ density lattices. For simplicity and without loss of generality, we assume square lattice, i.e. $F = T = \sqrt{L}$. So (3.4) can be modified as:

$$\sum_m (\varphi(\tau + m\sqrt{L}) \exp(j2\pi m\sqrt{L}\nu))^* \sum_n \varphi\left(\tau + (\frac{m}{L} - n)\sqrt{L}\right) \exp\left(j2\pi(\frac{m}{L} - n)\sqrt{L}\nu\right) = \sqrt{L} \tag{3.5}$$

With a variable change in (3.5) we get the orthonormality criterion for $1/L$ density lattice:

$$\sum_{r=0}^{L-1} \left| \sum_q \varphi\left(\tau + (q + \frac{r}{L})\sqrt{L}\right) \exp(j2\pi\nu(q + \frac{r}{L})\sqrt{L}) \right|^2 = \sqrt{L}. \tag{3.6}$$

For the unit density, $L = 1$, this expression simplifies to:

$$\left| \sum_q \varphi(\tau + q) \exp(j2\pi\nu q) \right|^2 = 1. \tag{3.7}$$

For the $\Delta = 1/2$ density lattice, the condition becomes:

$$\left| \sum_k \varphi(\tau + k\sqrt{2}) \exp(j2\pi\nu\sqrt{2}k) \right|^2 + \left| \sum_k \varphi\left(\tau + (k + \frac{1}{2})\sqrt{2}\right) \exp\left(j2\pi\nu\sqrt{2}(k + \frac{1}{2})\right) \right|^2 = \sqrt{2}. \tag{3.8}$$

This condition plays a similar role to the well known Nyquist criterion for non inter-symbol interference in 1 dimension. The $|\cdots|^2$ terms in (3.8) are periodic and also their sum is periodic in time and frequency with a common period $1/F = 1/T = 1/\sqrt{2}$.

3.2 Orthonormalization of a Mother Function

Other than the trivial functions such as rectangular or sinc functions or raised cosine filters, it is very difficult to find a set of $\varphi_{mn}(t) \in L^2(\mathbb{R})$ in order to satisfy the orthonormality condition given in (3.4). Here, we introduce a novel method to orthonormalize any given mother function $\psi(t)$ by combining time-frequency shifts of $\psi(t)$ as:

$$\phi(t) = \sum_k \sum_l a_{kl} \psi_{kl}(t), \tag{3.9}$$

where

$$\psi_{kl}(t) = \psi(t - kT) \exp(j2\pi lFt), \tag{3.10}$$

and a_{kl} are complex coefficients. Therefore, orthonormalizing the mother function reduces to finding the appropriate coefficient set $\{a_{kl}\}$. Using this condition directly in (3.4) for any irregular spacing leads to analytically intractable solutions. Hence, we again limit ourselves to the inverse integer density cases where $\Delta = 1/L$. If we combine (3.9) with the orthonormality condition of (3.6) , we end up with:

$$\sum_m \left(\sum_k \sum_l a_{kl} \psi_{kl}(\tau + m/F) \exp\left(j2\pi m\nu/F\right) \right)^*$$
$$\dots \sum_n \sum_{p,q} a_{p,q} \psi_{p,q}(\tau + m/F - nT) \exp(j2\pi(m/F - nT)\nu) = F. \tag{3.11}$$

If we replace the mother function shifts $\{\psi_{kl}\}$ by their expression given in (3.10), we can rewrite (3.11) as:

$$\sum_m \left(\sum_k \sum_l a_{kl} \psi_{kl}(\tau + m/F - kT) \exp\left(j2\pi m\nu/F\right) \exp\left(j2\pi l F(\tau + m/F)\right) \right)^*$$
$$\sum_n \sum_{p,q} a_{p,q} \psi_{p,q}(\tau + m/F - (n+p)T) \exp(j2\pi q F(\tau + m/F - nT)) \exp(j2\pi(m/F - nT)\nu) = F. \tag{3.12}$$

After rearranging the summations and using the density relation $F = T = \sqrt{L}$, (3.12) becomes:

$$\sum_k \sum_l \left[a_{kl} \exp\left(j2\pi\sqrt{L}(k\nu + l\tau)\right)\right]^* \sum_{p,q} a_{p,q} \exp\left(j2\pi\sqrt{L}(p\nu + q\tau)\right)$$
$$\dots \sum_m \left(\psi\left(\tau + (\frac{m}{L} - k)\sqrt{L}\right) \exp\left(j2\pi(\frac{m}{L} - k)\sqrt{L}\nu\right)\right)^*$$
$$\dots \sum_n \psi\left(\tau + (\frac{m}{L} - n - p)\sqrt{L}\right) \exp\left(j2\pi(\frac{m}{L} - n - p)\sqrt{L}\nu\right) = \sqrt{L} \tag{3.13}$$

After changes of variables and factorization, (3.13) can be written as:

$$\left| \sum_k \sum_l a_{kl} \exp\left(j2\pi\sqrt{L}(k\nu + l\tau)\right)\right|^2 \sum_{r=0}^{L-1} \left| \sum_n \psi\left(\tau + (\frac{r}{L} + n)\sqrt{L}\right) \exp\left(j2\pi(\frac{r}{L} + n)\sqrt{L}\nu\right)\right|^2 = \sqrt{L} \tag{3.14}$$

As it can be seen from (3.14), for inverse integer densities, the coefficients a_{kl} can be obtained by a two dimensional discrete Fourier transform. We can modify (3.14) as:

$$\sum_k \sum_l a_{kl} \exp\left(j2\pi\sqrt{L}(k\nu + l\tau)\right) = \frac{L^{1/4}\chi(\nu,\tau)}{\sqrt{\sum_{r=0}^{L-1} \left| \sum_n \psi\left(\tau + (\frac{r}{L} + n)\sqrt{L}\right) \exp\left(j2\pi(\frac{r}{L} + n)\sqrt{L}\nu\right)\right|^2}}. \tag{3.15}$$

where $\chi(\nu, \tau)$ is an arbitrary complex unit module function periodic in time and frequency with a period of $1/\sqrt{L}$. For simplicity purposes, we set the function to 1. Re-organizing and integrating both sides of (3.15) gives the equation for computing the coefficients a_{kl}:

$$a_{kl} = \int_{0<\nu,\tau<1} \frac{L^{5/4} \exp\left(-j2\pi\sqrt{L}(k\nu + l\tau)\right) d\nu d\tau}{\sqrt{\sum_{r=0}^{L-1} \left|\sum_n \psi\left(\tau + (\frac{r}{L} + n)\sqrt{L}\right) \exp\left(j2\pi(\frac{r}{L} + n)\sqrt{L}\nu\right)\right|^2}}. \tag{3.16}$$

By employing the coefficients obtained by using (3.16), any non-orthogonal function can be orthonormalized.

In the denominator of (3.16), L different values in the form of $|.|$ are summed. This forms a diversity since each term varies independently and hence the sum of the squared terms do not fluctuate considerably. As a consequence, the Fourier transform of the inverse takes negligible values for the high values of k and l, leading to very well localized orthonormalized functions, where $a_{00} = 1$ almost and the prototype function is very close to the mother function. Hence the prototype function is almost as well localized as the mother function. For example, the cases of $L = 1$ and $L = 2$ are given in (3.20) and (3.21) respectively:

$$a_{kl} = \int_{0<\nu,\tau<1} \frac{\exp\left(-j2\pi(k\nu + l\tau)\right) d\nu d\tau}{\sqrt{\left|\sum_n \psi\left(\tau + n\right) \exp\left(j2\pi n\nu\right)\right|^2}}, \tag{3.17}$$

$$a_{kl} = \int_{0<\nu,\tau<1} \frac{2^{5/4} \exp\left(-j2\pi\sqrt{2}(k\nu + l\tau)\right) d\nu d\tau}{\sqrt{\sum_{r=0}^{1} \left|\sum_n \psi\left(\tau + (\frac{r}{2} + n)\sqrt{2}\right) \exp\left(j2\pi(\frac{r}{2} + n)\sqrt{2}\nu\right)\right|^2}}. \tag{3.18}$$

The summation in the denominator of (3.21) increases the degree of freedom when compared to the case of $L = 1$ in the course of solving the equation, and helps to orthonormalize the signal while keeping the signal well localized. Next, the effect of diversity is further investigated in the light of the Balian - Low theorem.

The orthogonalization of well localized nonorthogonal signals was proposed in [3, 7]. However, in all of the cases that are present in the literature, the well localized nonorthogonal functions, which we refer to as the mother function from this point on, is chosen as the Gaussian function. The orthonormalization of Gaussian function results in the IOTA function of [3]. In the following section, it is shown that this is not the optimal choice for the mother function from a time-frequency localization point of view.

3.3 Ambiguity Function

Recalling equation (2.11), for a multi-carrier system to work, we want the ambiguity function to be zero at the integer multiples of time separation T and frequency separation F. However, this condition is sufficient only for ideal channel conditions when the effects of time or frequency dispersion are not considered.

For a multi-carrier system, in order to become robust against channel impairments, the ambiguity function must also have low values near the integer multiples of time separation T and frequency separation F. Furthermore, the ambiguity function must be a rapidly decreasing function. This property can be achieved by a fast decaying mother function $\psi(t)$ and a fast decaying orthonormalized function $\phi(t)$ derived from $\psi(t)$.

We can represent the ambiguity function $A(t,f)$ in terms of $\psi(t)$ by employing (3.9) and (3.10) as:

$$A(t,f) = \sum_k \sum_l \sum_{k',l'} a^*_{k,l} a_{k',l'} \int_{-\infty}^{+\infty} \psi^*(u-kT)\psi(u-t-k'T) \exp\left(j2\pi((l'-l)F+f)u\right) \exp(-j2\pi l'Ft)du. \tag{3.19}$$

In the following chapter, the choice of the mother function is investigated along with the comparison of different ambiguity functions resulting from employing different mother functions.

3.4 Parity Preservation after Orthonormalization

Next, our objective is to show that the previous orthonormalization procedure preserves the parity of the mother function $\psi(t)$. Hence, let us assume that $\psi(t)$ is of even or odd parity, with

$$\psi(-t) = (-1)^p \psi(t) \tag{3.20}$$

where $p = 0$ for even parity and $p = 1$ for odd parity. Then using (3.9) and (3.10), we can write $\phi(-t)$ as a function of p and $\psi(t)$ as

$$\phi(-t) = (-1)^p \sum_{k,l} a_{-k,-l} \psi_{k,l}(t) \tag{3.21}$$

To show that the parity is preserved we should just check whether , $a_{-k,-l} = a_{k,l}$ or not. Taking into account the time and frequency periodicity of the function within the integral giving the combination coefficients $a_{k,l}$ and using the variables changes $n \longrightarrow -(n+1)$ and $r \longrightarrow L - r$, we thus have

$$\begin{aligned} a_{-k,-l} = & \\ & \frac{\int_{0 \le \nu,\tau \le \frac{1}{\sqrt{L}}} L^{5/4} \exp\left(j2\pi\sqrt{L}(k\nu + l\tau)\right) d\nu d\tau}{\sqrt{\sum_{r=0}^{L-1} \left| \sum_n \psi\left(\tau + (\frac{r}{L} + n)\sqrt{L}\right) \exp\left(j2\pi(\frac{r}{L} + n)\sqrt{L}\nu\right) \right|^2}} \\ = & \frac{\int_{0 \le \nu,\tau \le \frac{1}{\sqrt{L}}} L^{5/4} \exp\left(-j2\pi\sqrt{L}(k\nu + l\tau)\right) d\nu d\tau}{\sqrt{\sum_{r=0}^{L-1} \left| \sum_n (-1)^p \psi\left(\tau - (\frac{r}{L} + n)\sqrt{L}\right) \exp\left(-j2\pi(\frac{r}{L} + n)\sqrt{L}\nu\right) \right|^2}} \end{aligned} \tag{3.22}$$

$$
\begin{aligned}
&= \frac{\int_{0\le\nu,\tau\le\frac{1}{\sqrt{L}}} L^{5/4}\exp\left(-j2\pi\sqrt{L}(k\nu+l\tau)\right)d\nu d\tau}{\sqrt{\sum_{r=1}^{L}\left|\sum_n \psi\left(\tau+(\frac{r}{L}+n)\sqrt{L}\right)\exp\left(j2\pi(\frac{r}{L}+n)\sqrt{L}\nu\right)\right|^2}} \\
&= \frac{\int_{0\le\nu,\tau\le\frac{1}{\sqrt{L}}} L^{5/4}\exp\left(-j2\pi\sqrt{L}(k\nu+l\tau)\right)d\nu d\tau}{\sqrt{\sum_{r=0}^{L-1}\left|\sum_n \psi\left(\tau+(\frac{r}{L}+n)\sqrt{L}\right)\exp\left(j2\pi(\frac{r}{L}+n)\sqrt{L}\nu\right)\right|^2}} \\
&= a_{k,l}
\end{aligned}
\tag{3.23}
$$

Hence, the parity of the mother function is preserved by orthonormalization. This characteristic is needed when half-density lattice is used as a starting point for the construction of an OFDM-OQAM lattice. In fact these lattices, when based on a half-density lattice, need that the orthonormal prototype function be of even or odd parity. Hence, to have one of these characteristics suffices to chose the mother function to have the desired parity. Also, the result shows the orthonormalization procedure is convergent, since the parity is not conserved, if the result is divergent.

3.5 Conclusion

In this chapter, we presented a novel orthonormality criterion for pulse shapes to be used in multi-carrier systems. We have derived the special lattice density cases for this criterion. We have also presented the ambiguity function in terms of the representations given for the orthonormality conditions.

Later, using this orthonormality criterion, we have given an orthonormalization procedure for any given mother function. In practice, as long as the desired orthogonal set is achieved, the way to achieve it is not of particular importance. However, the proposed method is utilized in the following chapters where heuristic search algorithms are employed and the function is computed many times. In this way, the methodology is fast and efficient.

Chapter 4

Choice of the Mother Function

In this chapter, we propose Hermite functions as the choice of mother functions to be orthonormalized. We start by presenting popular function families and their feasibility in multi-carrier systems. By employing the orthonormalization methods given in the previous chapter, Hermite functions are orthonormalized and utilized as pulse shapes in multi carrier systems. The coefficients for Hermite functions for a well localized pulse shape are calculated. The resulting ambiguity functions are plotted. Furthermore, the localizations of various pulse shapes are given.

4.1 Some unsuccessful alternatives

Prior to the investigation of the pulse shape for multi-carrier systems, we investigate some well known function families and demonstrate why they are not good candidates to be used in OFDM systems.

4.1.1 Wavelets

Just as time-frequency translations and modulation were first introduced in Physics as coherent states [44,45], wavelets have been proposed in Physics as 'affine coherent states' [46]. In communication theory, wavelets have been introduced by I. Daubechies in [35]. Wavelets, like the Weyl-Heisenberg frames, transform the continuous Hilbert space by the use of window functions. However unlike Weyl-Heisenberg frames, the translation and modulation operations are not accomplished by uniform time and frequency translations, but by position and dilation. The modified window function $h_{mn}(x) \in L^2(\mathbb{R})$ from the source window is given by:

$$h_{mn}(x) = |m|^{-1/2} h(\frac{x-n}{m}), \tag{4.1}$$

where $h(x)$ is a square integrable function. In $h_{mn}(x)$, m is the dilation and n is the position parameter. In the time-frequency analysis, dilation affects the frequency; hence it is similar to modulation whereas position is similar to translation.

When we compare the lattice structures of wavelets and Weyl-Heisenberg frames, the functions h_{mn} are more concentrated in the higher frequencies. The difference is depicted in Fig. 4.1 and Fig. 4.2.

As it can be seen in the figures, the wavelets divide the time-frequency plane non-uniformly. In multi-carrier communications, this results in non-uniform distribution for the sub-carriers resulting in favor of the subcarriers closer to the origin. Therefore, wavelet based frames are not suitable in terms of subcarrier location schemes. As a result, the application of wavelets in multi carrier systems has been limited to very few studies investigating the pulse shaping of MC-CDMA, still using Weyl-Heisenberg frame structure [47]. Hence, in this dissertation we limit our analysis to the Weyl-Heisenberg frames. An exception to this investigation is non-uniform systems providing non-uniform throughput distribution between subcarriers or unequal error protection. It

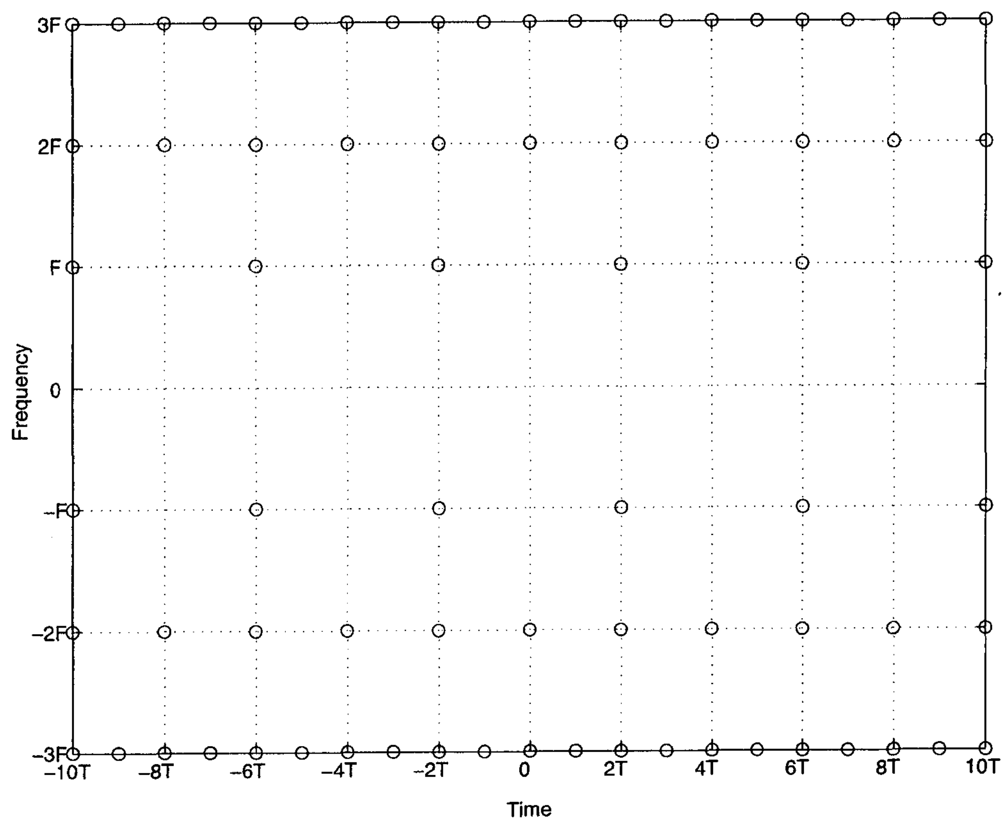

Figure 4.1: Time-Frequency distribution of the wavelet functions.

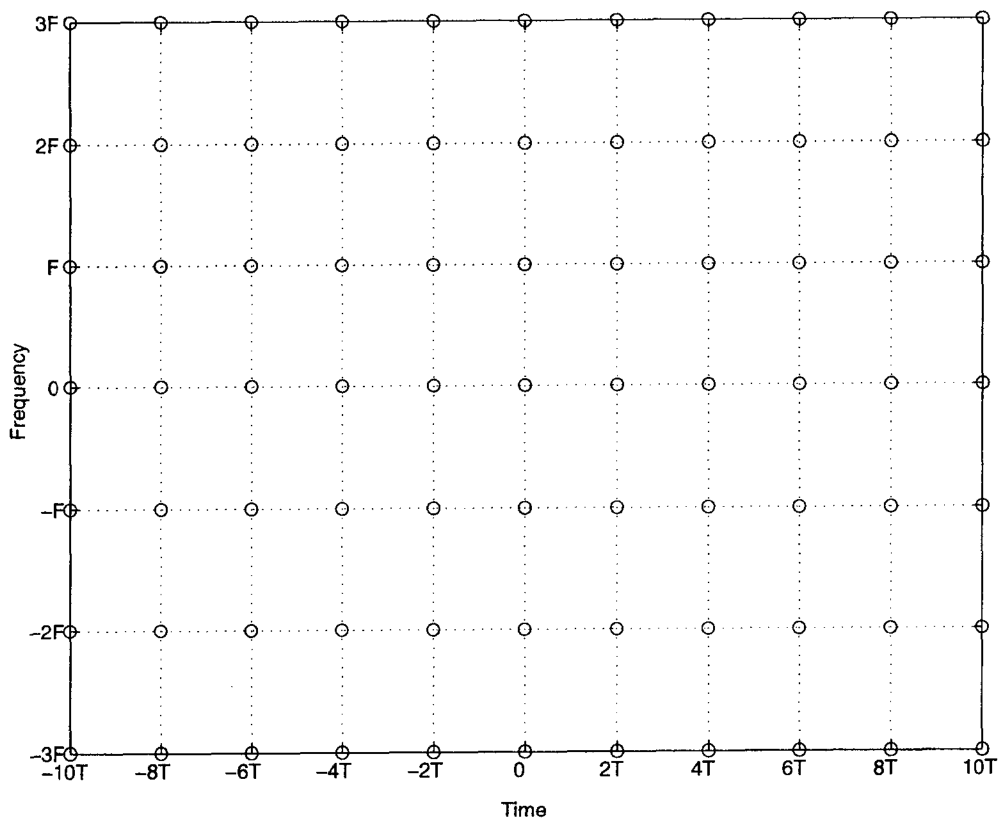

Figure 4.2: Time-Frequency distribution of the Weyl-Heisenberg functions.

is also possible to change the time-frequency spacings by modifying the wavelets, however for that case, they become equivalent to Weyl-Heisenberg frames.

4.1.2 Prolate Spheroidal Functions

Once the lattice structure is set, the second problem is setting the pulse shape to be used in the lattice. Prior to the discussion of well localized pulse shapes, we investigate another group of pulse shapes namely Prolate functions. Prolate spheroidal (PS) functions are initially proposed as solutions of a differential equation resulting from separating the variables to solve the Helmholtz equations in prolate spheroidal coordinates [48].

Their introduction to communication theory was done by Slepian in [49]. The importance of the PS functions in pulse shaping results from their spectral localization properties. A set of orthogonal PS functions forms the most spectral efficient orthogonal set of functions possible. A simple algorithm for generating numerical values of prolate functions is given in [50].

Even though the first discrete function converges to a Gaussian which is well localized in both time and frequency, the localization property of the PS functions is optimum in a single dimension only. Hence in communication systems, the applications of PS functions suffer under non-linear channel dispersions [51]. In order to facilitate the localization in two dimensions simultaneously, we investigate the choice of mother functions in the next section.

4.2 Choice of Mother Functions

The Gaussian function is the most localized function in terms of both time localization and frequency localization and the localization is given by $1/4\pi$, The main motivation of employing Gaussian functions is that when the Gaussian mother function is orthonormalized, the resulting orthonormal function $\psi(t)$ also has a localization very close to the Gaussian one. If we employ the Gaussian signal as:

$$\psi(t) = e^{-\pi t^2}, \tag{4.2}$$

and orthonormalize for the half density lattice, $1/L = FT = 2$, the resulting orthonormalized signal $\phi(t)$ is the IOTA function.

As a more general approach, we propose to combine Hermite functions for designing the mother function. This novel mother function can then be orthonormalized by any method proposed in the literature.

We form the mother function $\phi(t)$ by:

$$\phi(t) = \sum_{k=0}^{\infty} a_k H_k(t), \tag{4.3}$$

where $H_k(t)$ is the k^{th} Hermite function. The main motivation behind employing Hermite functions is that the first Hermite function is the Gaussian function given by (4.2) and the k^{th} Hermite function is the k^{th} best localized function that is orthogonal to the Gaussian and other Hermite functions. Hermite functions generate all square integrable functions that is, they form a base of $L^2(\mathbb{R})$, hence any arbitrary choice for the mother function can be obtained as a combination of these Hermite functions.

A good combination of Hermite functions must use very small combination coefficients for large indices. The reason behind this is the decreasing localizations of Hermite functions with increased index values.

In this work, these coefficients are optimized by brute force approach, using exhaustive search in order to maximize the localization. There are three main results that are obtained from the simulations:

- The coefficients $\{a_k\}$ decrease exponentially with increasing k, hence only 5 coefficients are satisfactory for convergence.
- Only the Hermite functions whose frequency transforms are the same as themselves, hence time-frequency symmetric Hermite functions give good localization performance. These Hermite functions are the ones where $k = 0 \ (\mathrm{mod} 4)$.
- The first coefficient a_0 can be set to 1 without loss of generality for normalized pulses. When we set $a_0 = 1$, all other coefficients a_k must be real. In general all complex coefficients must have the same phase for optimum localization with the exception of a $\pi/2$ degree phase shift.

Keeping these conditions in mind, the Hermite functions that are employed are given as:

$$
\begin{aligned}
H_0(t) &= \exp(-\pi t^2) \\
H_4(t) &= 16 \exp(-\pi t^2)(4\pi^2 t^4 - 6\pi t^2 + 0.75) \\
H_8(t) &= 256 \exp(-\pi t^2)(16\pi^4 t^8 - 112\pi^3 t^6 + 210\pi^2 t^4 \\
&\quad -105\pi t^2 + 11.67) \\
H_{12}(t) &= 4096 \exp(-\pi t^2)(64\pi^6 t^{12} - 1056\pi^5 t^{10} + 5940\pi^4 t^8 \\
&\quad -13860\pi^3 t^6 + 12993.75\pi^2 t^4 - 3898\pi t^2 162.42 \\
H_{16}(t) &= 65536 \exp(-\pi t^2).(256\pi^8 t^{16} - 7680\pi^7 t^{14} + 87360\pi^6 t^{12} \\
&\quad -480480\pi^5 t^{10} + 1351350\pi^4 t^8 - 1891890\pi^3 t^6 + 1182431.25\pi^2 t^4 - 253378.125\pi t^2 + 7918)
\end{aligned}
\tag{4.4}
$$

Various Hermite functions are depicted from Fig. 4.3 to Fig. 4.6.

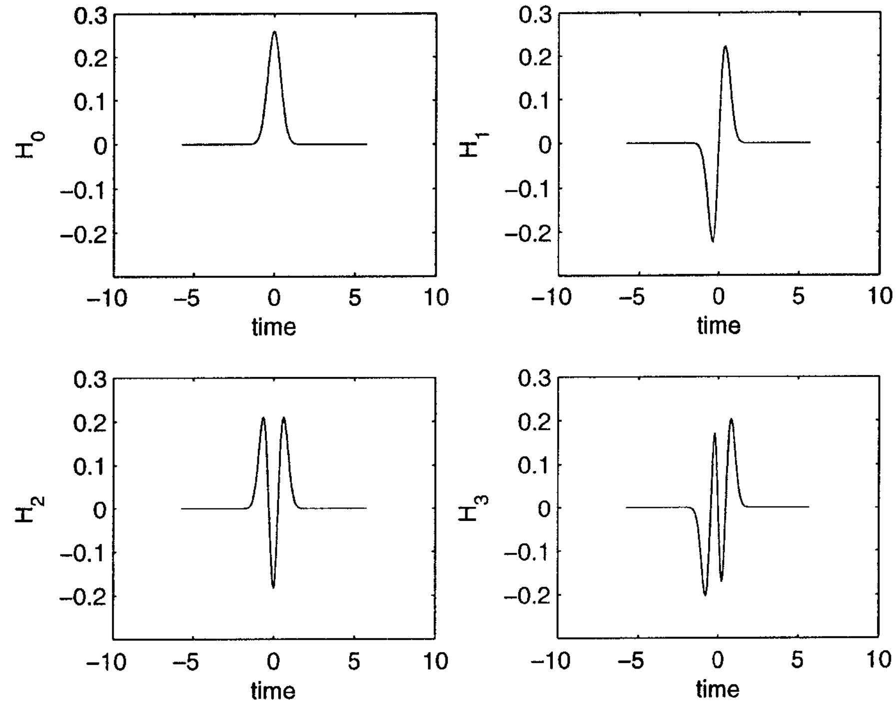

Figure 4.3: First four Hermite functions.

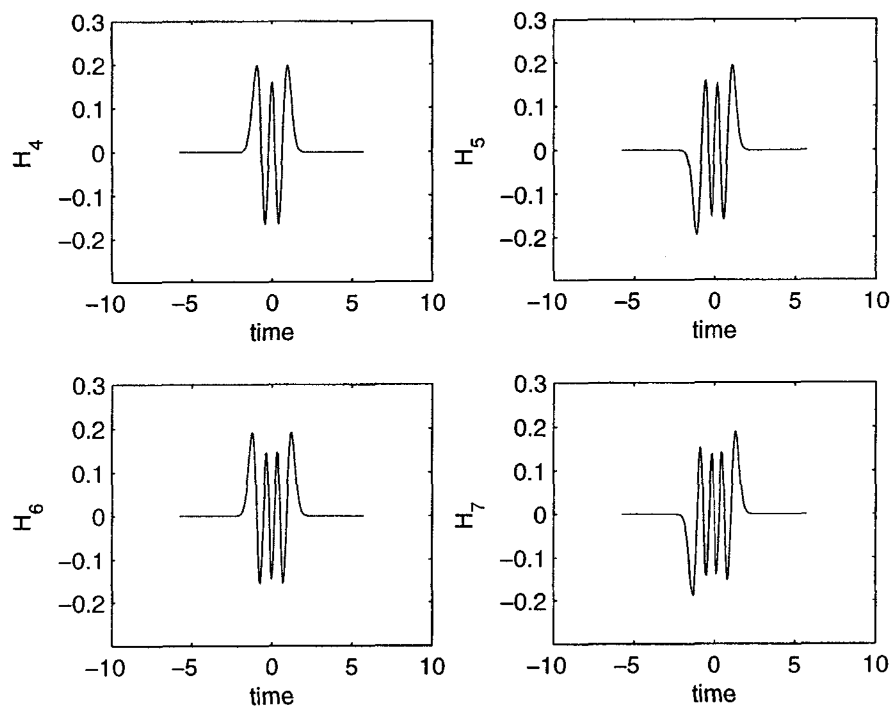

Figure 4.4: 5^{th} to 8^{th} Hermite functions.

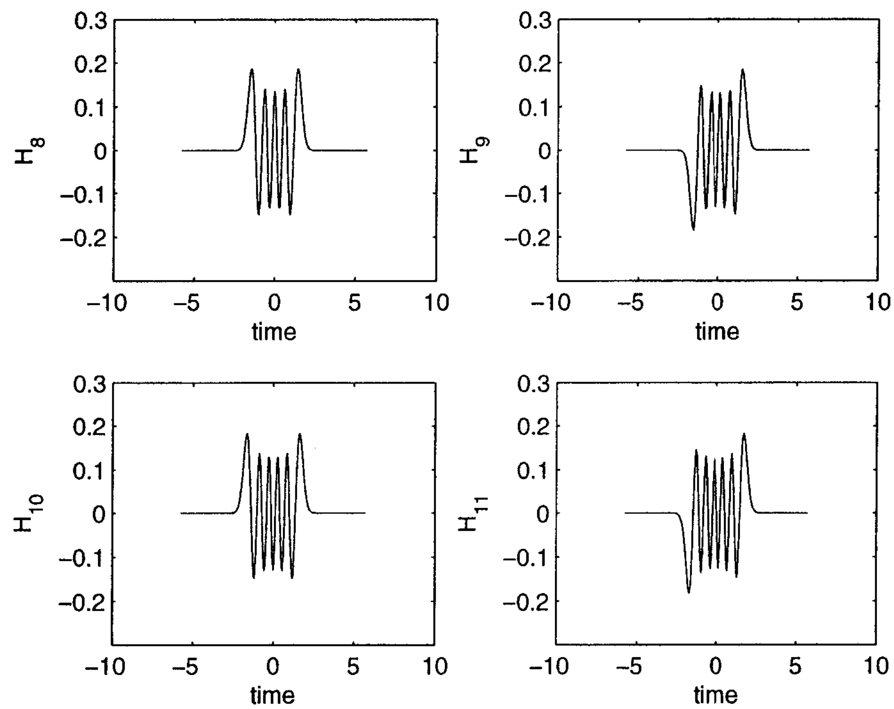

Figure 4.5: 9^{th} to 12^{th} Hermite functions.

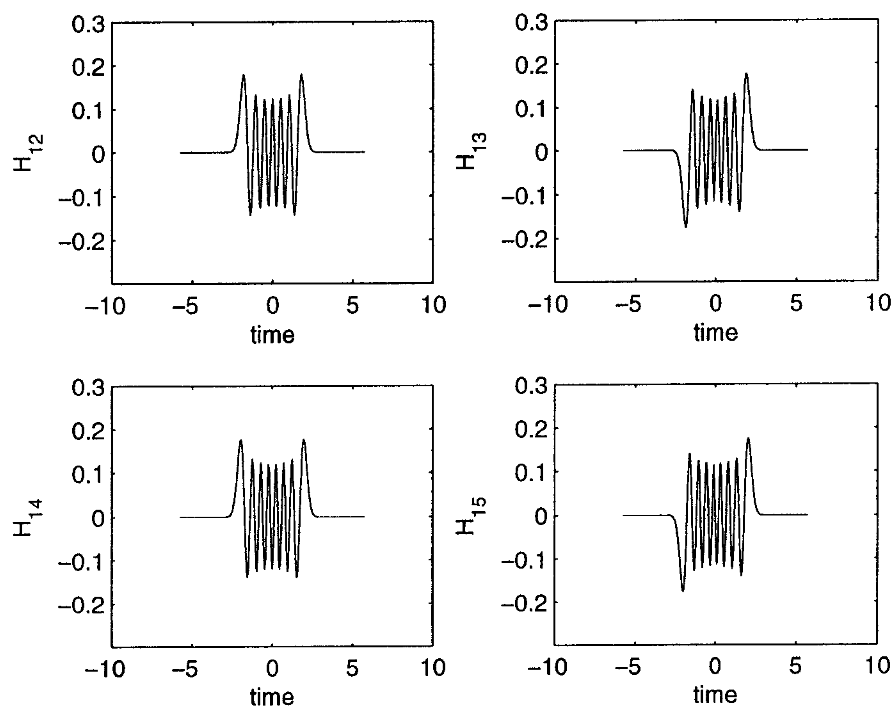

Figure 4.6: 13^{th} to 16^{th} Hermite functions.

Table 4.1: Coefficients for Hermite functions for well-localized pulses.

a_0	1
a_4	-1.5×10^{-3}
a_8	-3×10^{-6}
a_{12}	-2×10^{-10}
a_{16}	-2×10^{-13}

The coefficients to these functions are given in Table 4.1. We form our mother function by the coefficients given in Table 4.1 and orthogonalize it. The coefficients are calculated using a gradient-based optimization technique. The results converge to the coefficient set mentioned in the table regardless of the initial starting point. However, the optimization process is not linear. The reason is; even though the Hermite pulse shapes are orthogonal to each other, their time-frequency orthonormalized versions are not. In other words, the orthonormalization process does not conserve the orthogonality between the Hermite functions. For this reason, the coefficients were re-calculated each time a new Hermite is added to the optimization process.

The resulting orthogonal signal is plotted in Fig.4.7. In this figure, the Gaussian signal and the orthogonalized Gaussian signal (IOTA) as well as the raised cosine pulse are included. Although the functions are symmetric in time and frequency, we include the frequency response of Fig.4.8 for an extended range, in order to get a broader comparison between IOTA and our signal.

It is clearly seen in Fig. 4.7 and Fig. 4.8 that the proposed orthogonal signal is slightly more localized in both time and frequency when compared to the IOTA function. The time localization of the conventional raised cosine signal with 0.1 roll-off factor is much worse when compared to the other signals: 0.2188. Whereas, the time-frequency

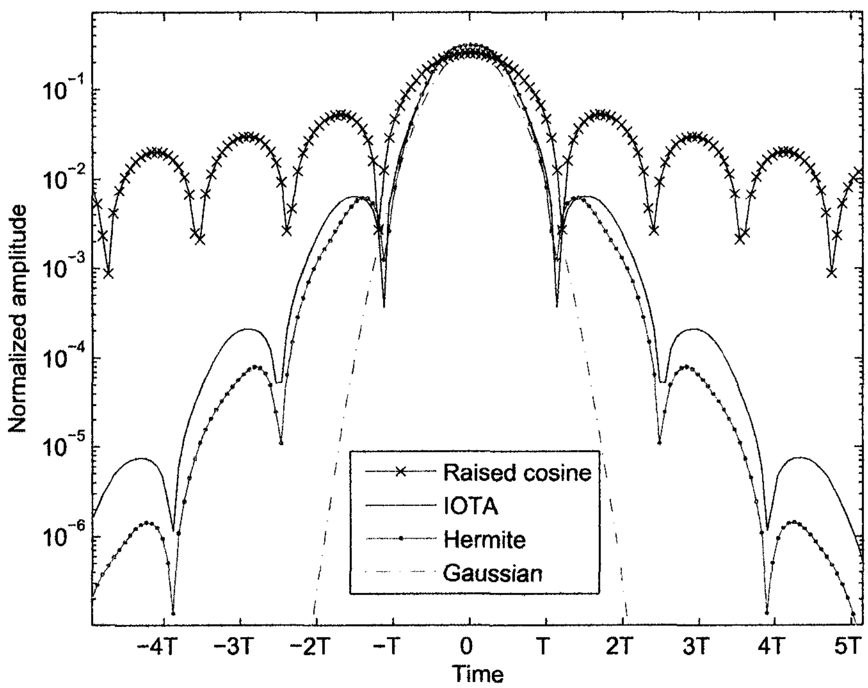

Figure 4.7: The proposed Hermite signal vs. the IOTA and the Gaussian in time domain.

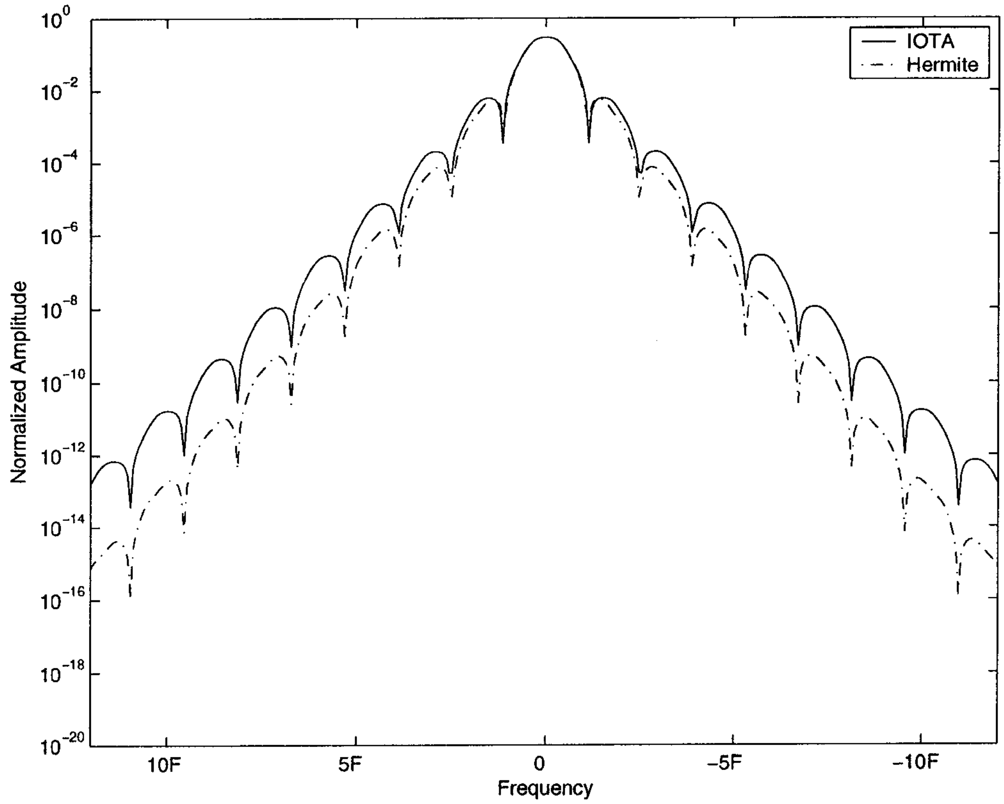

Figure 4.8: The proposed signal vs. the IOTA signal in frequency domain.

localization of a Gaussian pulse is $1/4\pi = 0.0796$, the localization of IOTA is 0.0815 and the proposed signal has a localization of 0.0811 (In the optimization process, the localization changes after each Hermite is given as $H_0 - 0.0815$, $H_4 - 0.0813$, $H_8 - 0.08114$, $H_{16} - 0.0811$). In Figs. 4.7 and 4.8, it can be seen that the proposed signal has the same nulls and smaller sidelobes when compared to IOTA, which makes it more robust the time and frequency dispersion effects of the channel.

The main motivation behind using half density is the Balian-Low theorem [5,6]. The Balian-Low theorem states that for a unit density lattice ($L = 1$), it is impossible to obtain well localized pulses that are orthonormal both in time and frequency. These pulse sets are also referred to as Weyl - Heisenberg bases. As a result, half density lattice structures are employed in most of the OFDM/QAM systems proposed in the literature [7,8]. The proposed cases in the literature can be derived with our method as specific cases of (3.4). Hence, the work presented here is the generalized and simplified orthonormalization procedure for any signal set, including the OFDM/QAM systems and the IOTA.

One must also note that, the orthonormalization method proposed in [3] for the IOTA function can only be applied to Gaussian functions, which limits the proposed orthonormalization procedure in [3].

Another important point for employing the proposed orthonormalization procedure is that the IOTA function has been proved to be a non optimum one as opposed to the conjecture in [3] and [7]. Hence by modifying the mother function, a better localized orthonormal signal set can be achieved.

We should also note that IOTA is just a special case of the method employed here by using only the first Hermite function. In terms of localization gains, the additional Hermite functions only provide marginal gains. However, the main advantage of Hermite functions is their flexibility with using different coefficients for different combinations. From this point on we will exploit this property to develop pulse shapes for unit-density cases as well as for overlapping Weyl-Heisenberg frames.

4.3 Ambiguity Functions for Different Pulse Shapes

In figures 4.9, 4.10, and 4.11, the ambiguity functions for the square pulse, the IOTA and the proposed Hermite functions are given respectively. As it can be observed in the figures, the sidelobe levels of the ambiguity function for the square pulse is very high. This would result in the leakage of interference power between subcarriers, if there is dispersion in the channel in either time or frequency. When we compare the ambiguity functions for the IOTA and Hermite, the latter has a marginally faster decaying ambiguity function. This results in a slightly better dispersion robustness as shown in the simulations of the next chapter. As afore-mentioned, the ambiguity functions present a measure of applicability as a pulse shaping methodology for MC systems.

In order to present the difference between the Hermite and IOTA ambiguity functions, the difference is plotted in Fig. 4.12. As it is shown in the figure, the ambiguity function of IOTA has lower values around the origin but higher values around the neighboring regions that may cause inter-symbol-interference or inter-carrier-interference.

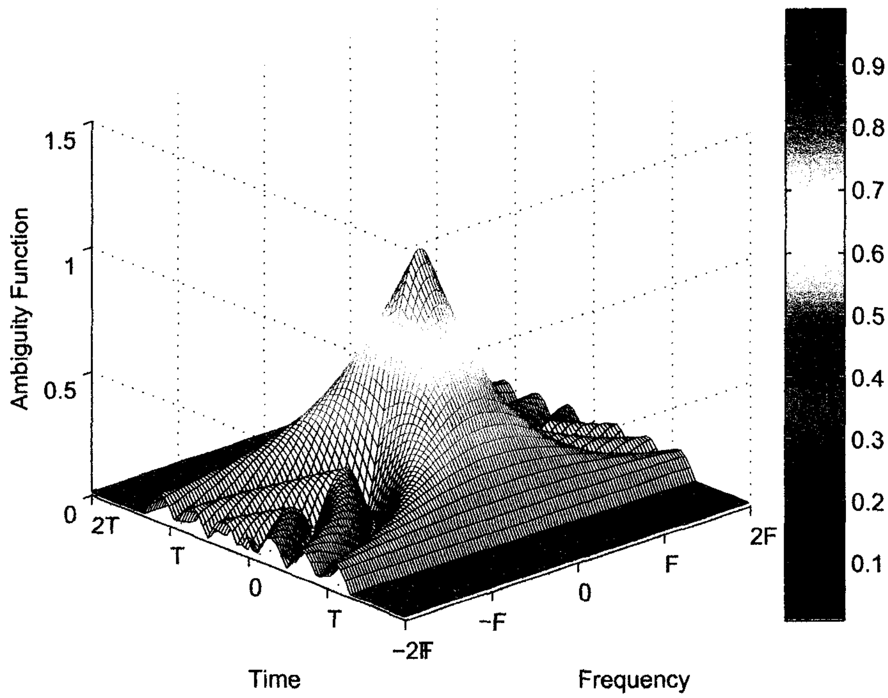

Figure 4.9: Ambiguity Function for Square Pulse.

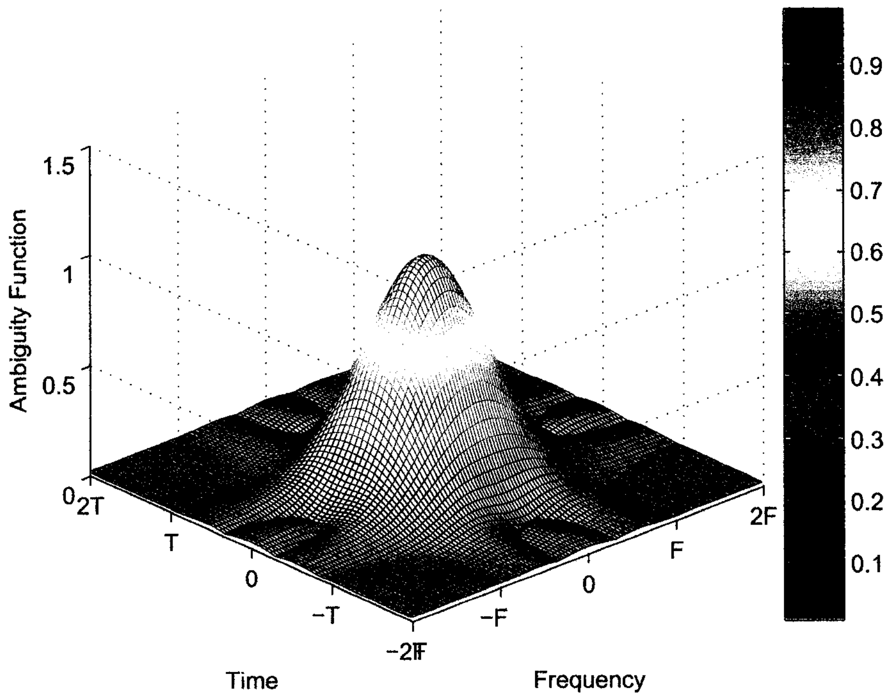

Figure 4.10: Ambiguity Function for IOTA.

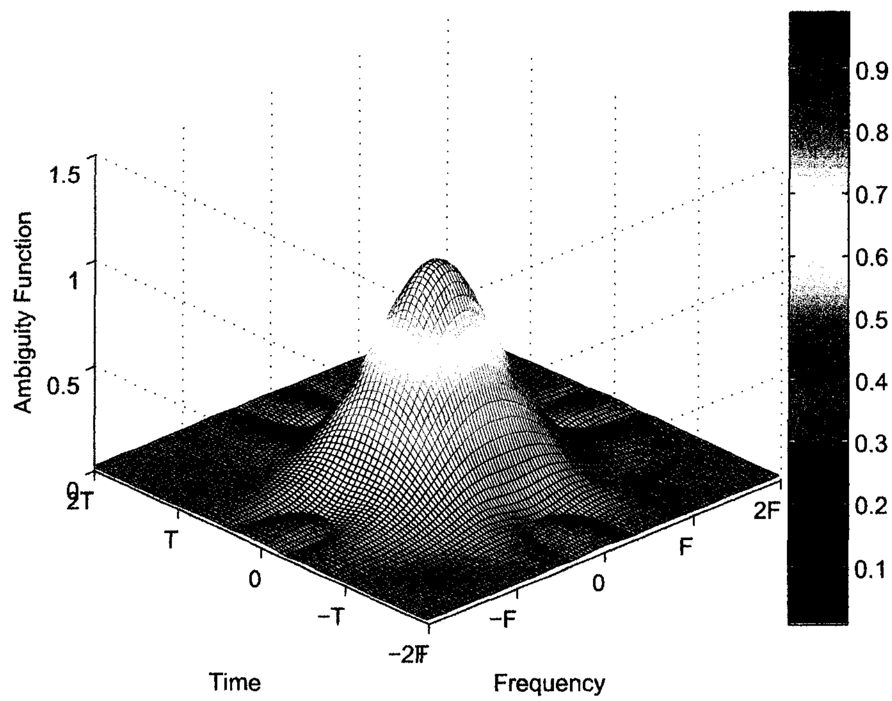

Figure 4.11: Ambiguity Function for Hermite.

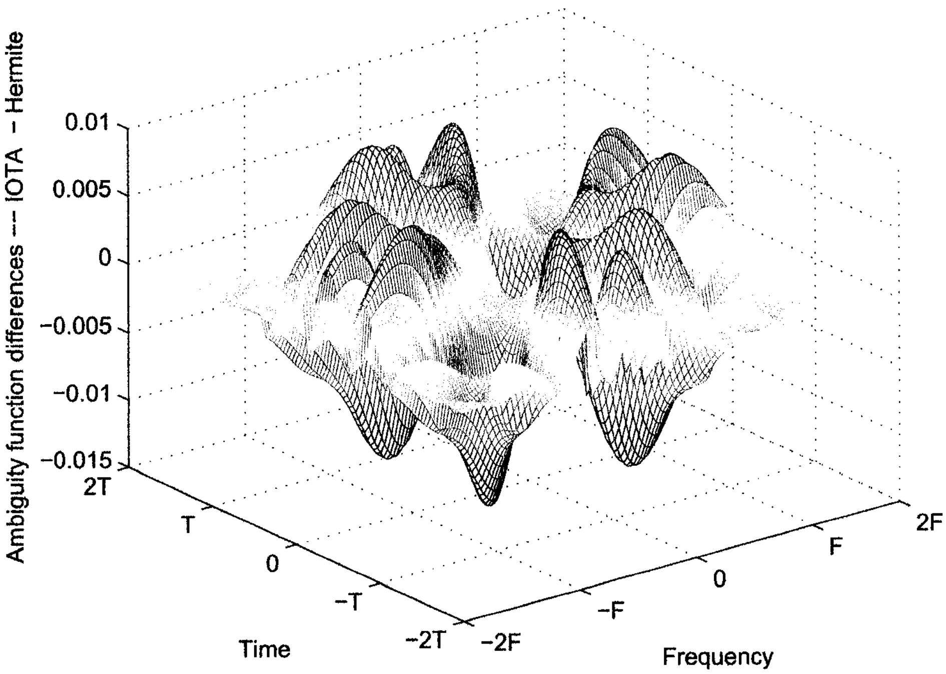

Figure 4.12: The difference between the ambiguity functions of Hermite and IOTA.

4.4 The Effect of Lattice Density

Up until this point, we investigated lattices with density of 0.5. However, Balian-Low theorem only dictates the localization condition for density, $\Delta < 1$. In this section, we investigate the localization of different pulse shapes in the region $\frac{1}{L} = \Delta \leq 1$. The various pulse shapes by orthonormalizing the Gaussian pulse for different lattice density values are given in Fig. 4.13.

The resulting densities are depicted in Fig. 4.14. As shown in Fig. 4.14, the localizations become worse as the density increases. On the other hand, the localization gain introduced by the Hermite functions becomes very significant. Hence for unit density, it does not make any sense to try to localize using only the Gaussian function. Also, it can be seen in the figure that going below half density lattice doesn't provide any additional localization advantage, since it is very close to the asymptote dictated by the Gaussian pulse around 0.0796.

In Fig. 4.15, the pulse shapes for IOTA and Hermite at unit density are compared. As can be seen in the figure, the localization of the Hermite based function is far superior. The Hermite coefficients employed to build the mother function to be orthonormalized are given in Table 4.2. The pulse shapes for Hermite functions are optimized for each lattice density and the resulting pulse shapes are plotted in Fig. 4.16.

Even though, for unit density the decrease in the pulse shape is not exponential, the decrease in the high amplitude areas are, making the introduced pulse shape an almost localized pulse which is from this point on, referred to as unit density axial-localized pulse (UDALOP). The importance of UDALOP is that, it can be employed with a unit density lattice and therefore 2D constellation diagrams can be employed. Hence, the localization advantage can be achieved without the limitations on the constellation shapes, increasing the overall capacity of the multi-carrier systems. Finally, in Fig. 4.17, the ambiguity

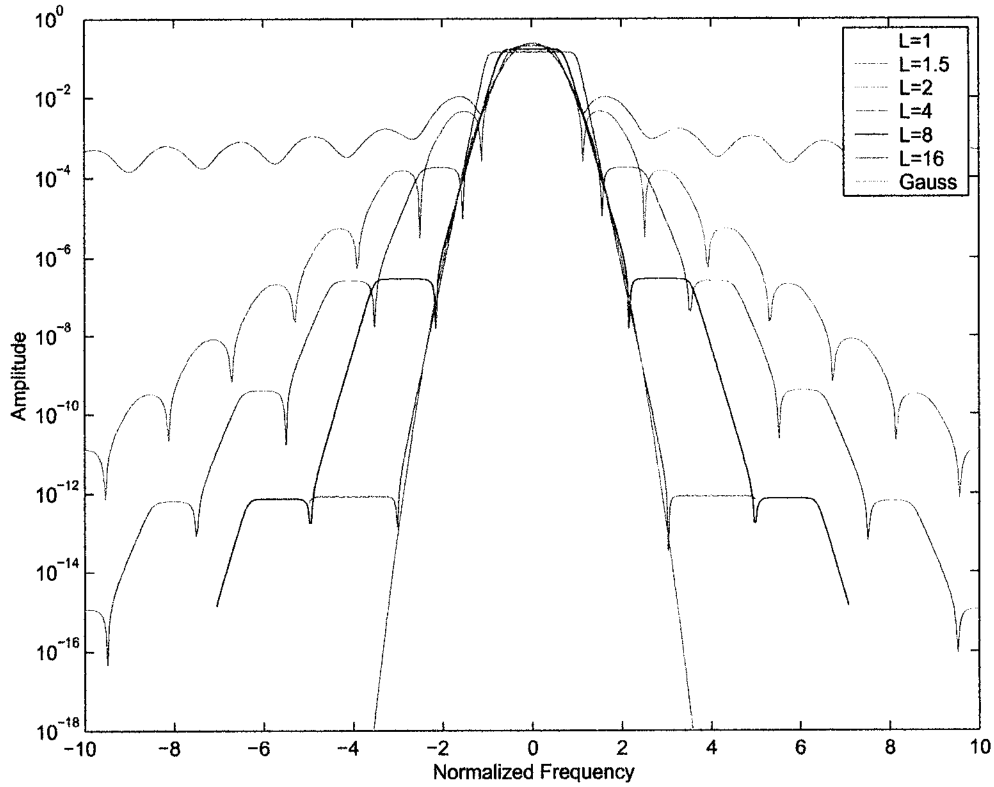

Figure 4.13: Comparison of pulse shape localizations for different lattice densities - Orthonormalized Gaussian pulse shapes.

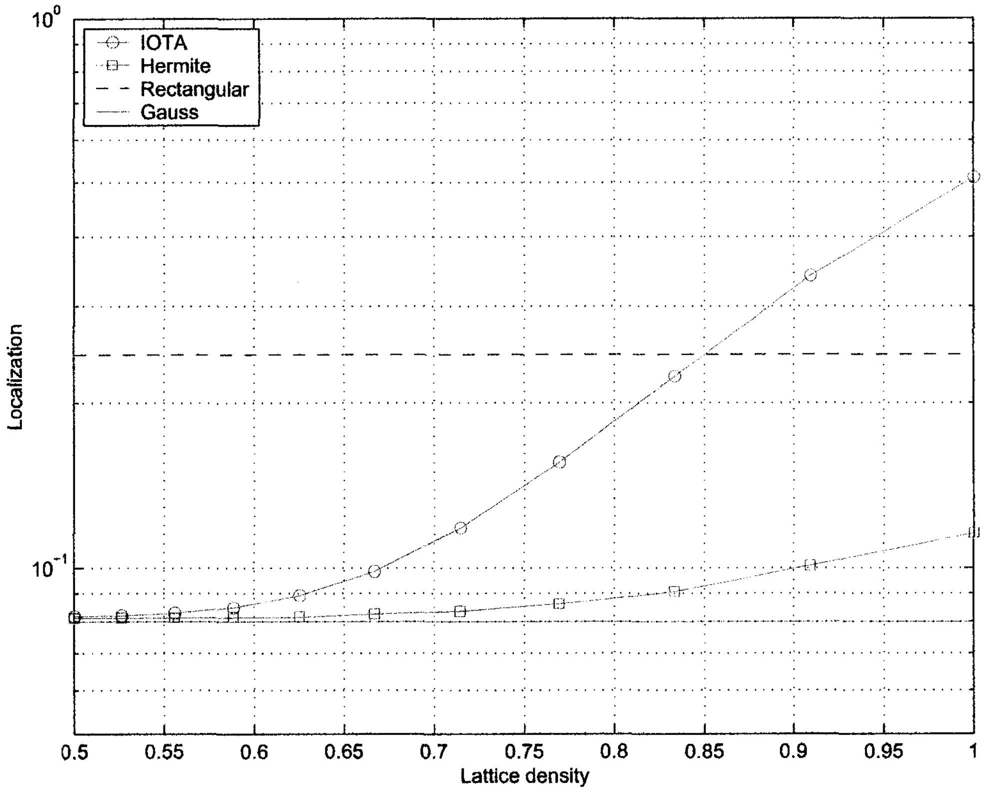

Figure 4.14: Comparison of pulse shape localizations for different lattice densities.

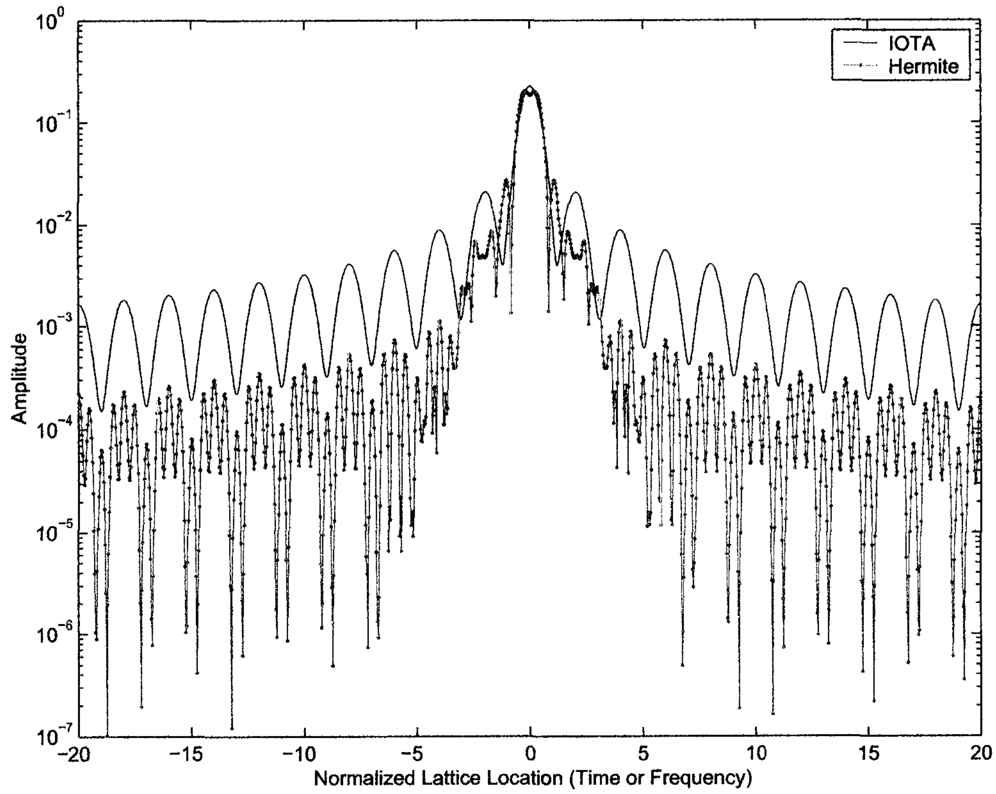

Figure 4.15: Comparison of pulse shapes at unit density: IOTA vs. Hermite.

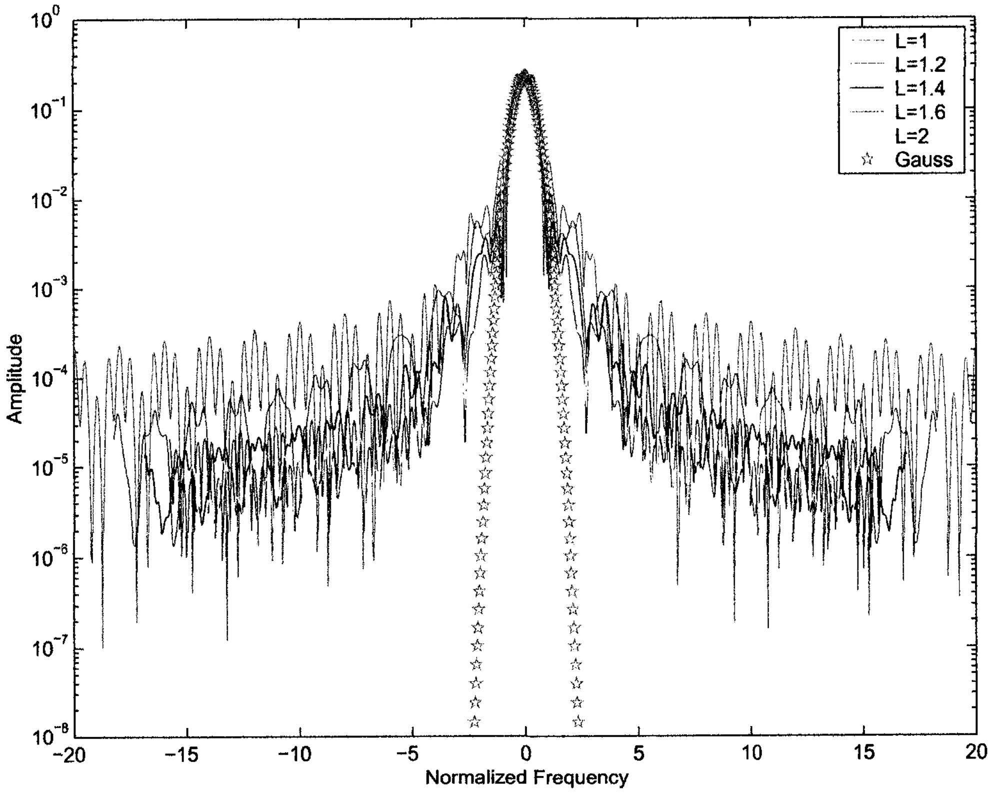

Figure 4.16: Orthonormalized Hermite pulse shapes for various densities.

Table 4.2: Normalized coefficients for Hermite functions at unit density.

Hermite Coefficient	Value
a_0	1
a_4	-0.2216
a_8	-0.0669
a_{12}	-0.0429
a_{16}	-0.0293
a_{20}	-0.0529
a_{24}	-0.0263
a_{28}	-0.0034

function for UDALOP is presented. In the following chapter, we investigate the effect of localization gains to the system performance.

4.5 Conclusions

In this chapter, we investigated possible pulse shapes to be used as mother functions to be orthonormalized. For our purposes, we found that Hermite functions forming Weyl-Heisenberg frames are the choice for mother functions.

We computed the optimum coefficients for combining Hermite functions in forming the mother function. This is accomplished with both 0.5 density lattices and unit density lattices.

We demonstrated that for 0.5 density lattices, the IOTA pulse shape is not optimal and a slightly better pulse shape can be achieved.

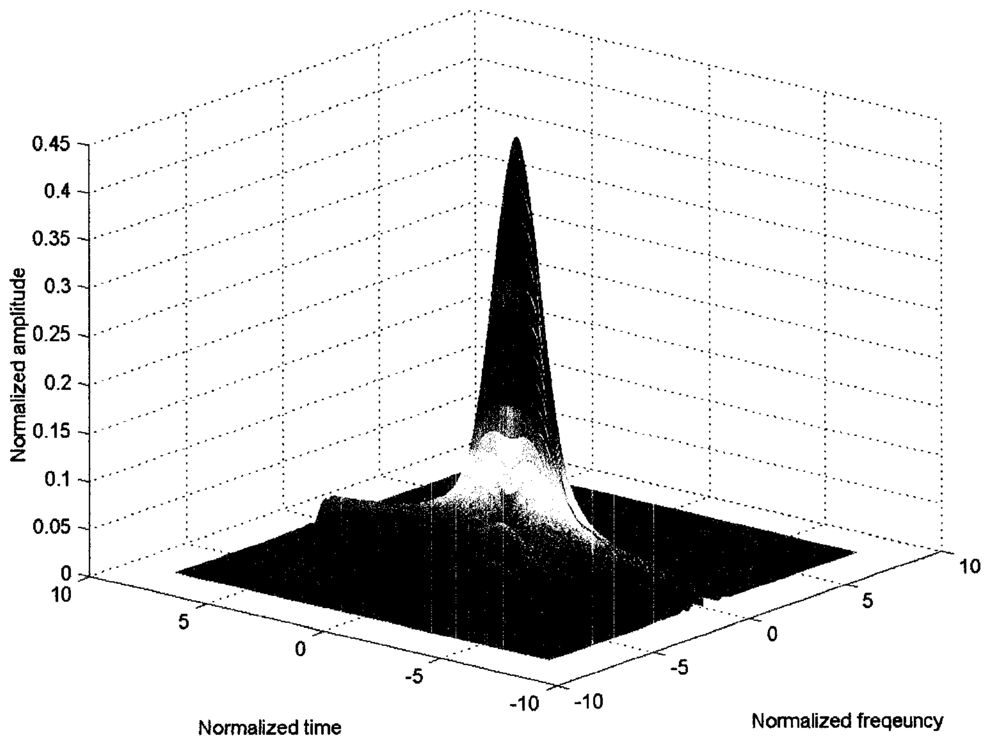

Figure 4.17: Ambiguity function for UDALOP.

For unit density, we showed that orthonormalization of the Gaussian pulse results in a pulse shape with very bad localization, whereas when different Hermite functions are combined a much better localization is achieved. The novel pulse shape is referred to as UDALOP. With the invention of UDALOP, we have provided a localized pulse shape for unit density. UDALOP is not localized in the sense of Balian-Low theorem, however it is localized for the values with high amplitude, therefore it can be considered localized for practical purposes.

Chapter 5

Applications of Hermite based Pulse Shapes in Wireless Communications

In this chapter, we investigate simulations of the results presented in the previous chapters in order to quantify the system performance. We start by investigating the effect of inter-carrier-interference. Then, we show the effect of the number of subcarrier to the inter-carrier-interference. We also give the effects of OFDM imperfections such as peak-to-average power ratio and phase jitter.

We investigate the inter-operability issues for systems that employ different pulse shapes in the transmitter and the receiver. We extend the results mentioned above for unit density lattices as well. We conclude the chapter by giving the effects of inter-symbol-interference.

5.1 Simulation Results

In this section, the simulation results of an OFDM system with different pulse shapes are presented. An OFDM system with 32 subbands and with a square lattice structure is considered. In our simulations, the OFDM system model presented in Chapter 2, is employed. Three different pulse shapes are considered. The first one is the well-known square pulse whose frequency response has the shape of a sinc function. The second one is the orthonormalized Gaussian function namely IOTA. The last one is the orthonormalized Hermite functions.

First we investigate the frequency spectrum of afore-mentioned OFDM system. In Fig. 5.1, the spectrum resulting from the employment of different pulse shapes are presented. As can be seen in the figure, both IOTA and Hermite pulse shaped OFDM give considerably less interference in the outband region and their powers are mostly concentrated on the desired frequency range.

5.1.1 The effect of Inter-carrier Interference for 32 subbands

Here, the effect of Doppler spread on system performance is investigated. One of the weakest points of the OFDM systems is that they are not robust against the frequency dispersion that appears due to high mobility. The reason behind this drawback is that for high speed users with high Doppler spread, the orthogonality between the subcarriers is lost, resulting in inter-channel interference (ICI). However by employing a pulse shape which rapidly decays in frequency, the amount of ICI can be reduced significantly.

In our simulation model, a Rayleigh fading channel is employed with a constant signal to noise ratio (SNR) of 5 dB. For the moment we neglect the effect of inter-symbol interference (ISI) by employing a cyclic prefix or any other means, and concentrate on

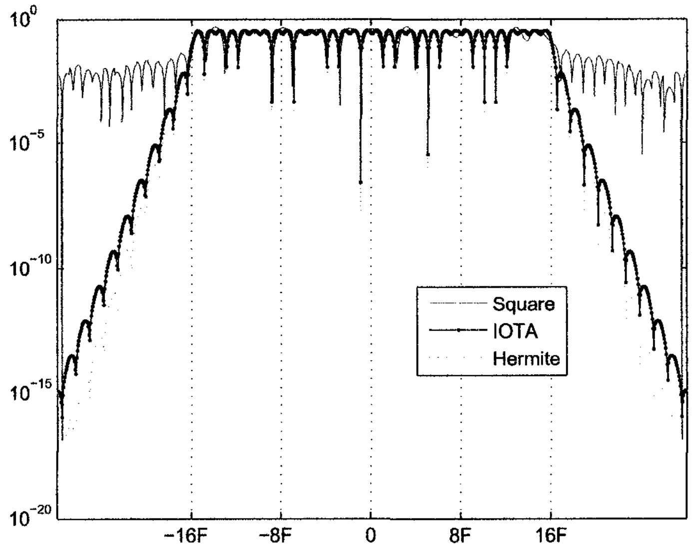

Figure 5.1: OFDM frequency spectrum employing IOTA signal, Hermite signal and square pulse.

ICI. In the simulations results represent independent run for 10^6 bits. We define the mobility as the product of Doppler frequency (f_D) and symbol time (T) as f_DT. Fig. 5.2 shows the effect of mobility on the performance of OFDM systems with different pulse shapes. As it is depicted in the figure, Hermite and IOTA based OFDM systems are much more robust against Doppler frequency shifts, the former being a little more robust than the latter.

Finally we look at the effect of the SNR. In this simulation we assume the product $f_DT = 0.0005$. As shown in Fig. 5.3, there exists a considerable performance gain by application of Hermite functions.

All of these results demonstrate that the robustness of the OFDM systems to the Doppler spread is increased when Hermite pulse shapes are introduced. The performance of the OFDM system with Hermite pulse shapes is slightly better than the OFDM systems employing IOTA pulse.

5.1.2 The Effect of Inter-carrier Interference for 128 subbands

In this section, we investigate the effect of the number of subcarriers on the system performance. As the number of subcarriers increases, the robustness of the system to dispersion decreases. The mobility effects are shown on the BER vs. normalized Doppler spread curves shown in Fig. 5.4. The results show that as the number of subcarriers increase, the system loses robustness against mobility. The same performance with the 32 subcarrier case could be achieved by a 3 dB increase in the SNR. This is an important factor for consideration in designing 4G systems, because the OFDM mode of operation in IEEE 802.16e standard has 256 subcarriers while OFDMA mode has 2048 subcarriers. In practice, 2048-OFDMA with mobility was unsuccessful due to this and applications of OFDMA mode consisted of 256-OFDMA proprietary systems and no IEEE standard

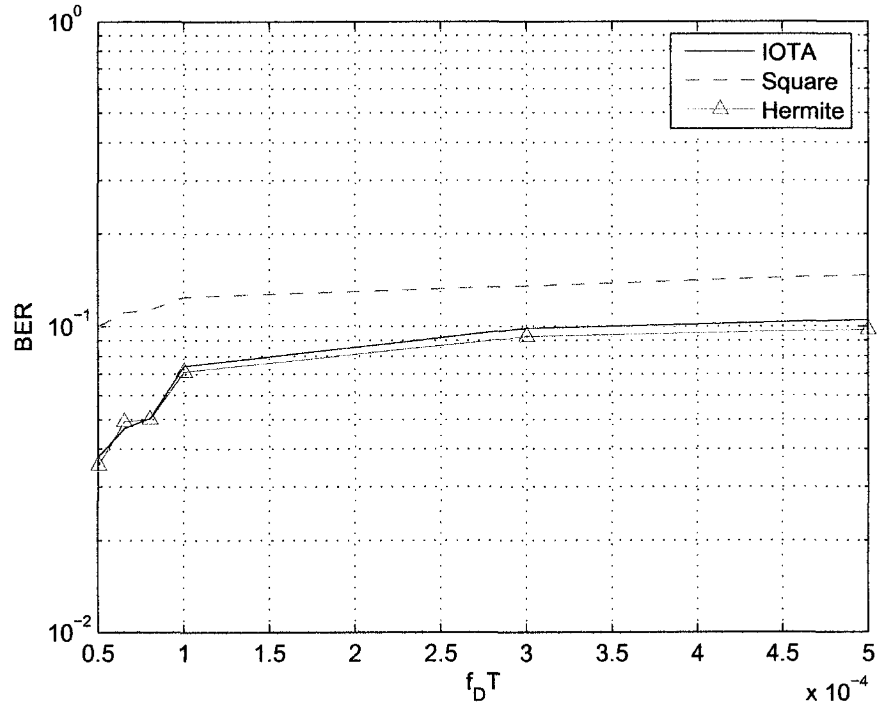

Figure 5.2: The effect of normalized Doppler spread on bit error rate (BER) for 32 subcarriers.

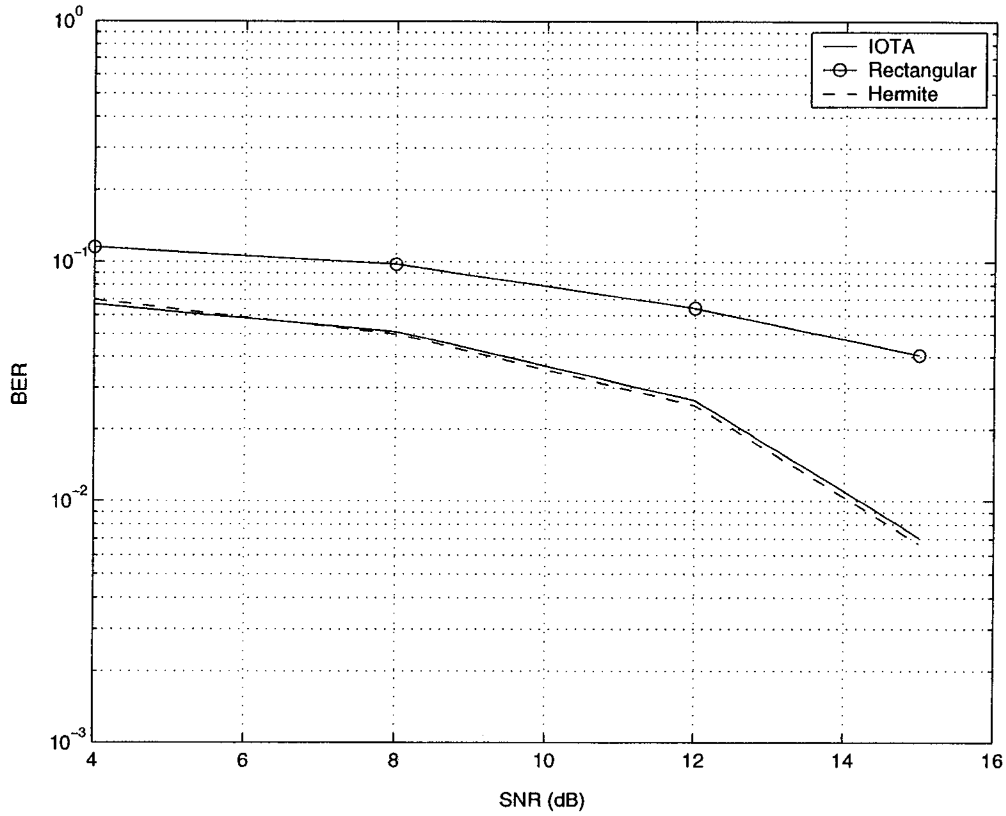

Figure 5.3: The effect of SNR on BER for 32 subcarriers ($f_D T = 0.0005$).

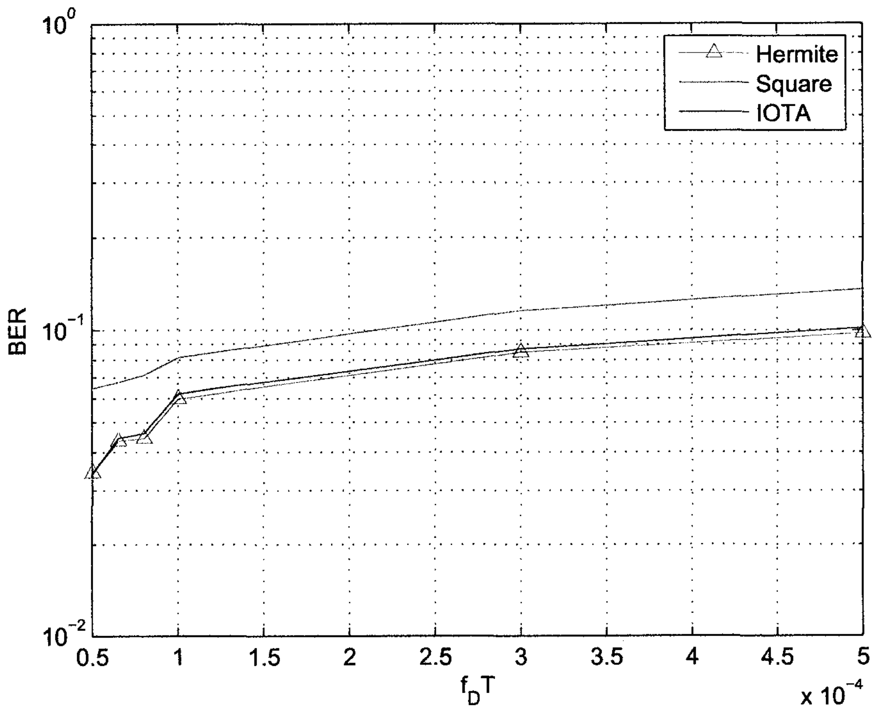

Figure 5.4: The effect of normalized Doppler spread on BER for 128 subcarriers for 8 dB SNR.

mobile OFDMA system found widespread application. Hence the introduction of pulse shaping is very critical in terms of success for 4G systems.

The effect of intersymbol interference is also investigated for the dissertation. However the effect of Doppler is more critical in terms of system performance.

5.2 Effects of OFDM based Imperfections

5.2.1 Peak to Average Power Ratio

One of the main problems in OFDM systems is the peak to average power ratio (PAPR) problem. In the system model after IFFT, the signal amplitude has a very high dynamic range. This causes problems in the amplifier design due to nonlinearities and imperfections in the amplifier. As a result, many different techniques have been proposed in order to combat PAPR problem [52–54].

The signal amplitudes that vary after the IFFT, are a function of the pulse shape as well. For a practical pulse shape, associated PAPR must be within acceptable limits. When the square pulse, which is the only constant amplitude pulse within the pulse interval, is replaced with another pulse, the PAPR increases. In other words, for pulse shape $\Psi(t)$, which is not a rectangular pulse, there exists a mean power level m which is the same as the mean power of the rectangular pulse shape $\Psi_R(t)$, if we assume that negligible amount of power is leaked outside the symbol interval. For $\Psi(t) \neq \Psi_R(t)$, there is a time t_1 such that $|\Psi(t_1)|^2 > m$, hence increasing the PAPR.

When Fig. 5.5 is investigated, we can see that the PAPR is increased by approximately 0.5 dB. This extra value must be taken into consideration in the system designs employing non-rectangular pulse shapes.

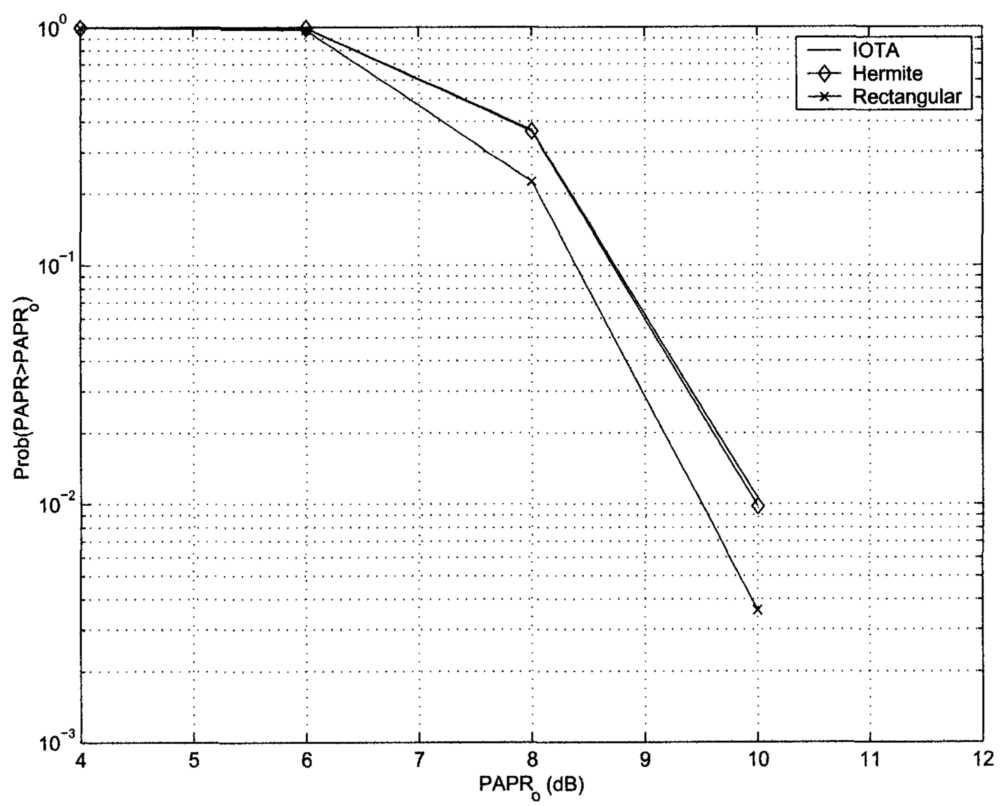

Figure 5.5: Probability of exceeding certain PAPR levels for different pulse shapes.

5.2.2 The Effect of Jitter

Another important problem in OFDM systems is the effect of phase jitter [55]. The phase jitter may result from the generation of sinusoidal signals in the system or by any other means. If there is a phase jitter in the system, which is usually the case to some extent in practical systems, the orthogonality of the carriers is affected. In [55], the effect is investigated for a rectangular pulse, where it is shown that the effect of jitter is independent from the jitter shape for multi-carrier systems. The degradation D_n is defined as loss in the SNR as dB:

$$D_n = 10 \log \left(1 + \frac{E_s \sigma_d^2}{E(|W_n(0)|^2)} \right), \tag{5.1}$$

where σ_d^2 is the jitter variance, E_s is the energy of the transmitted pulse and

$$W_n(0) = \frac{1}{N} \sum_{l=0}^{N-1} \exp(-j2\pi nl/N) \int_{-\infty}^{\infty} n(t) \Psi_n(t), \tag{5.2}$$

where n is the user index, N is the number of subcarriers, $n(t)$ is the AWGN, and $\Psi_n(t)$ is the pulse shape of the n^{th} user.

Since in (5.2), the normalized pulse shape is multiplied with the additive Gaussian noise, it does not change the result. As shown in Fig. 5.6, the distribution of the random variable $W_n(0)$ is independent of the pulse shape. Therefore the effect of jitter is independent of the pulse shape employed.

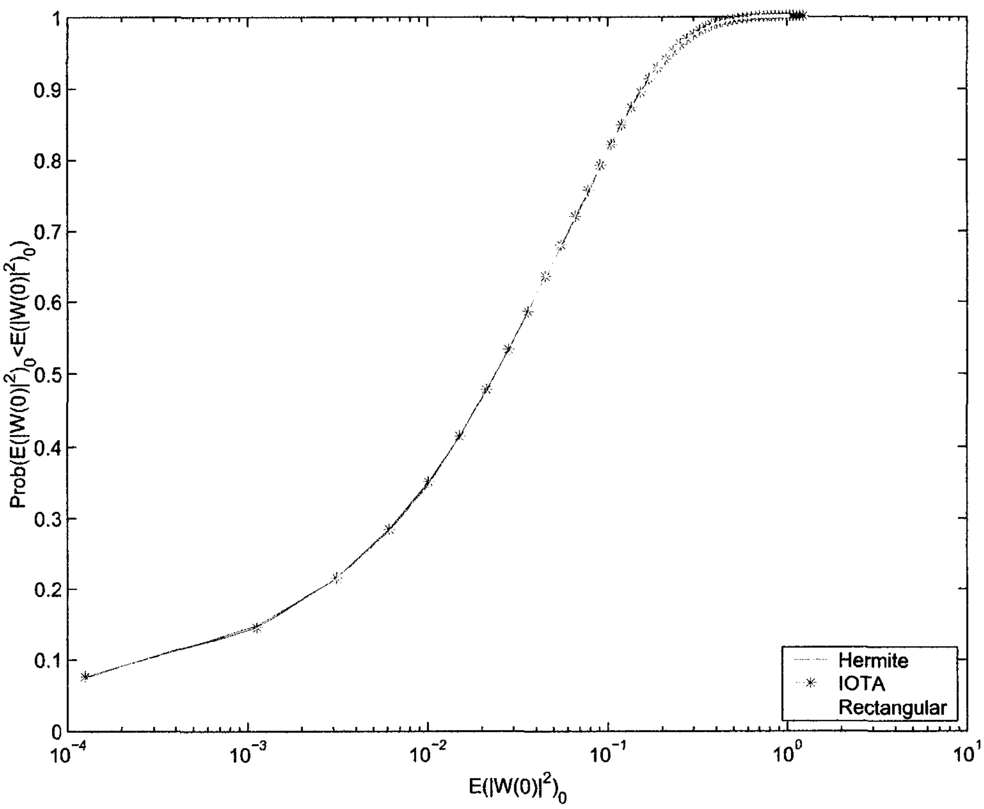

Figure 5.6: Cumulative distribution function of the colored noise as a result of pulse shaping.

5.3 Inter-operability Issues

It is very likely that future systems employing well-localized pulse shapes will have to work together with other various pulse shapes, in particular, rectangular pulses. In this section we investigate the performance of the system employing different pulse shapes at the transmitter and receiver.

In our system, we assume that the receiver has only the rectangular pulse shape defined in its hardware settings and there are three base stations employing a rectangular pulse, a Hermite pulse and a IOTA pulse respectively. The system model is depicted in Fig. 5.7.

We compare the performances of the three base stations under AWGN and fading channels. The results are given in Fig. 5.8 and Fig. 5.9 respectively.

When we compare the performances in the AWGN channel, as expected there is a performance loss. However, this performance loss occurs after $BER = 10^{-2}$, and for an uncoded performance, this is an acceptable degradation after error control coding for most of the practical applications. The performance loss is mainly due to unmatched filtering affecting the noise performance. However, in fading channel, the performance is still better for the IOTA and Hermite cases (even though degraded from the matched case) especially in high SNR levels, where the performance limiting factor is fading rather than noise.

This is a very important result, since it shows that the existing systems can be used together with new pulse shapes and performance gain can be achieved fully from the equipments that support the novel pulse shapes and partially from the ones that do not support.

One important issue is that the introduced pulse shapes do not introduce additional

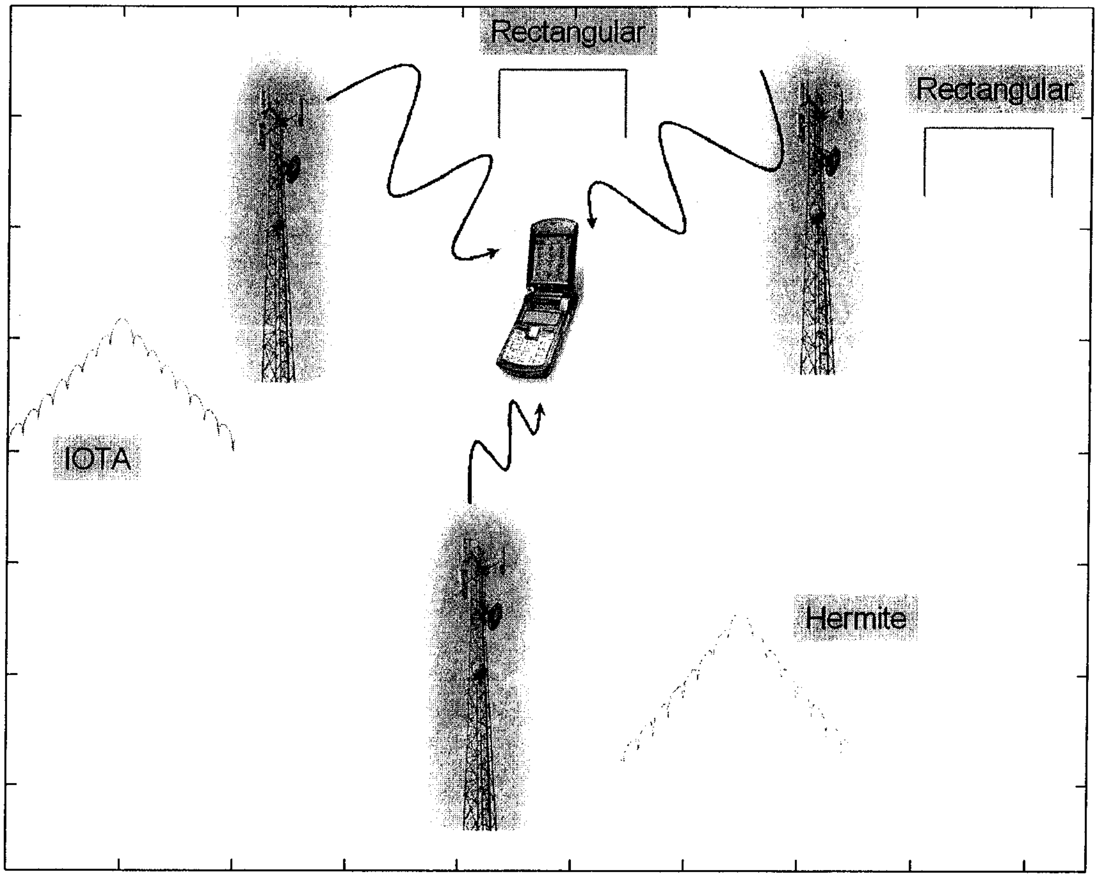

Figure 5.7: System model scenario for inter-operability.

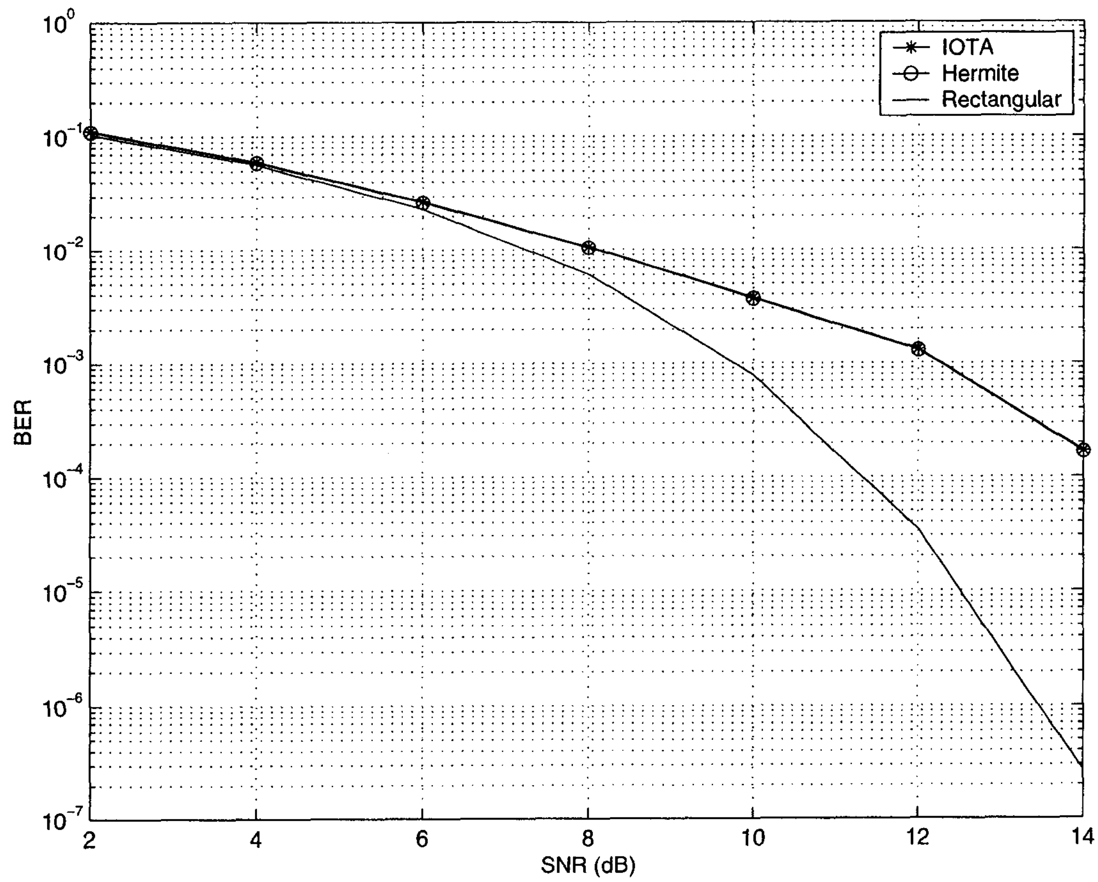

Figure 5.8: Performance comparison for Gaussian channel when the receiver uses rectangular pulse shapes whereas the transmitter employs Hermite, IOTA and rectangular pulse shapes.

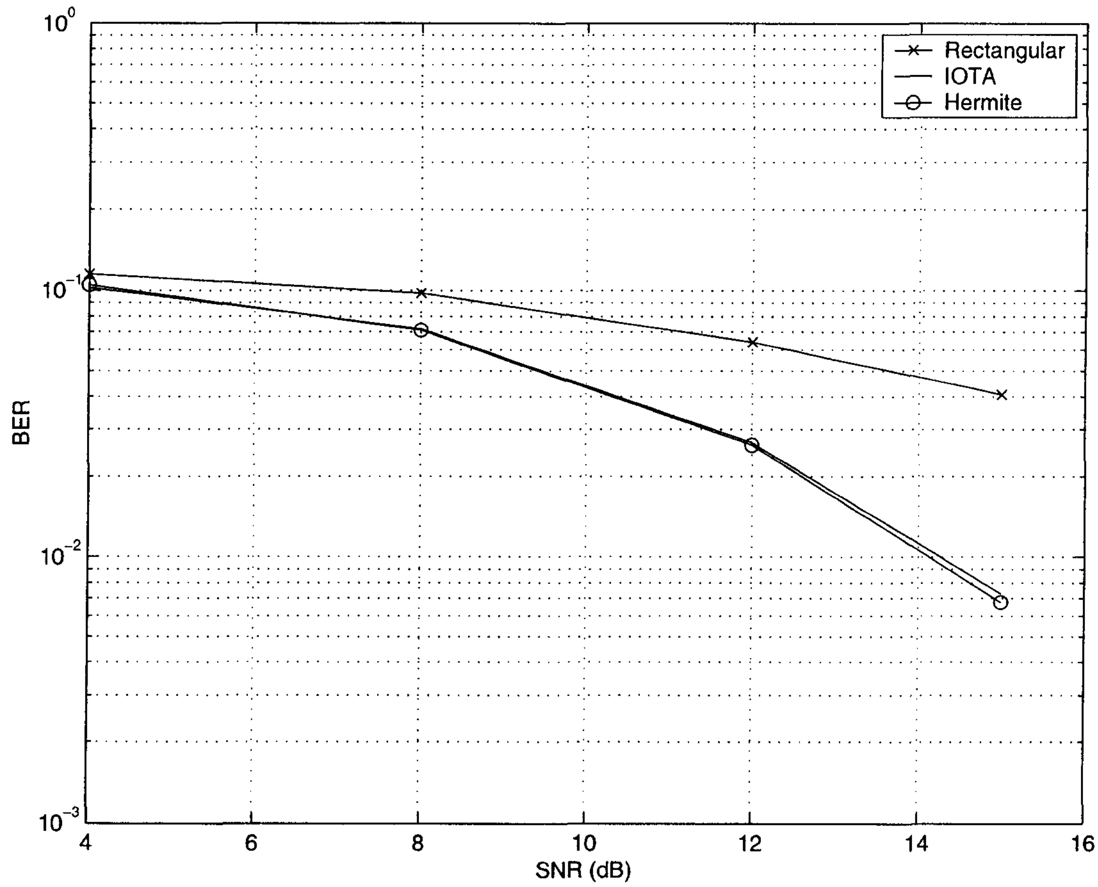

Figure 5.9: Performance comparison for fading channel with $f_D T = 0.0005$ when the receiver uses rectangular pulse shapes whereas the transmitter employs Hermite, IOTA and rectangular pulse shapes.

complexity to the system. The complexity is in the process of finding the pulse shapes. After finding the appropriate pulse shapes, they can be stored in the system.

5.4 Results for Unit Density

In the previous Chapter, we have shown that, it is possible to achieve localized pulse shapes for unit density lattices. In this section, we compare the performance of these pulse shapes against the rectangular pulse shape.

In Fig. 5.10, the results for various user velocities are depicted for SNR= 5 dB. It can be seen from the figures that better localization results in better BER performance. Also since unit density is employed 2D constellation can be used, therefore increasing the capacity. This is especially important for systems employing adaptive modulations.

Next in Figs. 5.11 and 5.12, the BER vs. SNR curves are depicted for $f_D T = 0.00005$ and $f_D T = 0.0005$ respectively. It is shown that the pulse shape UDALOP, which was proposed in the previous chapter, performs better than the classical rectangular pulse shape in various fading and noise environments.

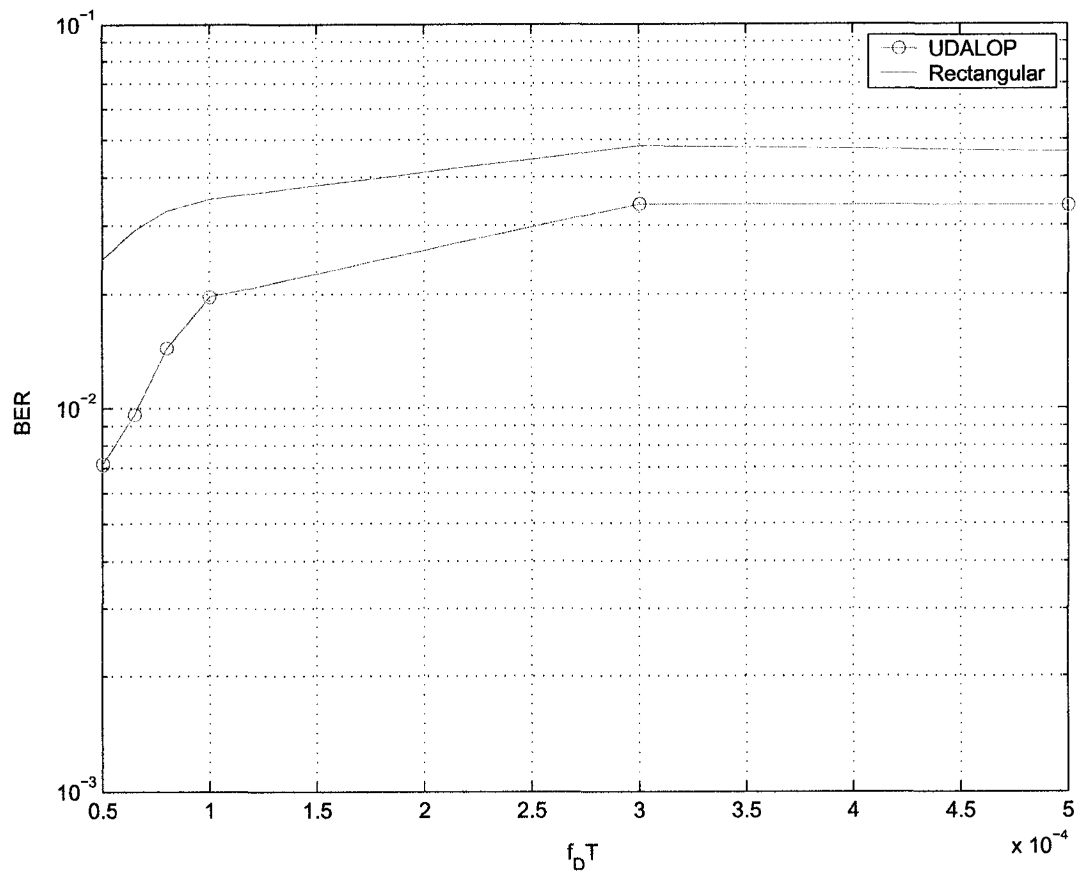

Figure 5.10: Performance comparison for fading channel with SNR= 5 dB for unit density lattice.

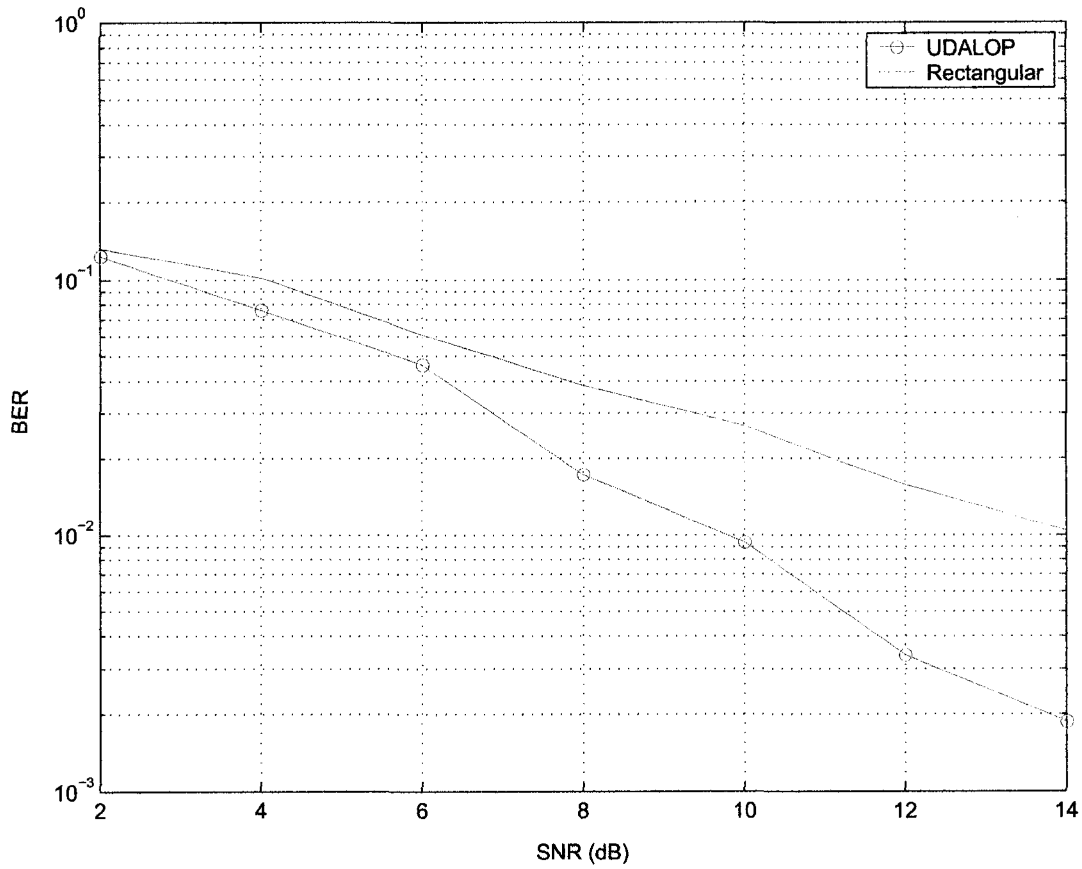

Figure 5.11: Performance comparison for fading channel with $f_D T = 0.00005$ for unit density lattice.

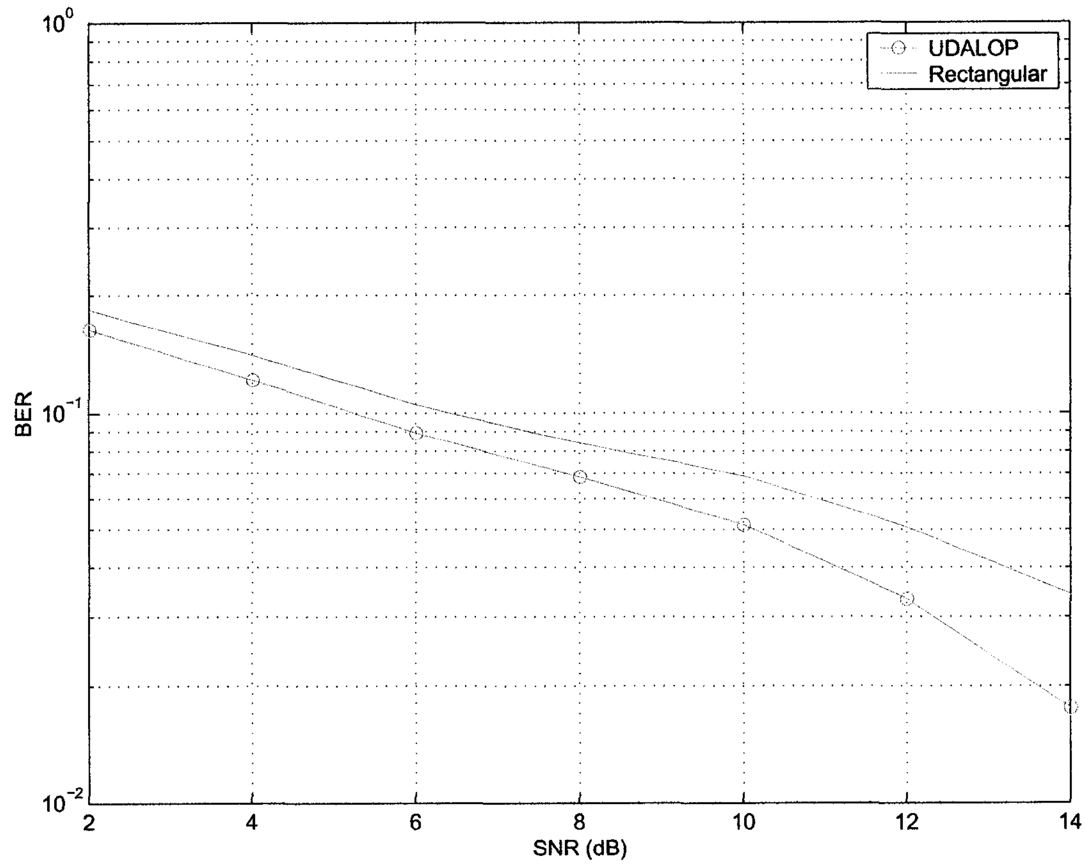

Figure 5.12: Performance comparison for fading channel with $f_D T = 0.0005$ for unit density lattice.

5.5 Effect of Inter-symbol Interference

Even though the rectangular pulse has bad frequency localization, it has a fairly good time localization. So, in order to make a fair comparison, next we test the performance of the pulse shapes under a time-frequency dispersive channel. We set the frequency dispersion $f_D T = 0.0005$, and SNR= 6 dB and vary the delay spread of the channel. The channel is modeled as an exponentially decaying channel.

The delay spread σ_τ^2 is defined as:

$$\sigma_\tau^2 = \bar{\tau^2} - \bar{\tau}^2, \tag{5.3}$$

where

$$\bar{\tau^n} = \frac{\int_{-\infty}^{\infty} \tau^n S_H(\tau)}{\int_{-\infty}^{\infty} S_H(\tau)}, \tag{5.4}$$

$S_H(\tau)$ is the delay spectrum.

We first analyze the performance for $L = 2$. 32 subcarriers are employed in a symbol time of $2.8\mu s$. In order to present the effect more clearly, the cyclic prefix has been eliminated from the channel. The results are depicted in Fig. 5.13. As shown in the figure, time dispersion closes the performance gap between the pulse shapes, the frequency dispersion is still the determining factor for the performance and Hermite pulse shape outperforms the rectangular pulse shape.

Next we investigate the performance for unit lattice density. The results are depicted in Fig. 5.14. The results are similar to the half lattice density case. The performance of UDALOP is still better than the rectangular based pulse shape.

The delay spread in wireless channels are typically in the order of $100ns$ to $10\mu s$ [56,57]. Therefore the results contain the worst case scenarios as well. As it can be seen in the results, even though the rectangular pulse is more robust to time dispersion, the

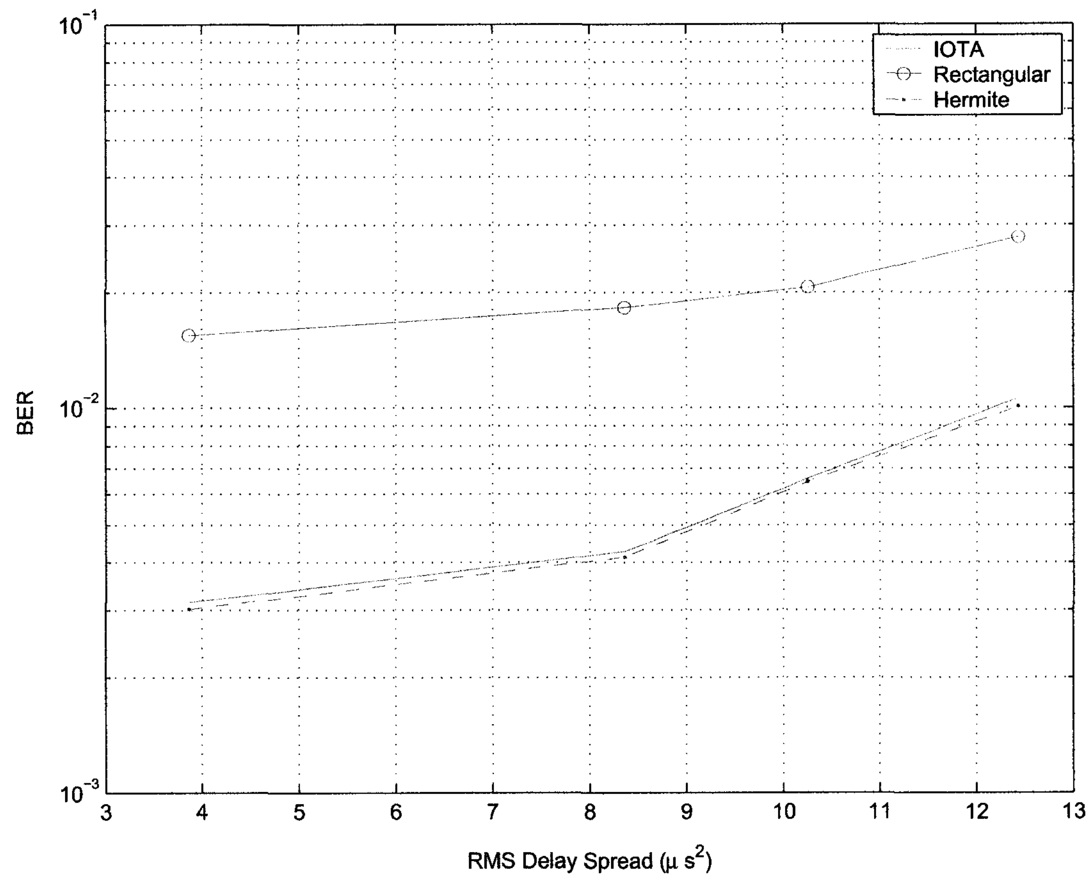

Figure 5.13: Performance of pulse shapes under inter-symbol interference for half density lattice, $f_D T = 0.0005$, and SNR= 6dB.

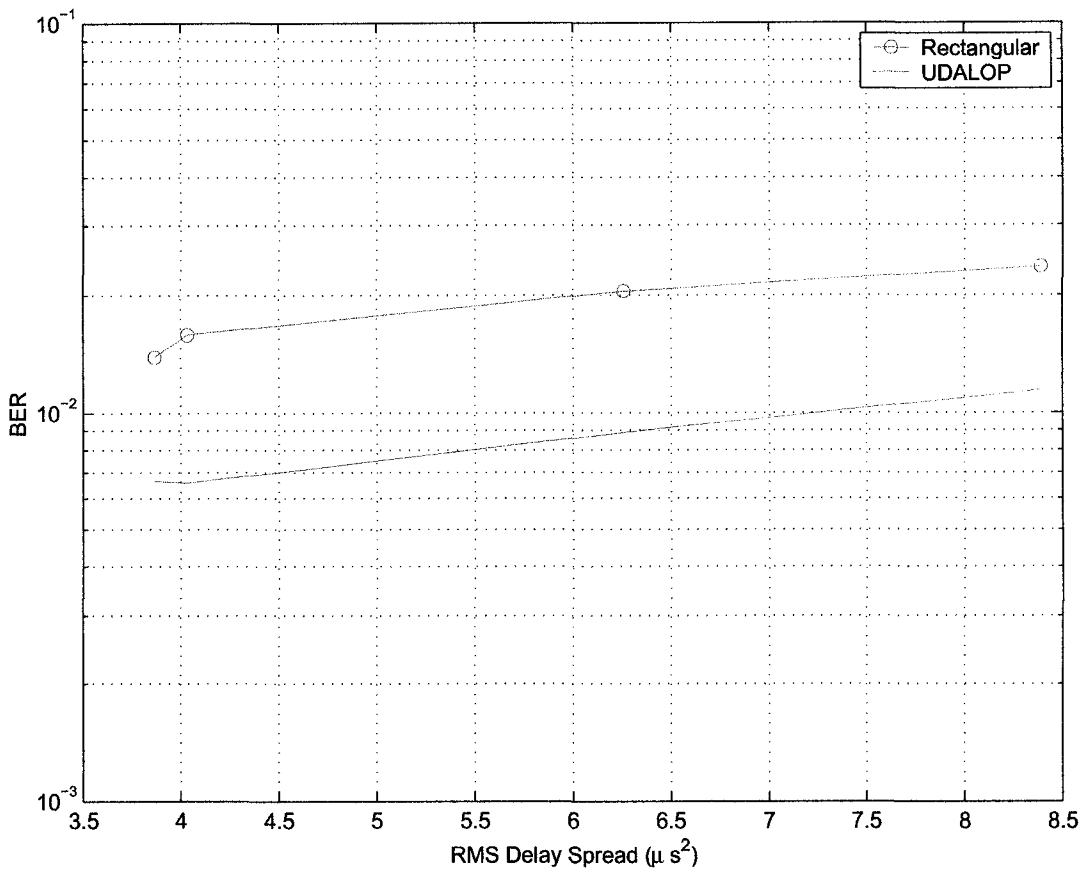

Figure 5.14: Performance of pulse shapes under inter-symbol interference for unit density lattice, $f_D T = 0.0005$, and SNR= 6dB.

performance difference compensates the difference. So regardless of time dispersion level, the localized pulses perform better than the square pulse.

5.6 Conclusions

In this chapter, we have presented various simulation results supporting the theoretical studies accomplished in previous chapters.

In particular, we have investigated the effect of ICI and number of subbands for 0.5 and unit density lattices. Results show that, for 0.5 density cases, the performance of Hermite based pulse shapes are slightly better than IOTA and much better than rectangular pulse. For UDALOP, in the unit density case, the results are much better than rectangular and IOTA.

It is shown that rectangular pulse shape is the optimum pulse shape for PAPR levels in OFDM. However, the performance reduction is at acceptable levels for most practical applications.

When there is also ISI in the system, rectangular pulse provides quite good performance. However, simulation results show that it is not sufficient to compensate for the performance loss due to possible ICI or inter-subchannel interference (ISCI).

Finally, we have presented an inter-operability analysis for the pulse shapes that are presented. Our analysis shows that even if rectangular pulse shapes are employed at one end of the communication system and Hermite pulse shapes are used in the other end, performance is still better than having rectangular pulse shapes at both ends. This is a very important result in terms of the practical applicability of the Hermite based pulse shapes.

Further system level simulation results are presented in the next chapter.

Chapter 6

A System Level Evaluation of Pulse Shapes for WiMAX

In this chapter, a system level evaluation of the effect of pulse shaping on WiMAX systems is presented. WiMAX is an industry collaboration for interoperability of devices using IEEE 802.16 standards. WiMAX systems employing OFDM are main competitors to high-speed downlink packet access (HSDPA) systems in terms of mobile broadband applications. HSDPA is the extension of 3G systems for higher rate data communications.

However, due to the frequency dispersion effects, WiMAX systems lose performance when the users are traveling at high velocities. In this chapter, we provide various comparisons of the high-speed broadband systems including the effect of pulse shaping with Hermite functions, which is proposed in Chapter 4 of this dissertation.

In this chapter, we start by giving overview of the standards related to high speed data transmission. Then, we provide the system. The simulations are accomplished by using TEMS Planet software [58]. An overview of the signal strength estimation methodology is given. The adaptive modulation architecture is presented. The simulation results showing the system level effects of multiple access scheme changes, smart antennae, carrier frequency are given. Finally, we present the effect of Doppler spread and the results of utilization of Hermite based pulse shapes.

6.1 Introduction

The broadband wireless access (BWA) area is currently one of the fastest-growing areas in wireless network access. It includes technologies that aim at providing wireless access to data networks with high data rates. BWA started as an alternative to digital subscriber lines (DSL) in urban areas or as a competitor to DSL technologies in rural areas. It has also been proposed as a backhaul application for WiFi networks.

The first BWA standard (IEEE 802.16 in April 2002) covered operations in line-of-sight environments ranging from 10 to 66 GHz. The 802.16-2004 (January 2003) standard that covered only fixed wireless systems was introduced for operations in non-line-of-sight (NLOS) environments between 2 and 11 GHz with a variable channel size. The standard includes two OFDM-based physical layers, namely orthogonal frequency division multiplexing (OFDM) and orthogonal frequency division multiple access (OFDMA). The IEEE 802.16-2004 standard was introduced in November 2004 [30] and replaced all other drafts. The IEEE 802.16-2004 standard introduced the concept of adaptive modulation. Most BWA systems follow the IEEE 802.16 standards as well as ETSI HiperMAN [29]. In most applications of both standards, orthogonal frequency division multiplexing (OFDM) is used. In late 2005, the standard was extended to cover mobile systems with the IEEE 802.16-2005 [32]. Also, a joint industry initiative to standardize products using IEEE 802.16 and HiperMAN standards, namely WiMAX, was initiated in order to support technology penetration [31].

OFDM is a candidate for future wireless broadband communications because of the way it effectively handles channels with large delay spreads [1]. OFDM divides the frequency selective wideband channel into multiple-frequency, flat fading, narrowband channels. In the time domain, this leads to a larger symbol period, which is accompanied by a cyclic prefix (CP) to handle the inter-symbol interference (ISI). One main advantage of OFDM-based systems, when compared with the CDMA based systems; the OFDM based systems are more robust to non-line of sight conditions. This is due to the multiple flat fading frequency structure of OFDM.

HSDPA was introduced in Release 5 of the third generation partnership project (3GPP) standards, whose aim is to standardize the 3G wireless communication architectures. With peak data rates of up to 10.8 Mbps [59, 60], the standard improves the throughput by four to five times during an average downlink packet session when compared with the downlink shared channel (DSCH) standards detailed in Release 99 of the 3GPP standard. High-speed uplink packet access (HSUPA) is part of Release 7 of the 3GPP standards while OFDM is a work item of Release 7 of the 3GPP standard. A new high speed-downlink shared channel (HS-DSCH) transport channel was introduced in Release 5 [61]. HS-DSCH has a spreading factor of 16 and supports adaptive modulation and coding (AMC) with QPSK/16QAM modulations. The transmission time interval (TTI) or interleaving period has been defined as 2 ms (3 slots) to achieve a short round-trip delay for the operation between the terminal and the base station (Node B) for retransmissions. The HS-DSCH 2-ms TTI is short compared with the 10, 20, 40 or 80-ms TTI sizes supported in Release 99 [60]. Adding a higher order modulation scheme, 16 QAM, as well as a lower coding redundancy increased the instantaneous peak data rate. The maximum number of codes that can be allocated is 15, but depending on the terminal capability, individual terminals may receive a maximum of 5, 10 or 15 codes.

HS-DSCH does not use fast power control. Data rates change along with changing radio conditions and the available transmission power in the Node B. The power assigned to HS-DSCH is the power that remains after serving common and dedicated channels [62]. Capacity increases with HSDPA by two to three times when compared with the DCH systems. This can be attributed to the inclusion of link adaptation, the use of the maximum cell power, and the scheduling and use of 16 QAM.

In terms of performance analysis, it is a challenging task to compare the performances of OFDM-based WiMAX and CDMA-based HSDPA systems. It is important that this comparison be done in various scenarios where both technologies are candidates in data communication solutions. The comparison extends to multiple layers of the system. In this chapter, however, a system level performance comparison of the CDMA and OFDM systems using the parameter settings of HSDPA and WiMAX respectively is undertaken. A more general performance comparison of OFDM and CDMA technologies were made in [63–65], but did not address specific WiMAX configurations.

Many performance-enhancing features are considered with the deployment of these technologies as well. One typical example is the application of smart antennae. Smart antennae enhance the capacity and quality of communication systems by reducing the total interference [66]. The cost of deploying smart antennae versus the performance improvement must be carefully studied. In this work, we also compare the performance enhancements of WiMAX and HSDPA systems with the introduction of smart antennae. In order to recreate a realistic scenario, the network planning and optimization tool TEMS Planet was used. This software was developed by Ericsson TEMS.

6.2 System Model

For our investigation, Vienna, Austria is selected as the simulation area. Dense urban as well as sub-urban areas around Vienna are included in the analysis. Vienna is selected due to this heterogeneous structure of urban and rural areas. The total area under investigation is 53 square kilometers. From the possible IEEE802.16 system profiles, OFDM is used unless stated otherwise. The parameters used in the simulations are summarized in Table 6.1. The different system level features (OFDMA, smart antennae) are included in order to show that the gains that can be achieved by features other than pulse shaping will still exist after the pulse shaping is employed.

The area of investigation is given in Fig. 6.1 and the dense urban area within that area is depicted in Fig. 6.2.

We will first compare these two technologies under rectangular pulse shaping using various combinations. Then, we utilize Hermite pulse shapes and present the improvements in the system performance result. This way, we compare the improvements with respect to pulse shape with other improvements in the system such as smart antennae and multiple access techniques.

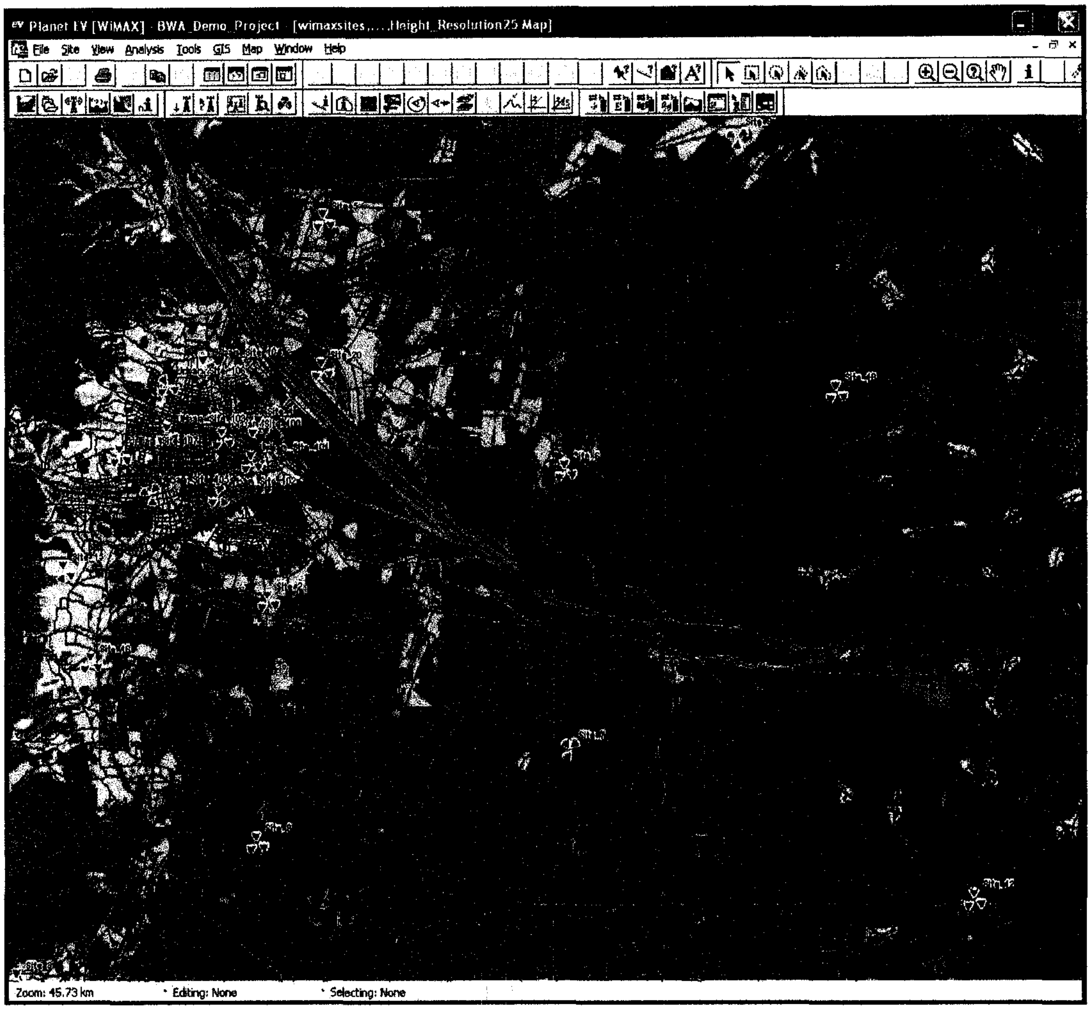

Figure 6.1: The area of simulation for system level tests throughout Vienna (TEMS Planet).

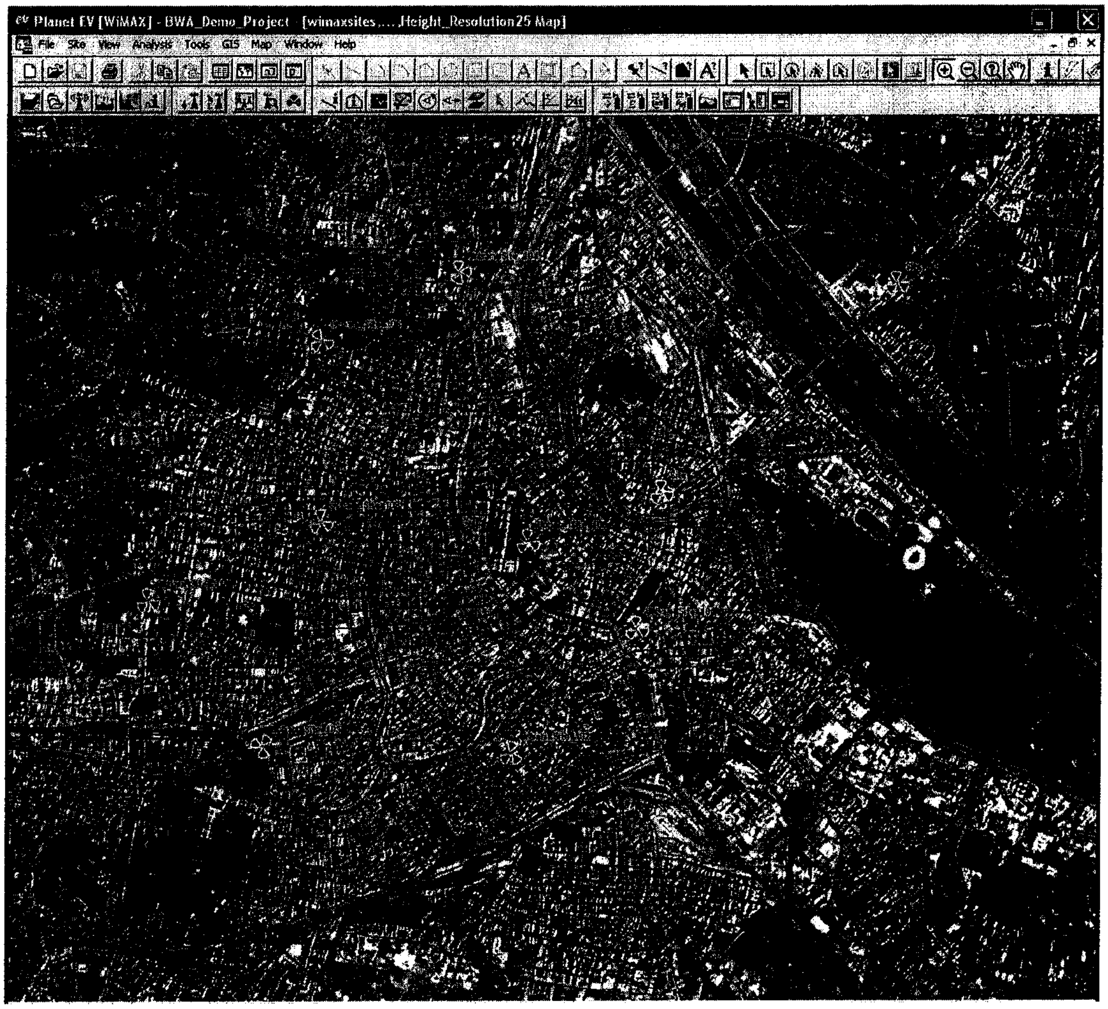

Figure 6.2: The dense urban area of simulation for system level tests throughout Vienna (TEMS Planet).

Table 6.1: Simulation Settings.

	WiMAX	HSDPA
Number of BSs	25	25
Number of Sectors/BS	75	75
Carrier Frequencies	2.1 GHz, 2.5 GHz, 3.5 GHz	2.1 GHz
EIRP	53 dBm	53 dBm
Antenna Gain	15 dBi	15 dBi
Electrical Tilt Range	0-6^o	0-6^o
Antenna Beamwidth (-3 dB)	60^o	60^o
Diversity	RX,TX	RX,TX
Smart Antenna	Phased Array	Phased Array
Channels	3 x 5MHz	3 x 5MHz
Frequency Reuse	1/3	1/3
CP Duration	1/32	NA
Antenna Noise Temperature	290 K	290 K
Cable Loss	2 dB	2 dB
Filter Loss	1 dB	1 dB
Front-end Amplifier Noise Figure	5 dB	5 dB
Measured Noise Density	-196.72 dBW/Hz	-196.72 dBW/Hz
Subchannelization Allowed	1/16,1/8,1/4,1/2	NA
Number of subchannels	16	NA
Number of Subcarriers/Subchannel	16	NA
Number of Subcarriers	256	NA
Maximum Phase Jitter Interference	0.5 dB	NA
Number of HSDPA codes	NA	15
Available Modulations	QPSK, 16QAM,64QAM	QPSK,16QAM
Mobile Speed Range	3-120 km/h	3-120 km/h

6.2.1 CRC-Predict

For the signal strength predictions, we used the analytic propagation model CRC-Predict 4.0, which was originally developed at the Canadian Communication Research Center (CRC) [67], and later improved upon by Ericsson TEMS.

Some traditional approaches to radio-wave propagation are empirical in nature and begin with the collection of real-world measurements. These measurements are then fitted to curves and applied to similar geographic areas. The limitation of these approaches is that they do not take into account the infinite variety of landscapes that can occur. In contrast, CRC-Predict is a deterministic model based on physical optics, a form of wave theory. Predictions are based on a detailed simulation of diffraction over terrain (including clutter), and include an estimate of local clutter attenuation.

As a result, predictions of coverage gaps and interference areas are based specifically on the particular terrain in question and are more likely to be accurate, given that the terrain and clutter data are accurate.

6.2.2 Adaptive Modulation

Modulations used in both WiMAX and HSDPA systems are adaptive in the sense that they change according to channel conditions. However, the available modulation types, the requirements and their related throughputs are different for HSDPA and WiMAX.

The available modulations and their corresponding requirements for WiMAX and HSDPA are summarized in Table 6.2. From the tables, it can be seen that WiMAX is approximately 12% more bandwidth efficient in terms of bits/sec/Hz. In the simulations, we used the throughput levels and coverage thresholds listed in the tables.

Table 6.2: Adaptive Modulation Settings.

5 MHz WiMAX			
Modulation	Required C/I	Required Power	Throughput
QPSK-1/2	9.4 dB	-86.3 dBm	4 Mbps
QPSK-3/4	11.2 dB	-82.5 dBm	6 Mbps
16QAM-1/2	16.4 dB	-78.3 dBm	8 Mbps
16QAM-3/4	18.2 dB	-76.1 dBm	12 Mbps
64QAM-1/2	22.7 dB	-71.6 dBm	16.3 Mbps
64QAM-3/4	24.4 dB	-69.9 dBm	18.4 Mbps
5 MHz HSDPA			
Modulation	Required Es/Nt	Throughput per code	Throughput for 15 codes
QPSK-1/4	-3 dB	119 Kbps	1.785 Mbps
QPSK-1/2	0 dB	237 Kbps	3.555 Mbps
QPSK-3/4	4 dB	356 Kbps	5.340 Mbps
16QAM-1/2	6 dB	477 Kbps	7.115 Mbps
16QAM-3/4	12 dB	712 Kbps	10.68 Mbps

6.3 Simulation Results

In the simulations, we examined an HSDPA system at 2.1 GHz and compared it with WiMAX systems in three different scenarios: 2.1 GHz, 2.5 GHz and 3.5 GHz. Frequency bands located at 2.5 GHz and at 3.5 GHz are typical WiMAX scenarios, and 2.1 GHz is included in order to compare the technologies in the same frequency band. For the sake of comparison, the gross physical layer throughput levels are calculated at each location on the map. Results are displayed in Fig. 6.3 - Fig. 6.6 and summarized in Table 6.3. In this work, we have considered that all the traffic allocated in the HSDPA network is data traffic and that there is a 100% power allocation to HSDPA. However, it is important to note that in a typical scenario, HSDPA is used with a release 99 (R99) carrier for voice data as well. This reduces the power available for data transmission, hence the total throughput available for HSDPA. In addition, in a WiMAX system, it is possible to include voice over IP (VoIP), or build the system with a voice network overlay. However, for the sake of fairness, we assumed an all data network where the voice is either non-existent or converted to VoIP.

The simulation results depicted through Fig. 6.3 - Fig. 6.6 show that when WiMAX is deployed around 3.5 GHz a severe coverage disadvantage results when compared with the 2.1 GHz HSDPA system. This is mainly due to the increased propagation loss that results at a higher frequency. There are two different solutions to this problem. The first approach is to apply subchannelization in the downlink direction and increase coverage. With both OFDM and OFDMA, this increases the coverage although the extended areas have low throughput levels. In the case of OFDM, this leads to reduced utilization as well because in OFDMA, the subchannels of the same time slot can be shared by different users. The second approach is to add more sites. Our analysis shows that 4 (15%) more sites are needed in a 3.5 GHz OFDM system in order to compensate for the extra path loss.

It can be shown that both approaches could compensate for the excess path loss but with different costs. Due to increased spectral efficiency, NLOS advantages, and the inclusion of 64 QAM constellations, the average throughput levels of the OFDM and OFDMA systems are higher when coverage was satisfied.

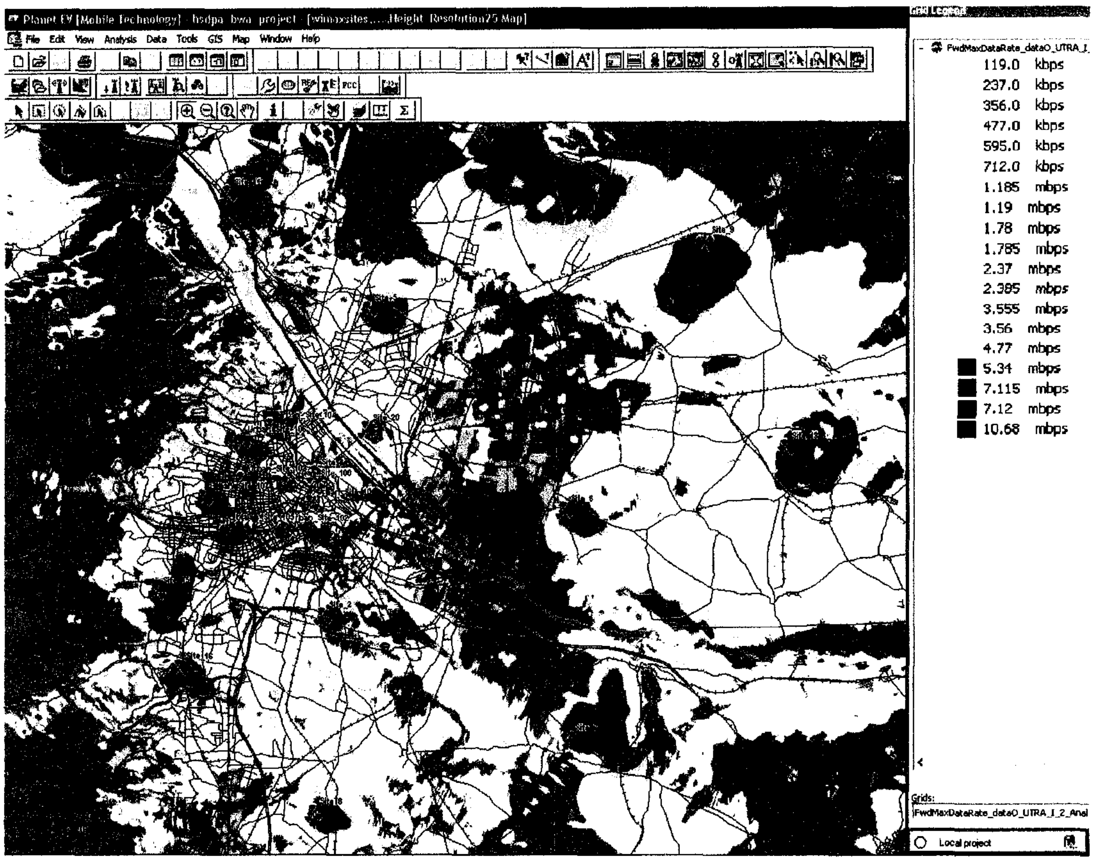

Figure 6.3: Distribution of Throughput Levels (in kbps) around Vienna for HSDPA with carrier frequencies in the range of 2.1 GHz.

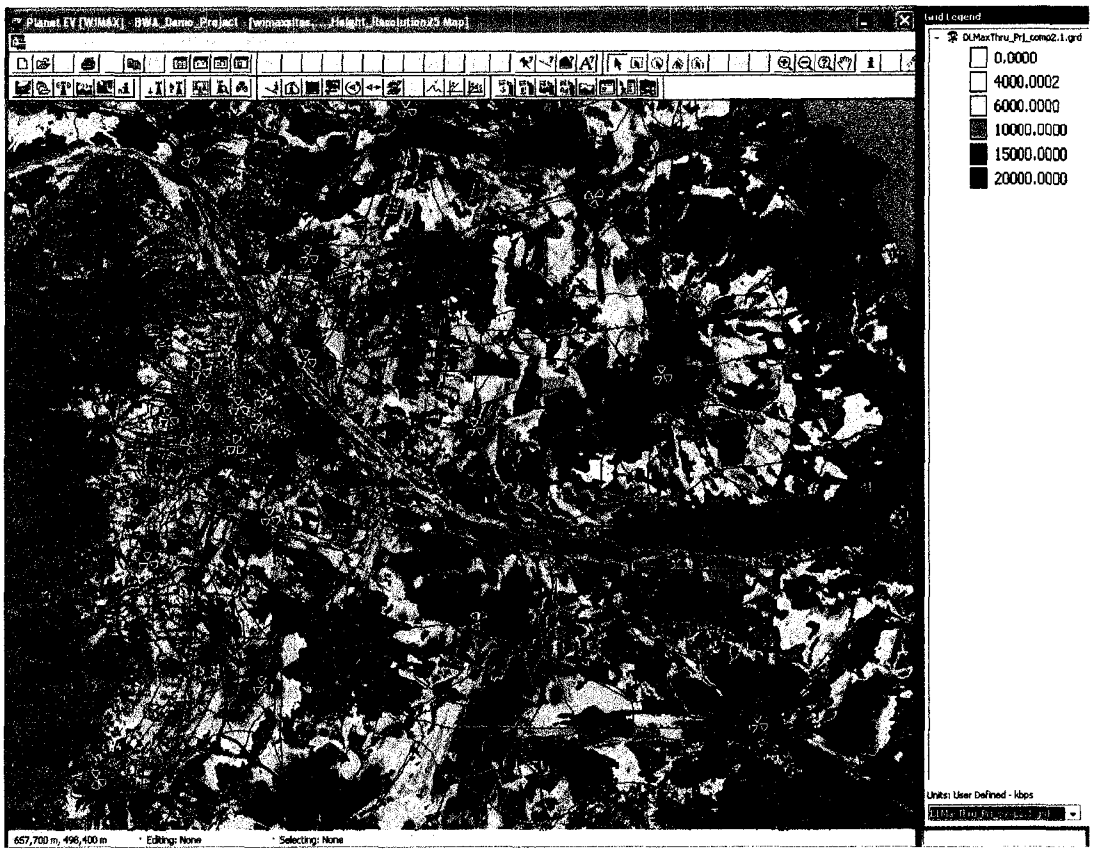

Figure 6.4: Distribution of Throughput Levels (in kbps) around Vienna for WiMAX with carrier frequencies in the range of 2.1 GHz using OFDM mode of IEEE 802.16.

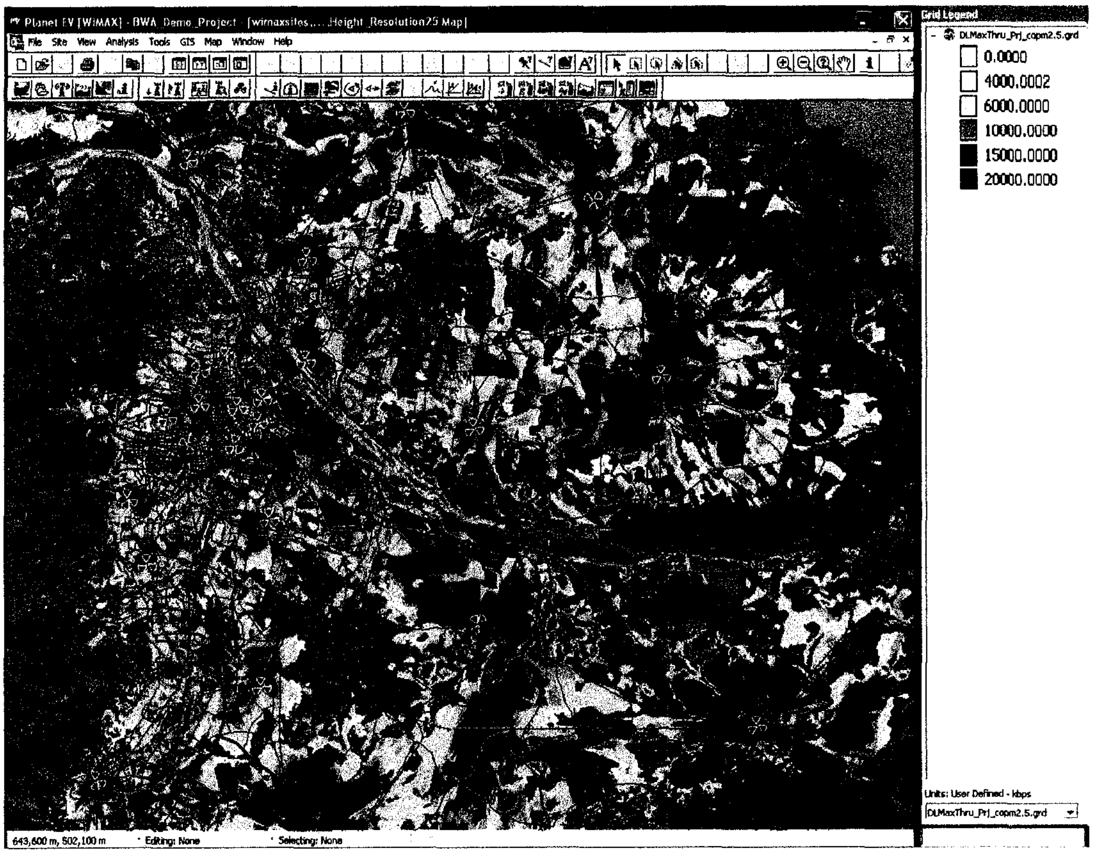

Figure 6.5: Distribution of Throughput Levels (in kbps) around Vienna for WiMAX with carrier frequencies in the range of 2.5 GHz using OFDM mode of IEEE 802.16.

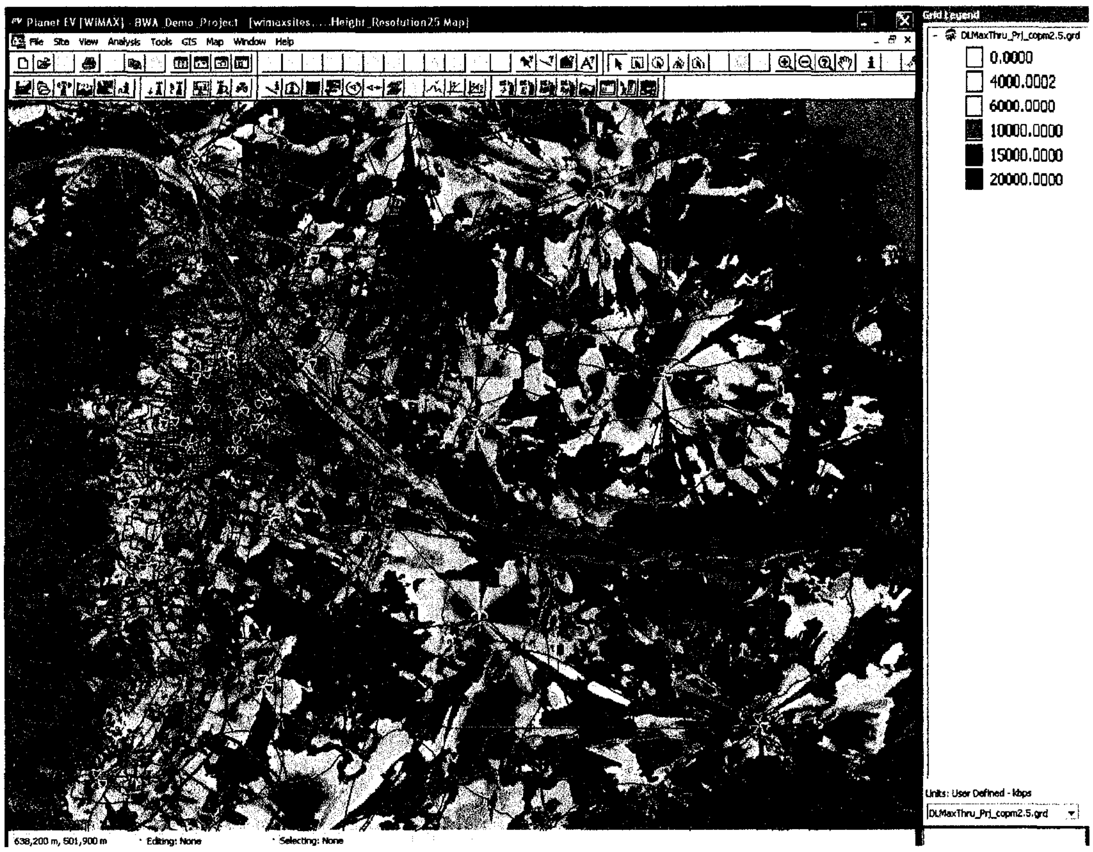

Figure 6.6: Distribution of Throughput Levels (in kbps) around Vienna for WiMAX with carrier frequencies in the range of 3.5 GHz using OFDM mode of IEEE 802.16.

6.3.1 Effect of OFDMA

OFDMA allows users to share resources in the subcarrier level of the orthogonal frequency division multiplexing (OFDM) based modulation. This is accomplished by assigning subcarriers to subchannels and assigning subchannels to users depending on the data rate and QoS requirements.

Data subcarriers are grouped between pilots, and each subchannel acquires a single subcarrier from each group depending on the permutation formula that is given in the IEEE 802.16-2004 standard. The assignments are orthogonal within a cell; however, they are not orthogonal between different cells. Because of this, there is the occasional collision and this impacts the performance especially in the case of 1/1 frequency re-use [68]. When network resources were not fully loaded, however, the collision-based architecture provided certain interference gains. In order to quantify this effect, we used OFDMA in the 3.5 GHz WiMAX system. Results are summarized in Table 6.3. The analysis shows that OFDMA significantly improves system performance, mainly due to the decreased interference levels that result from using sub-channel hopping mechanisms [32, 68]. The difference is more visible in dense urban areas, where in most cases interference is the limiting factor.

The simulation results for OFDMA for a lightly loaded (30%) system is shown in Fig. 6.7 for carrier frequency around 3.5 GHz. When we compare this figure with 6.6, it can be seen that both the coverage and throughput levels are increased due to the collision based architecture of the OFDMA system.

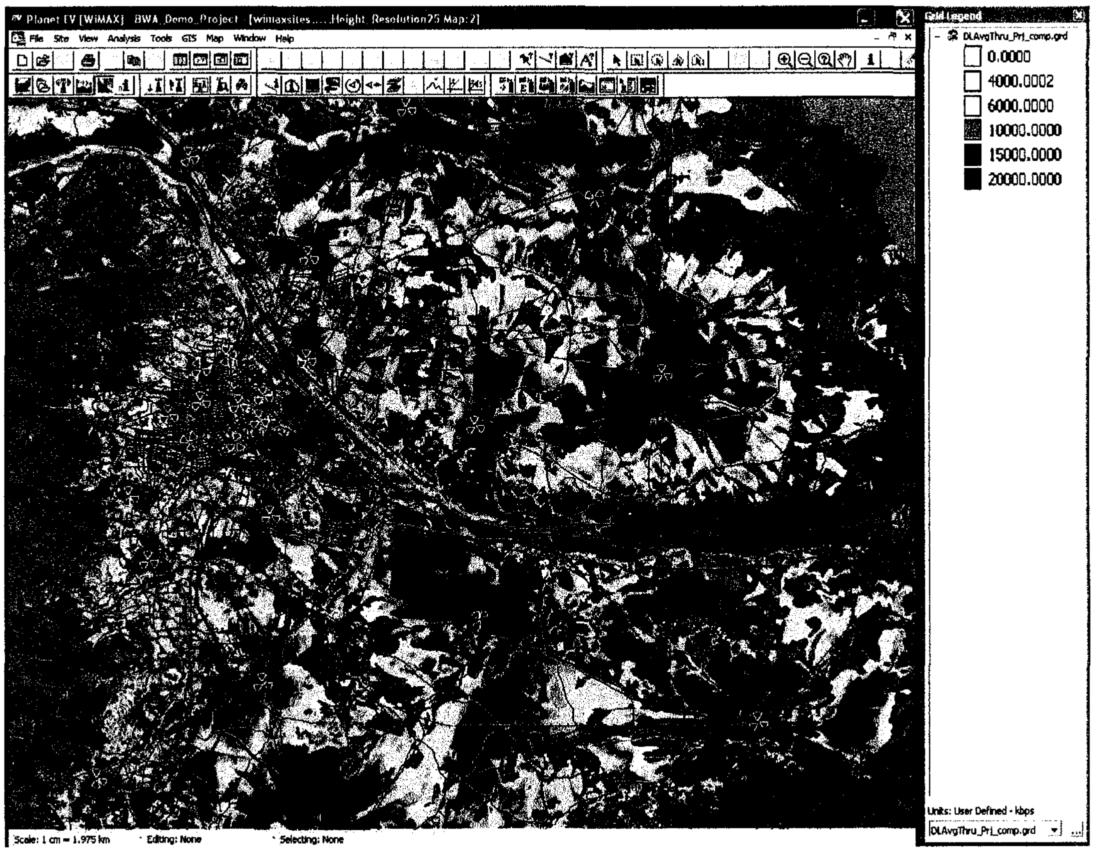

Figure 6.7: Distribution of Throughput Levels (in kbps) around Vienna for WiMAX with carrier frequencies in the range of 3.5 GHz using OFDMA mode of IEEE 802.16.

6.3.2 The Effect of Smart Antennae

Wide-scale deployment of smart antennae in cellular networks is generally unheard of; in fact, one rarely finds smart antennae used in mobile networks. The main reason for this is the lack of necessary gains that can be achieved with respect to implementation costs. This is especially true in dense urban environments, where the angular spread is in the order of 20^o [56] and the gains achieved using smart antennae are marginal. Also, the cusping loss that results from overlapping smart antenna beams further reduces performance.

However, the introduction of WiMAX and HSDPA systems with adaptive modulations may change this and, as a result, the deployment rate of smart antennae is expected to increase. Hence, in order to quantify the effect on the entire network, smart antennae are included in the simulations. To simulate a smart antenna, a switched-beam antenna pattern with five beams is used.

The combined beam pattern is shown in Fig. 6.8. Depending on the location of the user, the beam with the maximum gain was selected. In this way, the coverage pattern can be modeled as a combined beam pattern.

When determining the coverage of a sector with a smart antenna, the coverage changes to reflect the gains of the smart antenna. When determining the interference from neighboring sectors, the interference from the sectors using the smart antenna was edited accordingly. The interference pattern is actually a weighted combination of the beams, with the weights corresponding to the underlying traffic of each beam. We must also note that, in the simulations, it is assumed that the correct beam is selected and how the angle of arrival estimations is performed is not included in the results.

Next, the smart antennae are applied to both 3.5 GHz WiMAX (OFDM and OFDMA) and HSDPA systems. The results are depicted in Figs. 6.9 to Fig. 6.11 as well as in

Table 6.3. All these figures show that when compared to the results without smart antennae that are given in Figs. 6.3 to 6.7, both the coverage and the throughput levels are increased significantly.

In order to show the differences more clearly, the throughput levels for dense urban areas are given in Fig. 6.12 and 6.13 for HSDPA and WiMAX respectively. It can be seen from the figures that the coverage of HSDPA when smart antennae are used is very high, while the throughput levels of the OFDM and OFDMA systems are much higher still.

On average for all technologies, smart antennae increased the network coverage by 30%. When the throughput levels were considered, HSDPA and OFDM throughputs were increased by 130%, whereas for OFDMA, the throughput increased by 30%. The relatively low increase is due to the maximum throughput limits dictated by the available modulations. For further enhancements, higher order constellations such as 256-QAM are required. In dense urban regions, the gains achieved by OFDM and OFDMA tends to be relatively high, since in dense urban areas, as the interference levels drop, the availability of higher order modulations dominates the performance.

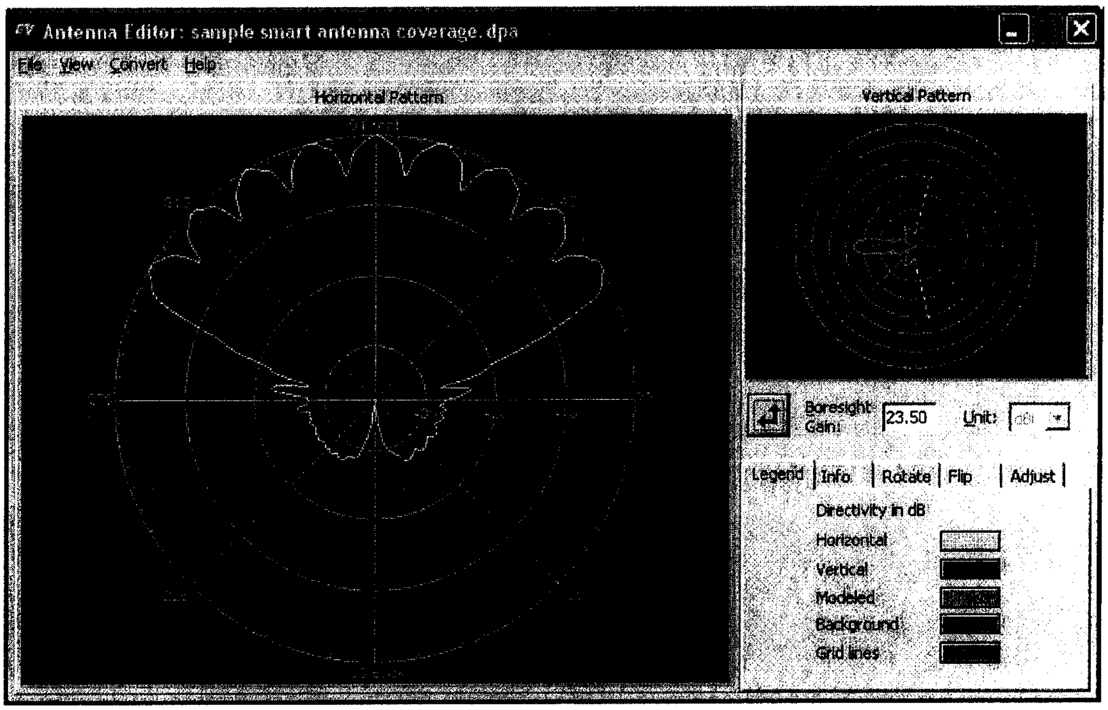

Figure 6.8: Smart antenna results pattern used for coverage calculations around Vienna.

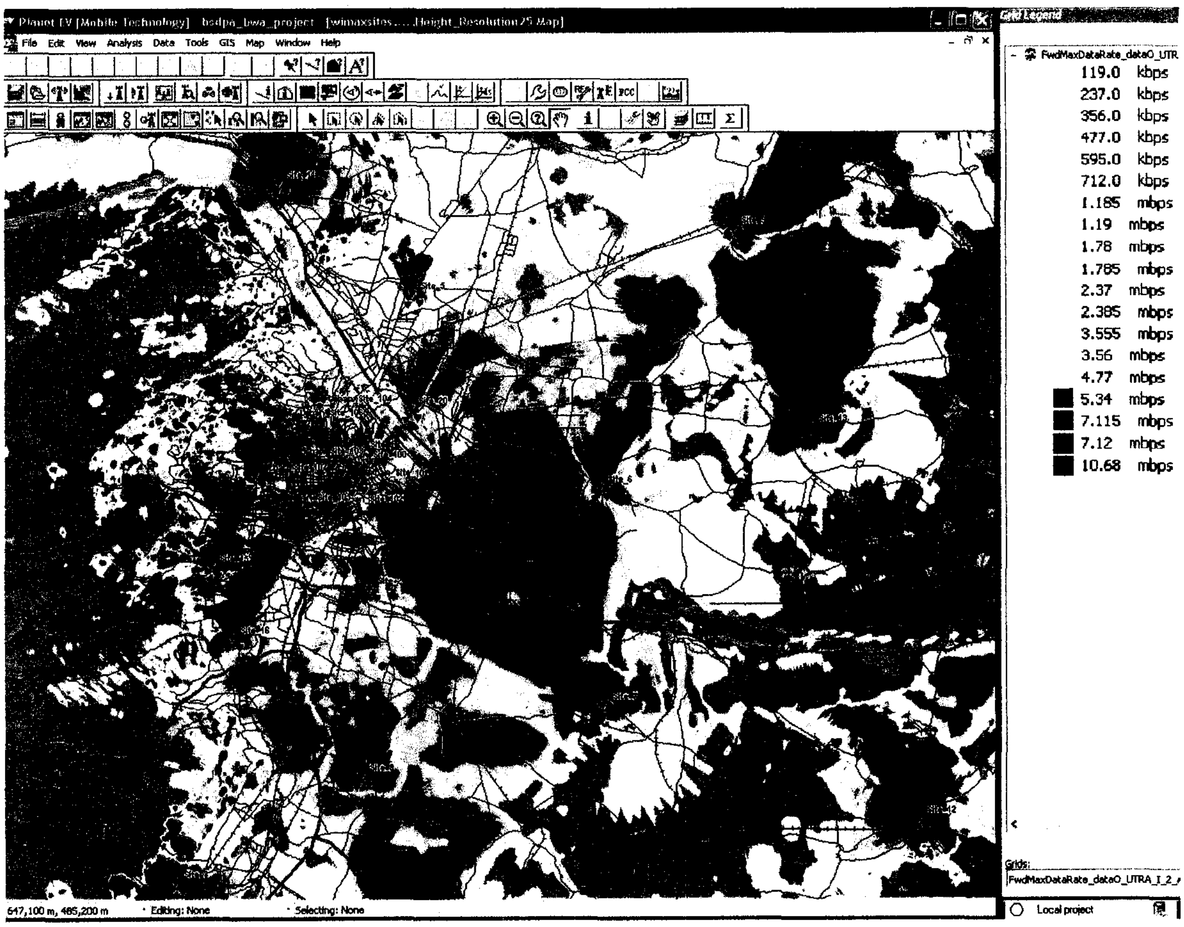

Figure 6.9: Throughput results for Vienna for base stations employing smart antennae and using HSDPA around 2.1 GHz.

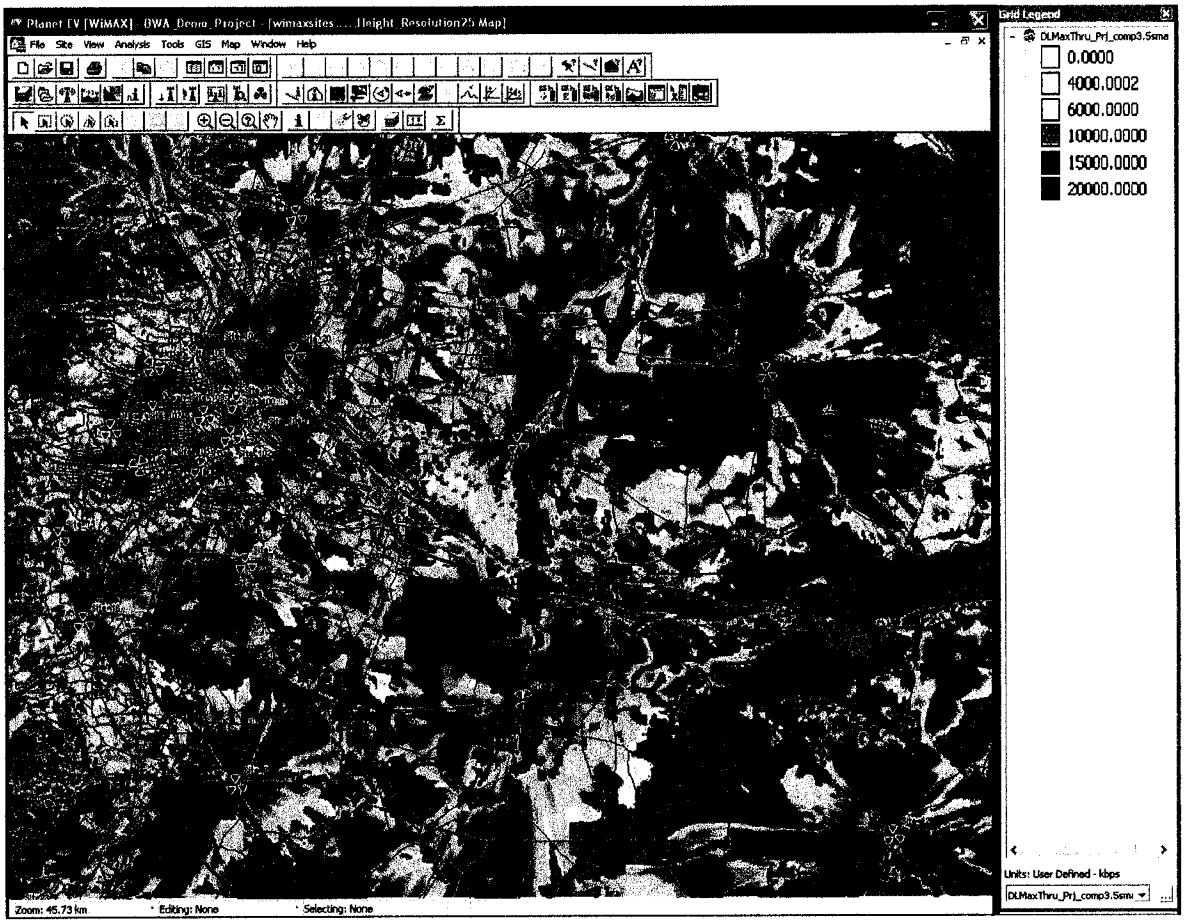

Figure 6.10: Throughput results for Vienna for base stations employing smart antennae and using WiMAX (OFDM mode) around 3.5 GHz.

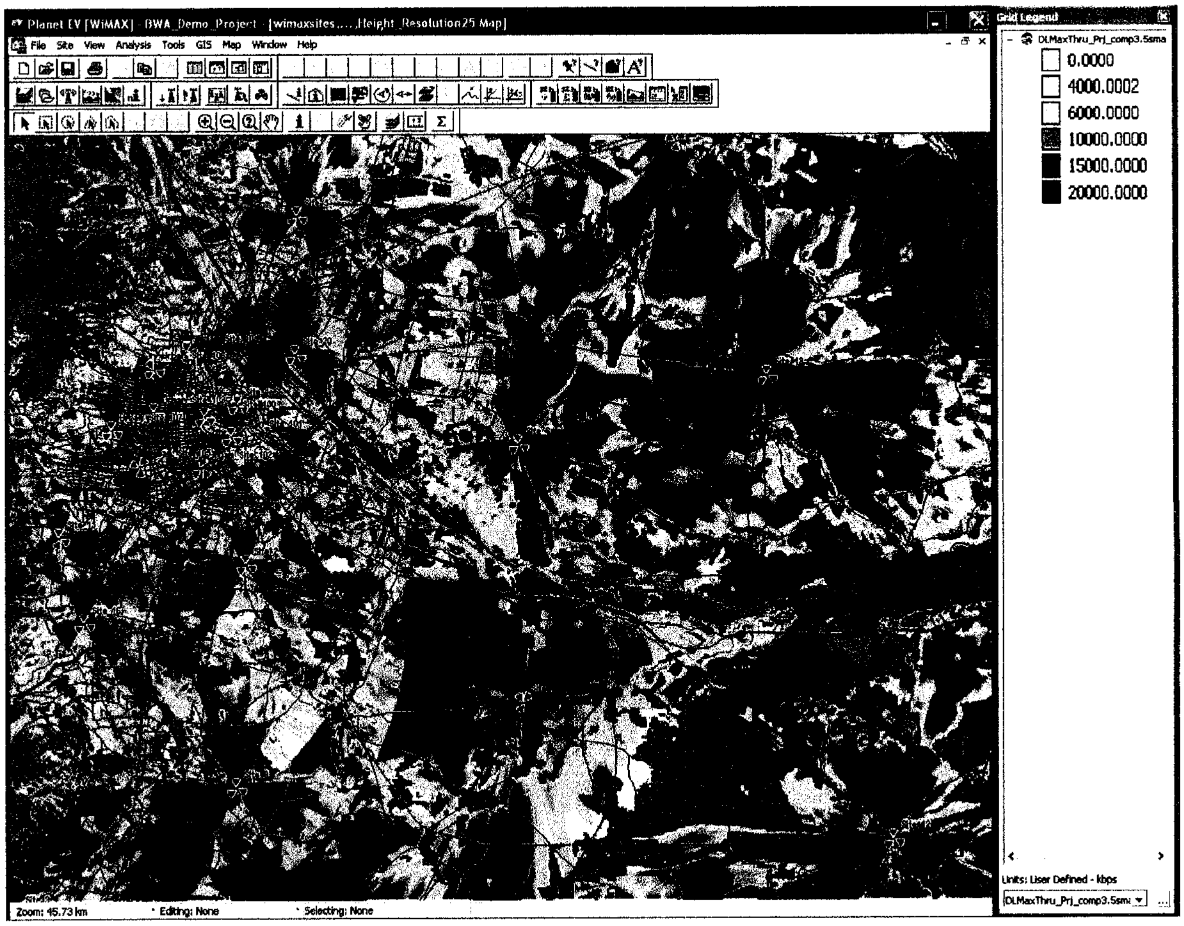

Figure 6.11: Throughput results for Vienna for base stations employing smart antennae and using WiMAX (OFDMA mode) around 3.5 GHz.

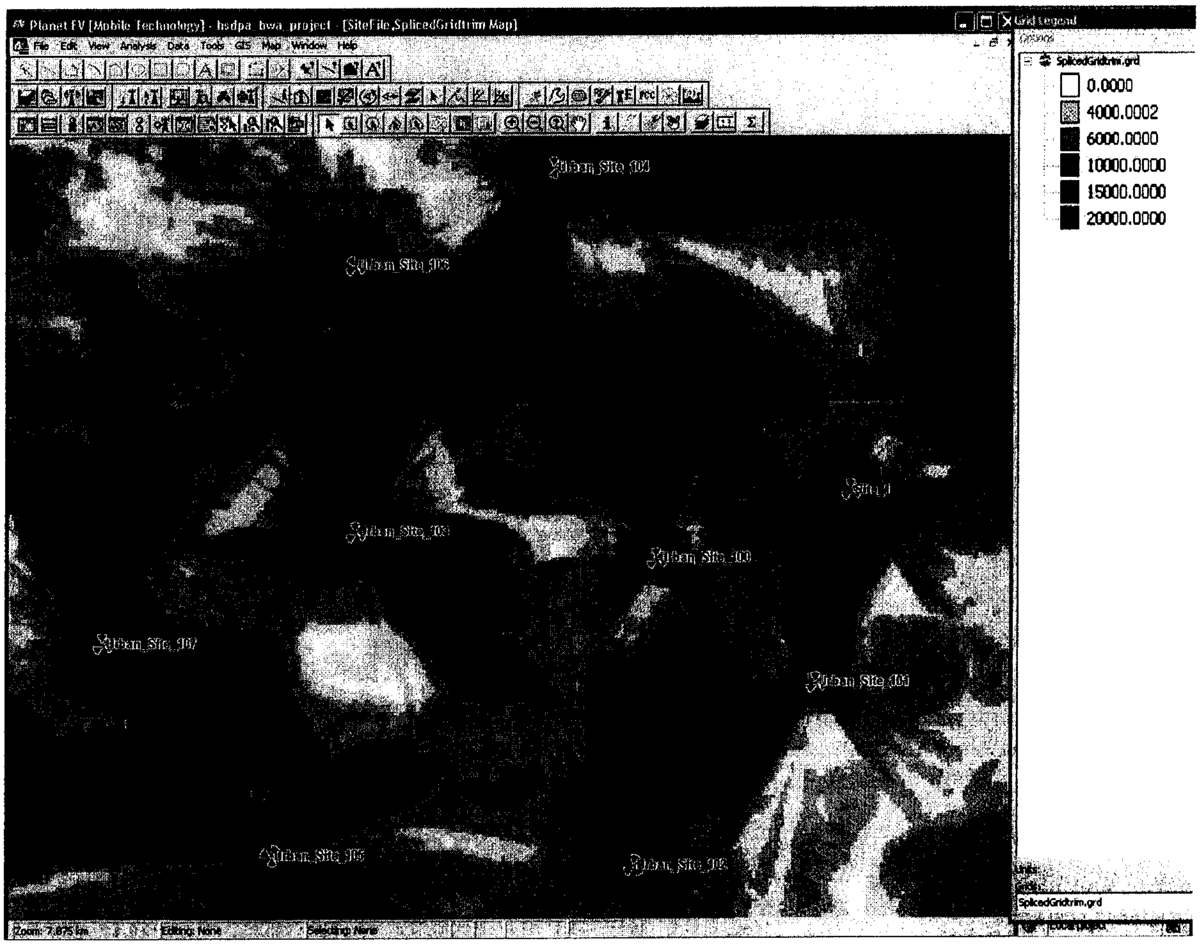

Figure 6.12: Throughput results for dense urban Vienna for base stations employing smart antennae and using HSDPA around 2.1 GHz.

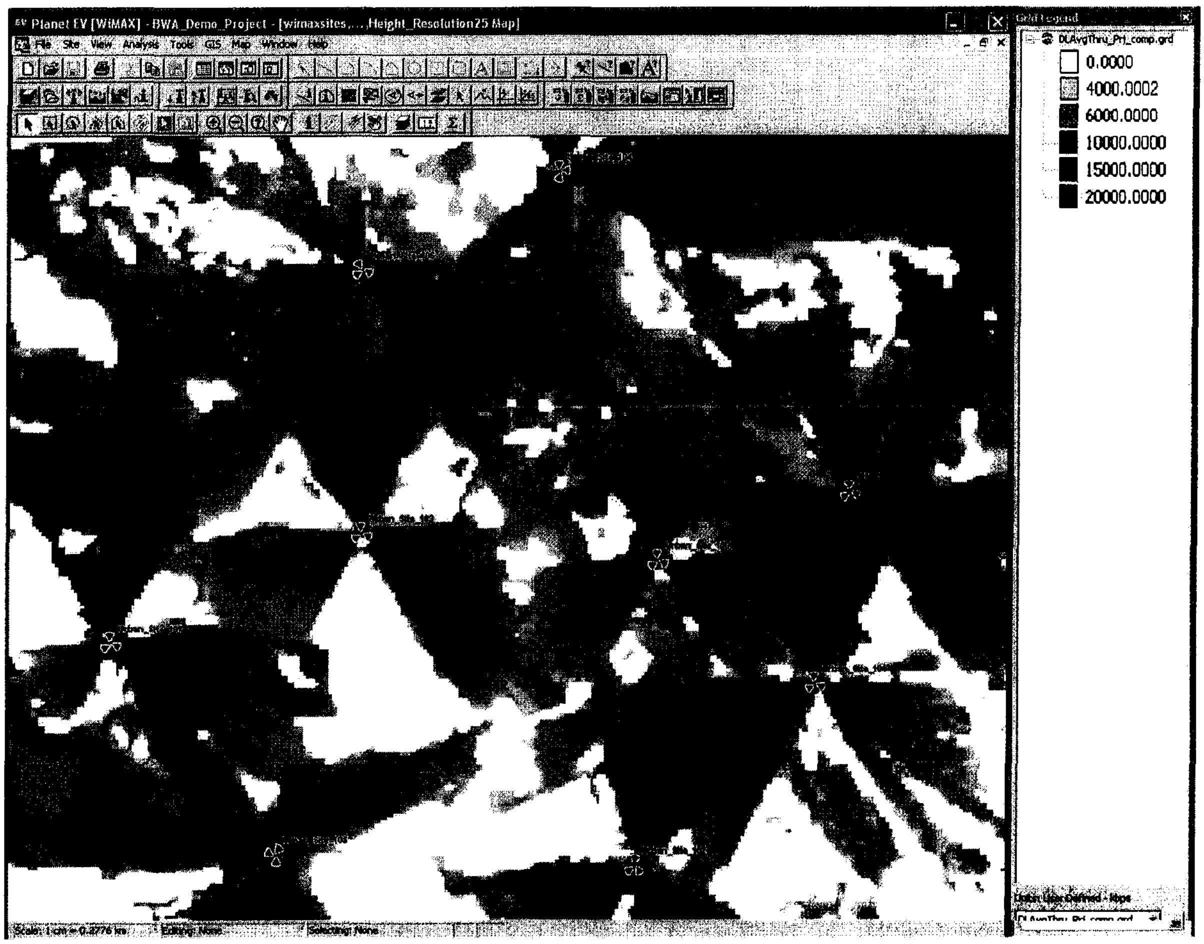

Figure 6.13: Throughput results for dense urban Vienna for base stations employing smart antennae and using WiMAX (OFDMA mode) around 3.5 GHz.

6.3.3 The Effect of User Velocity

In HSDPA, varying radio conditions are dealt with using fast link adaptation, a fast hybrid automatic repeat request (HARQ) with soft combining, and fast channel dependent scheduling. The scheduler uses the channel quality indicator (CQI) reports from the user equipment (UE) when deciding which UE to schedule [69]. The CQI reports are subject to signaling delays so the system performance is sensitive to the UE speed. The performance of the system degrades when the speed increases due to a less accurate link adaptation and poor packet scheduling. The cell capacity decreases when the UE speed increases [69]. The antenna diversity schemes add robustness to the system and account for the signaling delays for CQI reports [69]. In order to show the effect of velocity in HSDPA systems, the system performance degradation curves given in [60] are used.

Although CP provides protection against multi-path delay spread or channel dispersion in time, the OFDM systems are vulnerable to dispersion in frequency, namely the Doppler spread. Since the subbands of the OFDM systems are very densely packed, with the increasing speed of the receiver and transmitter with respect to each other, orthogonality between sub-carriers is disrupted and performance degradation is observed.

This is one of the major challenges of OFDM systems that are geared to mobile applications. In this work, we use both a rectangular pulse and a Hermite based pulse in order to tackle this problem. The simulations of the previous sections are repeated at a user speed of 120 km/h in order to clearly demonstrate the effect of high velocity.

In [70, 71], it is shown that, when either low-density parity check codes (LDPC) or convolutional codes are used, the uncoded bit error rate (BER) of 0.05 corresponds to a coded BER of 0.001. Hence, using the methodology in [72], we investigated the performance degradation with respect to inter-subcarrier interference as a result of user velocity around 120 km/h.

Table 6.3: Throughput and coverage results for OFDM and HSDPA.

Technology	Frequency	Coverage	Average Throughput	Dense Urban Throughput
Fixed and Pedestrian Environment (< 3 km/h)				
HSDPA	2.1 GHz	69%	3.10 Mbps	3.71 Mbps
OFDM	2.1 GHz	54(69)%	5.26(4.3)Mbps	5.74 Mbps
OFDM	2.5 GHz	51%	4.79 Mbps	5.33 Mbps
OFDM	3.5 GHz	40%	3.03 Mbps	3.32 Mbps
OFDMA	3.5 GHz	59%	5.92 Mbps	6.74 Mbps
Smart antennae				
HSDPA-S	2.1 GHz	88%	7.10 Mbps	8.18 Mbps
OFDM-S	3.5 GHz	67%	6.97 Mbps	8.66 Mbps
OFDMA-S	3.5 GHz	77%	7.75 Mbps	10.08 Mbps
High Velocity (120 km/h)				
HSDPA-HV	2.1 GHz	55%	2.22 Mbps	NA
OFDMA-Sq	3.5 GHz	35%	1.54 Mbps	NA
OFDMA-Hm	3.5 GHz	45%	1.97 Mbps	NA

The results of the simulations are shown in Table 6.3. It can be seen that due to inter sub-channel interference, at high velocities there is a significant performance loss when compared with the HSDPA system. But also, the application of a better pulse shape helps to increase robustness to velocity, therefore increasing the average throughput. It must also be noted that the results reflect the worst-case scenario where all the users are traveling at 120 km/h. In a real network, depending on the distribution of speed, the degradation is expected to be less.

6.4 Conclusions

In this chapter, we compare the performance of the physical layer of WiMAX and HSDPA technologies in various scenarios. Simulation results included detailed hardware component characteristics, multiple access issues, propagation characteristics, and detailed geographical information. It is found that maximum performance is achieved in a network using OFDMA and smart antennae. The simulation results show that when WiMAX and HSDPA networks are compared, the WiMAX network suffered from coverage issues related to the higher carrier frequency even though it provided much higher maximum throughput levels.

When OFDMA is used instead of OFDM in networks that are not congested, interference decreased and as a result both coverage and capacity improved.

Simulation results also showed that, due to the adaptive modulations, smart antennae provided huge gains in both systems. In order to increase the gains in networks using smart antennae, it might be very beneficial to include higher order constellation modulations such as 256 QAM.

Investigations of user velocity showed that for highly mobile users, there are problems in both WiMAX and HSDPA. Of the two, however, HSDPA is shown to perform better in these cases. Also, pulse shaping in OFDM systems proved to be critical in the performance of high velocity OFDM networks.

In deciding which technology to deploy for next generation wireless data networks, the work undertaken in this chapter showed that the carrier frequency, available modulations, spectral efficiency and degradations with respect to mobility are critical deciding factors. When these are kept in mind, from the given alternatives, OFDMA and HSDPA with smart antennae proved to be the best options for the specific scenario depending on the requirements of coverage and capacity. Due to the heterogeneous structure of the area studied in this work, similar results are expected in other scenarios as well.

Chapter 7

Capacity Enhancement in Multi-Carrier Systems

In this chapter, we extend our analysis from single lattice structures to multiple lattices. By doing this, we intend to use more than one lattice in the same time frequency range. However, by minimizing the interference between those frames, the overall capacity of the system is doubled.

We start by presenting the problem definition for multiple lattice structures for MC communications. We present the required conditions and structure for multiple lattices. Then, by using non-linear optimization methods and Hermite functions, we provide the lattices for MC systems.

We show the capacity enhancements employing Matlab simulations for AWGN as well as fading channels. We extend this analysis to unit lattice density cases and provide mother functions for lattices as well as simulation results supporting the capacity enhancement.

Finally, we present system level simulation results, depicting the effect of multiple lattices in a simulated WiMAX network. All these results show that by employing multiple lattices, very important capacity increases on the order of 100% can be achieved.

7.1 Introduction

In the previous chapters, we have considered a single pulse shape and the Weyl-Heisenberg frame formed by its shifts. In this chapter, we extend the analysis to multiple pulse shapes employed jointly at the same transmission duration and transmission frequency.

We start our investigation by considering two pulse shapes both of which constitute an orthogonal basis and transmitted via the same time-frequency lattice at the same time effectively doubling the capacity of the system. Hence we pursue two orthogonal pulse shapes which are practically orthogonal to each other as well.

In the previous analysis in Chapter 2, we have also seen that due to the Balian-Low theorem, pulses with fast decays do not exist with unit lattice density. Hence in O-QAM OFDM systems, Wilson expansions with half density lattices are utilized. As explained earlier, the density of these systems is increased to unity by employing phase shifted pulses. However, this approach limits the constellation to real valued elements. In this chapter, we look into two frames which are structured in a lattice that are offset from each other and employ different pulse shapes. By doing this we overcome the reduced density effect caused by the Balian-Low theorem.

7.2 Multiple Lattice Structures

We start our analysis by considering two lattice structures with pulse shapes φ and ξ satisfying the following criteria:

$$\int_{-\infty}^{\infty} \varphi_{00}^{*}(t)\varphi_{mn}(t)dt = \delta_m(t)\delta_n(t), \tag{7.1}$$

$$\int_{-\infty}^{\infty} \xi_{00}^{*}(t)\xi_{mn}(t)dt = \delta_m(t)\delta_n(t). \tag{7.2}$$

On the other hand, in order to double the capacity, it is desired to have:

$$\int_{-\infty}^{\infty} \varphi_{00}^{*}(t)\xi_{mn}(t)dt = 0, \qquad \forall m, n \in \mathbb{Z}. \tag{7.3}$$

In other words, any time frequency shift of both pulses must be orthogonal to all frequency shifts of both pulses, other than the pulse itself. For practical purposes, the interference from one pulse shape to other does not necessarily need to be zero. As a result we need to satisfy:

$$\int_{-\infty}^{\infty} \varphi_{00}^{*}(t)\xi_{mn}(t)dt \simeq 0, \qquad \forall m, n \in \mathbb{Z}. \tag{7.4}$$

Hence, if the interference is negligible enough, then the capacity can be increased without introducing significant interference.

In this problem, we again employ Hermite functions since they constitute an orthogonal basis for $L_2(\mathbb{R}^2)$. As a result any function in $L_2(\mathbb{R}^2)$ can be written as a linear combination of Hermite functions.

Hermite functions have been previously employed as orthogonal pulse shapes in the single carrier literature particularly in ultra-wideband systems [15, 16]. However the applications in single carrier systems are different than the multi-carrier ones due to two reasons. First in a single carrier system, the orthogonal pulses are just an alternative to further divide the time or frequency resources. However in a tight multi-carrier lattice, this is not an option. Having time and frequency at the maximum density, and another dimension is required to further enhance the capacity.

The second reason is that the orthogonalization procedure is a nonlinear transformation. Hence the orthogonalization transforms of two orthogonal Hermite functions do not remain orthogonal. As a result, in this dissertation, we seek the optimal weights for two different weighted sums of Hermite functions that are optimal in the sense that they minimize the interference between the two lattices in the orthogonal domain.

In order to construct the mother functions, we use linear combinations of Hermite functions that are symmetric in time and frequency. The mother functions to be orthogonalized are represented by $\phi_1(t)$, $\phi_2(t)$ and are evaluated as:

$$\begin{aligned} \phi_1(t) &= \sum_{k=0}^{\infty} a_k H_{4k}(t), \\ \phi_2(t) &= \sum_{k=0}^{\infty} b_k H_{4k}(t). \end{aligned} \tag{7.5}$$

Due to practical reasons, in the optimization process the number of symmetric Hermite functions are restricted to 8, hence the mother functions are calculated as:

$$\begin{aligned} \phi_1(t) &= \sum_{k=0}^{7} a_k H_{4k}(t), \\ \phi_2(t) &= \sum_{k=0}^{7} b_k H_{4k}(t). \end{aligned} \tag{7.6}$$

The Hermite functions are listed below.

$$
\begin{aligned}
H_0(t) &= \exp(-\pi t^2) \\
H_4(t) &= 16\exp(-\pi t^2)(4\pi^2 t^4 - 6\pi t^2 + 0.75) \\
H_8(t) &= 256\exp(-\pi t^2)(16\pi^4 t^8 - 112\pi^3 t^6 + 210\pi^2 t^4 \\
&\quad -105\pi t^2 + 11.67) \\
H_{12}(t) &= 4096\exp(-\pi t^2)(64\pi^6 t^{12} - 1056\pi^5 t^{10} + 5940\pi^4 t^8 \\
&\quad -13860\pi^3 t^6 + 12993.75\pi^2 t^4 - 3898\pi t^2 162.42 \\
H_{16}(t) &= 65536\exp(-\pi t^2).(256\pi^8 t^{16} - 7680\pi^7 t^{14} + 87360\pi^6 t^{12} \\
&\quad -480480\pi^5 t^{10} + 1351350\pi^4 t^8 - 1891890\pi^3 t^6 + 1182431.25\pi^2 t^4 - 253378.125\pi t^2 + 7918) \\
H_{20}(t) &= 1048576\exp(-\pi t^2)(1024\pi^{10} t^{20} - 48640\pi^9 t^{18} \\
&\quad +93024\pi^8 t^{16} - 9302400\pi^7 t^{14} + 52907400\pi^6 t^{12} - 174594420\pi^5 t^{10} + 327364537.5\pi^4 t^8 \\
&\quad -327364537.5\pi^3 t^6 + 153452126.953125\pi^2 t^4 - 255753554.49\pi t^2 + 639383.8625) \\
H_{24}(t) &= 16777216\exp(-\pi t^2)(7.72057\times 10^7 - 3.70587\times 10^9\pi t^2 + 2.7176372\times 10^{10}\pi^2 t^4 \\
&\quad -7.2470324489\times 10^{10}\pi^3 t^6 + 9.31761315\times 10^{10}\pi^4 t^8 \\
&\quad -6.625858239\times 10^{10}\pi^5 t^{10} + 2.810970162\times 10^{10}\pi^6 t^{12} \\
&\quad -7.41354768\times 10^9\pi^7 t^{14} + 1.23559128\times 10^9\pi^8 t^{16} - 1.2921216\times 10^8\pi^9 t^{18} \\
&\quad +8.160768\times 10^6\pi^{10} t^{20} - 2.82624\times 10^5\pi^{11} t^{22} + 4.096\times 10^3\pi^{12} t^{24}) \\
H_{28}(t) &= 268435456\exp(-\pi t^2)(1.302845\times 10^{10} - 7.29592933\times 10^{11}\pi t^2 \\
&\quad +6.323138\times 10^{12}\pi^2 t^4 - 2.023404400791212\times 10^{13}\pi^3 t^6 \\
&\quad +3.179635486957619\times 10^{13}\pi^4 t^8 - 2.826342655073440\times 10^{13}\pi^5 t^{10} \\
&\quad +1.541641448221876\times 10^{13}\pi^6 t^{12} - 5.421156741\times 10^{12}\pi^7 t^{14} \\
&\quad +1.2649365729\times 10^{12}\pi^8 t^{16} - 1.984214232\times 10^{11}\pi^9 t^{18} \\
&\quad +2.08864656\times 10^{10}\pi^{10} t^{20} - 1.4466816\times 10^9\pi^{11} t^{22} \\
&\quad +6.28992\times 10^7\pi^{12} t^{24} - 1.548288\times 10^6\pi^{13} t^{26} + 1.6384\times 10^4\pi^{14} t^{28}).
\end{aligned}
$$

7.2.1 Non-linear Optimization Methods

In order to find a good pair of mother functions $\phi_1(t)$, $\phi_2(t)$, we employed two optimization algorithms. The first one is the Nelder-Mead optimization algorithm [73].

Nelder-Mead algorithm (NMA) was first published in [74] and quickly became popular in the field of chemistry, physics and engineering. NMA is a direct search algorithm which doesn't utilize derivative information. In the algorithm, each iteration method begins with a simplex, specified by its vertices and the associated function values. One or more test points are computed, along with their function values, and the iteration terminates by updating vertices with a descent condition. The details of the algorithm can be found in [74]. However the algorithm is very sensitive to local minima and the starting position is very critical. Hence we first use the second algorithm prior to local fine tuning with NMA.

The second algorithm that is used is based on interior-reflective Newton method, proposed in [75, 76]. At each iteration, the algorithm uses preconditioned conjugate gradients in order to approximate the solution of a linear equation set. This approach is a subspace trust region method. The idea is to approximate the approximation function, with a simpler function so that the simpler function approximates the behavior of the original function within a neighborhood of the initial start point, i.e. the trust region. More details about trust region methods can be found in [77].

7.3 Optimization Results

As the result of the interference minimization accomplished by the algorithms mentioned above, the weights of the mother function employed to generate two Weyl-Heisenberg frames with low correlation have been found. These coefficients are tabulated in Table 7.1.

Table 7.1: Normalized coefficients for Hermite functions for capacity enhancement.

Hermite Coefficient	Pulse-A	Hermite Coefficient	Pulse-B
a_0	1	b_0	2.4×10^{-2}
a_4	-8.4×10^{-2}	b_4	1
a_8	-9.2×10^{-2}	b_8	-7.7×10^{-1}
a_{12}	9.9×10^{-2}	b_{12}	-7×10^{-1}
a_{16}	-6.7×10^{-2}	b_{16}	-1.5×10^{-2}
a_{20}	1×10^{-10}	b_{20}	-1.1×10^{-2}
a_{24}	-1.4×10^{-2}	b_{24}	5.2×10^{-2}
a_{28}	-7×10^{-1}	b_{28}	1.5×10^{-3}

The pulse shapes that are built by orthonormalizing the mother function formed by Hermite pulses with the weights given in Table 7.1 are given in Fig. 7.1. These pulse shapes are symmetric in time and frequency, hence the plots represent pulse shape and the spectrum at the same time.

As a result of the correlation, to some extent interference occurs from the pulses employed in each and every lattice point in the time frequency plane. However the total interference depends on the transmitted symbols on these lattice points as well. Hence the total interference is probabilistic and the cumulative distribution function of interference is depicted in Fig. 7.2. Mean of this interference distribution is located at -17.1 dB.

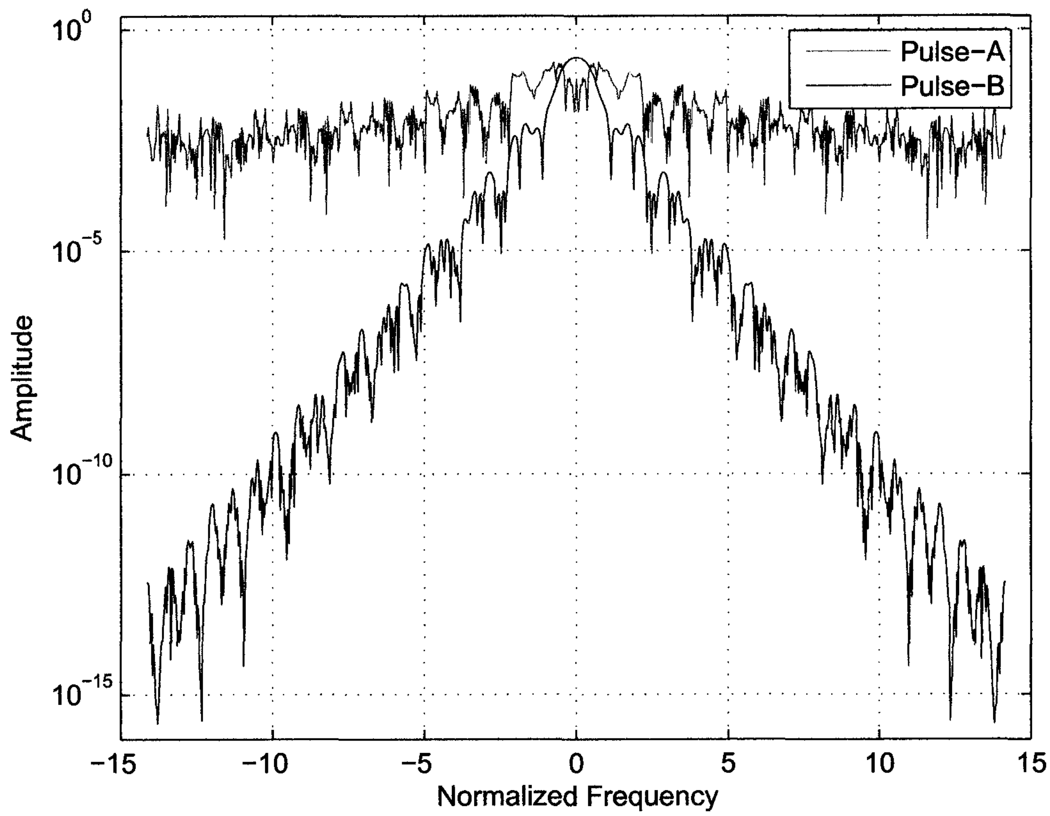

Figure 7.1: Orthonormal pulses with low correlation between each other.

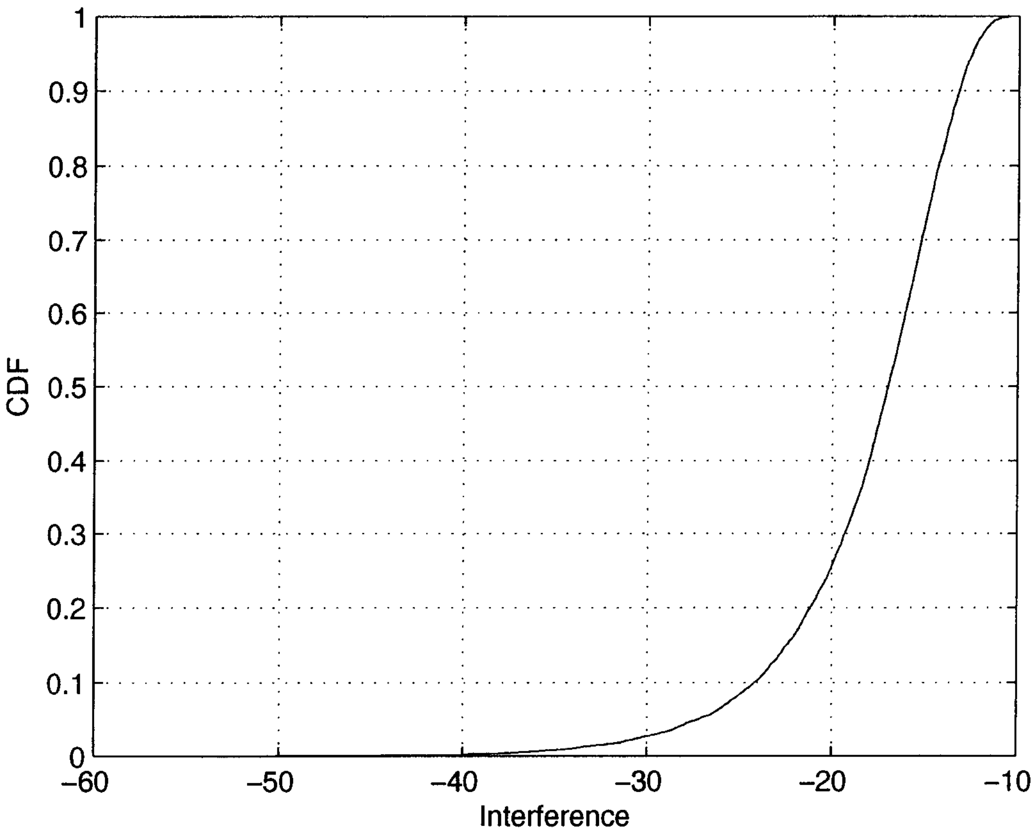

Figure 7.2: Cumulative distribution function for total interference.

As can be seen in Fig. 7.2, the interference is less than 10 dB for all of the cases. If we consider IEEE 802.16e specifications, even under -10 dB interference, the quality is sufficient to have transmission for 16QAM transmission with 3/4 coding rate [32]. We claim that the interference is very insignificant for most practical applications and in the following sections, we support this claim by simulation results in different channels. Furthermore, since the interference level is not constant and it is randomly changing with the transmitted bits, the system performance can be improved significantly by making use of error control coding.

7.3.1 Performance in Gaussian Channels

We first start by analyzing the performance of the system in additive white Gaussian channel. The performance for 32 subcarrier system is depicted in Fig. 7.3. As can be seen in the figure, there is very insignificant performance loss due to the interference between pulse shapes and it is very close to single carrier BPSK performance. Hence the capacity is effectively doubled. Simulation results are also repeated with QPSK, and as expected the BER results are the same as the case for BPSK.

7.3.2 Performance in Fading Channels

In this section, we investigate the performance in Rayleigh fading channels. For the fading channel, the equalization is accomplished at the frequency domain. It is assumed that the channel coefficient of each subcarrier is perfectly known to the detector in order to exclude the channel estimation performance.

The comparison is depicted in Fig 7.4. There is very insignificant performance loss, and the effective capacity is doubled for the fading channel as well. Also in Fig. 7.4, it

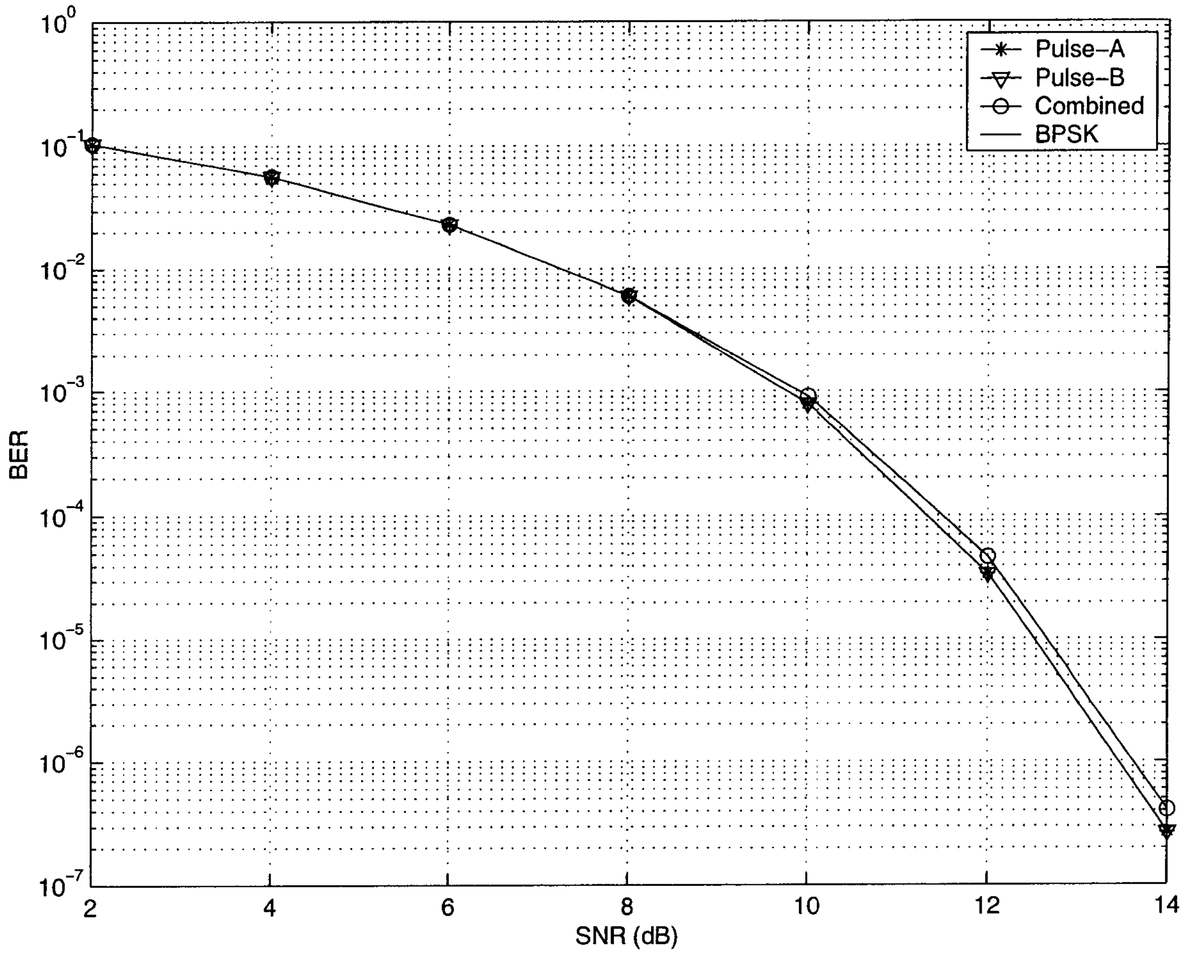

Figure 7.3: Comparison of BER in additive Gaussian channel.

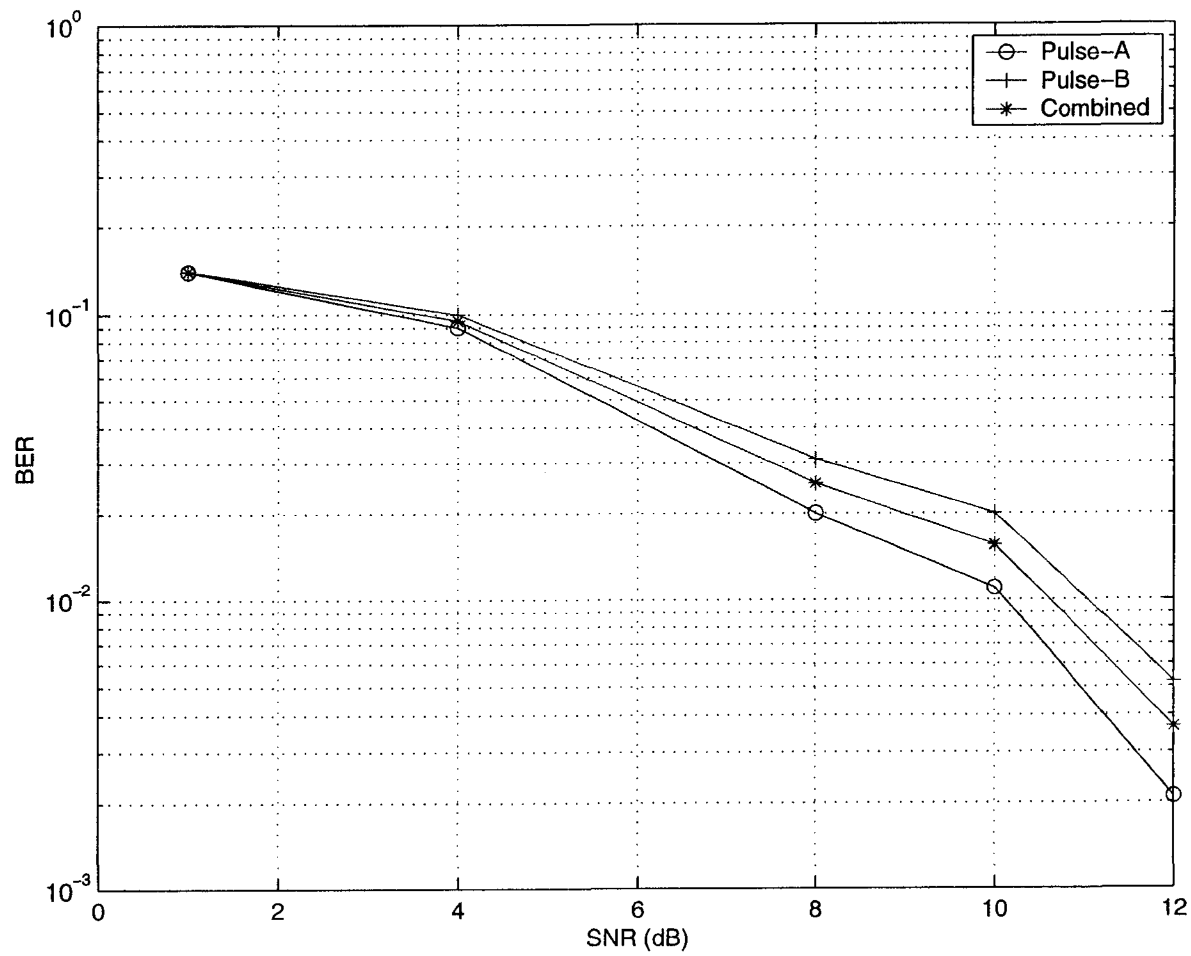

Figure 7.4: Comparison of BER in Rayleigh fading channel for $f_D T = 0.0005$.

can be seen that one of the pulses has better performance in fading channel.

7.4 Employing Multiple Pulse Shapes for Unit Density

In this section, we apply the same analysis given in the previous section to the lattice density of 1. The optimization methodology introduced in the previous section is employed. The optimization results for mother function construction are given in Table 7.2

Table 7.2: Normalized coefficients for Hermite functions.

Hermite Coefficient	Pulse-A	Hermite Coefficient	Pulse-B
a_0	1	b_0	7.2×10^{-2}
a_4	-4.93×10^{-2}	b_4	1
a_8	2.8×10^{-4}	b_8	-2.8×10^{-3}
a_{12}	-5.4×10^{-2}	b_{12}	-2.8×10^{-2}
a_{16}	-4.1×10^{-3}	b_{16}	-1.78×10^{-2}
a_{20}	7.34×10^{-2}	b_{20}	4.74×10^{-2}
a_{24}	1.72×10^{-2}	b_{24}	4.6×10^{-3}
a_{28}	1.32×10^{-2}	b_{28}	-7.39×10^{-2}

The resulting orthonormalized pulse shapes are given in Fig. 7.5.

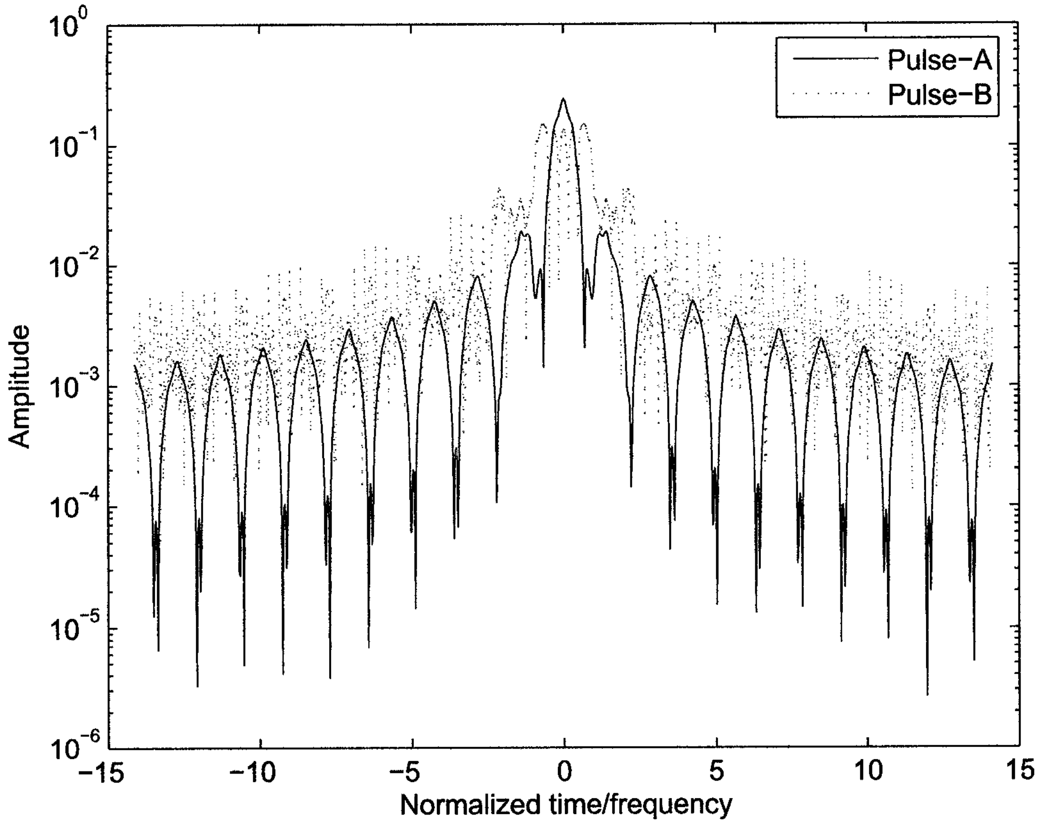

Figure 7.5: Orthonormal pulse couple for unit density lattice.

The optimization results show that the correlation between the pulses of the two frames is less than 4×10^{-4}, resulting in extremely low interference, making the pulses practically orthogonal.

We also investigate the performance in fading channel. The results are depicted in Fig. 7.6. As expected the pulse shape that employs the Gaussian pulse (Hermite function with coefficient 0) with more weight in its mother function performs better in fading channel. The Pulse A, which has more weight on fourth Hermite instead of the Gaussian pulse, performs poorly compared to the others. The performance of the system that uses both pulse shapes at the same time has the performance which is exactly half of the performances of the other pulse shapes.

The performance in the Gaussian channel is depicted in Fig. 7.7. The performance of the system using combined pulses is the same with the system using the pulses separately. Therefore, the capacity is effectively doubled.

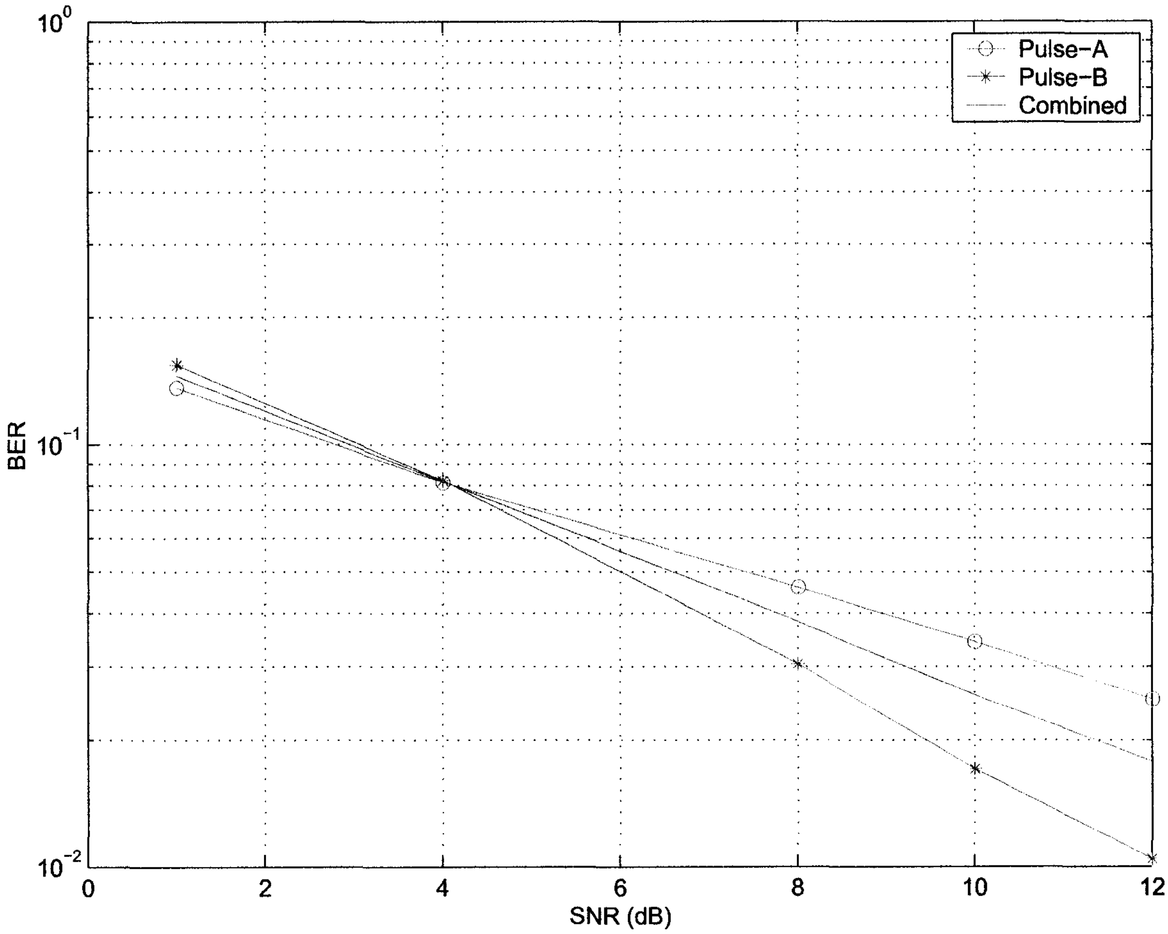

Figure 7.6: Performance of orthogonal pulse shapes in fading channel with $f_D T = 0.0005$.

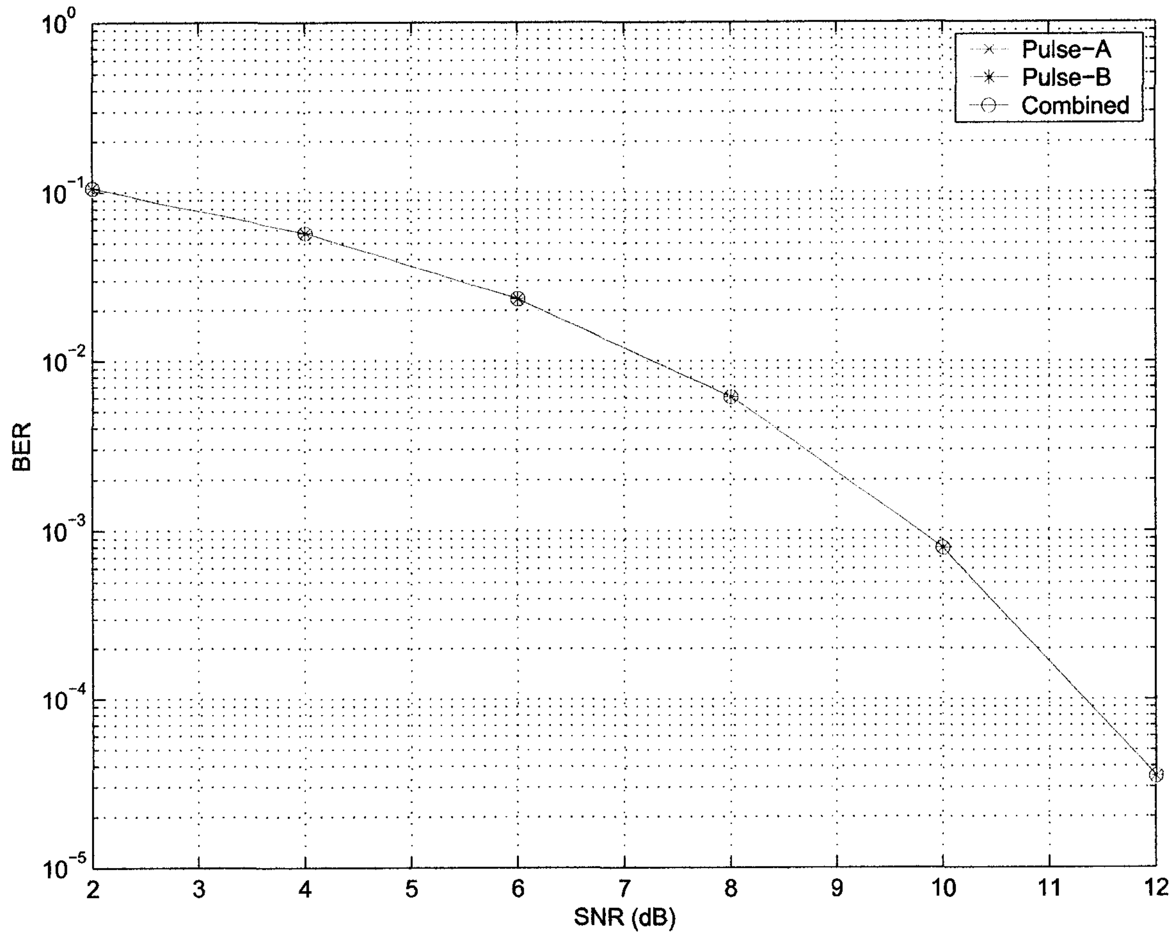

Figure 7.7: Performance of orthogonal pulse shapes in AWGN channel.

7.4.1 Employing More Than Two Pulse Shapes

Up to this point, we have investigated the cases, with two overlapping frames. Even though it is possible to include more and more frames for further increasing the capacity, the approach is only valid for AWGN channels. As the number of distinct frames in the channel increase, the weights of the higher order Hermite functions in the mother pulses also increase. This results in decreased localization values. The resulting frames are badly localized; therefore the systems are more prone to fading, Doppler and phase jitter. However for future work, the multiple frame structure for AWGN channels can be investigated.

7.5 System Level Simulation of Capacity Enhancement Using Multiple Weyl-Heisenberg Frames

Using the same system settings in the previous chapter, this time we have replaced the pulse shapes used in the base stations and customer premise equipments with different pulse shapes that are orthogonal to the ones employed in the other base stations. We have chosen the OFDM mode with 3 different carrier frequencies and repeated the simulations with additional pulse shapes.

The transmitted bands are divided into two. Hence, instead of three 5 MHz bands, six 2.5 MHz bands are employed. On the other hand, for each band, both pulse shapes are employed at the same time, therefore increasing the capacity employed per allocated frequency band. The results are shown in Fig. 7.8. The increase in throughput is significantly visible. The changes in the throughput and coverage levels are given in Table 7.3. As it is seen in the table, with the introduction of the orthogonal pulse shapes, the interference levels have decreased significantly due to lower frequency re-use ratio. The decrease in interference levels resulted in a more than double coverage and throughput levels. Hence, for this specific scenario, huge gains have been accomplished comparable to the gains experienced when a smart antenna is added to the system.

7.6 Conclusions

In this chapter, we have presented a novel methodology which doubles the effective capacity of OFDM systems. We have employed two practically orthogonal Weyl-Heisenberg frames on top of each other for both 0.5 density and unit density lattices.

The increase in capacity is achieved with the sacrifice of localization for the second

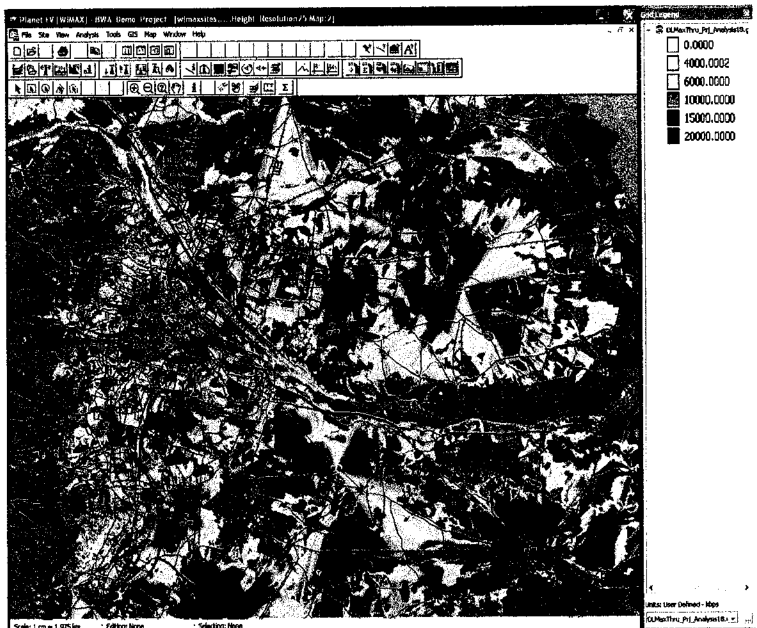

(a)

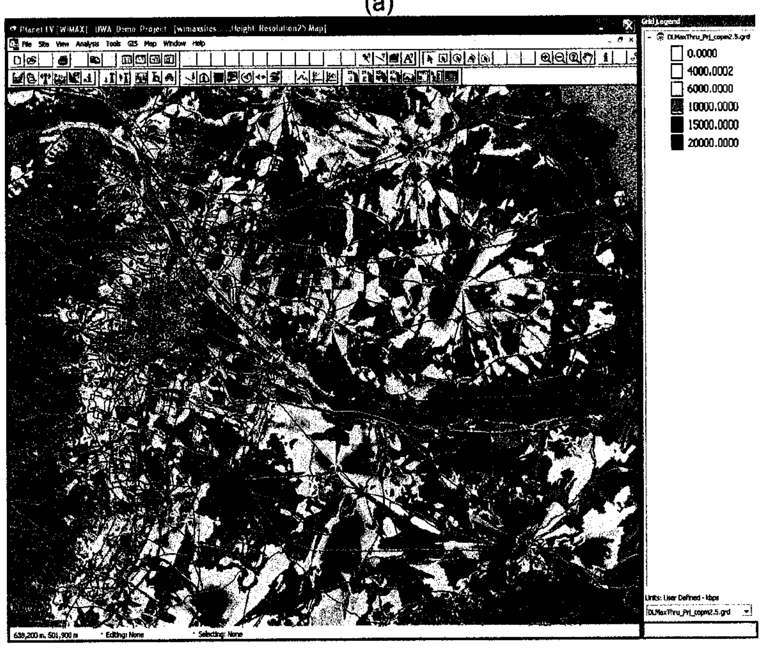

(b)

Figure 7.8: Distribution of Throughput Levels (in kbps) (a) WiMAX 3.5 GHz with double orthogonal pulse shapes (b)WiMAX 3.5 GHz with single pulse shape.

set of Weyl-Heisenberg frame since Gaussian pulses can only be utilized in one of the frames. However, for low velocity mobility and fixed applications, the results presented are extremely important. In order to identify this importance, system level simulations are performed employing the network planning tool TEMS Planet. Results show that the throughput and capacity performance can be doubled for a single base station, therefore possibly reducing the costs to half.

Table 7.3: Throughput and coverage comparison.

5MHz WiMAX			
Modulation	Ratio	Coverage Area	Throughput
No coverage	60.7%	1704.5 km^2	0 Mbps
QPSK-1/2	7.4%	207.7 km^2	0.29 Mbps
QPSK-3/4	16.5%	466.29 km^2	1 Mbps
16QAM-1/2	4.1%	116.6 km^2	0.33 Mbps
16QAM-3/4	9.8%	275.6 km^2	1.17 Mbps
64QAM-1/2	0.7%	19.4 km^2	0.11 Mbps
64QAM-3/4	0.67%	18.7 km^2	0.12 Mbps
Total	100%	2809 km^2	3.037 Mbps
2×2.5MHz WiMAX with two pulses			
Modulation	Ratio	Coverage Area	Throughput
No coverage	35.6%	1000 km^2	0 Mbps
QPSK-1/2	6.5%	182.7 km^2	0.26 Mbps
QPSK-3/4	19.4%	545.1 km^2	1.16 Mbps
16QAM-1/2	6.19%	174.1 km^2	0.49 Mbps
16QAM-3/4	21.6%	607 km^2	2.59 Mbps
64QAM-1/2	2.86%	80 km^2	0.46 Mbps
64QAM-3/4	7.77%	218 km^2	1.43 Mbps
Total	100%	2809 km^2	6.41 Mbps

Chapter 8

Conclusions

Multi-carrier systems are critical for next generation high speed mobile data communications. In this dissertation, we proposed a novel orthonormality criterion as well as a novel orthonormalization methodology for multi-carrier systems. The methodology is efficiently used in optimization algorithms. Then by employing this methodology, due to the Balian-Low theorem, Wilson frames of half densities are employed for multi-carrier systems and a very well localized pulse shape has been proposed which proved to be more localized than IOTA for half density and much more localized than IOTA at unit density.

We have evaluated and compared the performance gains associated when using these pulses. We also provided the effects of imperfections such as phase jitter and peak to average power ratio to the system performance. The system-level coverage and quality analysis for OFDM systems with different pulse shapes are presented. We have investigated the effects of ISI and ICI with simulation results and supported the theoretical analysis.

In addition to those, compatibility of multiple pulse shapes have been investigated. Since most of the equipments installed will be using rectangular pulse shapes, the transceivers with novel pulse shapes are shown to be compatible with the rectangular pulse. It is shown that even if at one end of the communication system, a rectangular pulse shape is employed and at the other end Hermite based pulse shape is employed, the performance is better than the system that employs rectangular pulse shapes at both ends of the system. This is due to the fact that the effect of Doppler spread is higher than the effect of mismatch between the pulse shapes.

Balian-Low states well localization as exponentially decaying pulses for all frequency band and time durations. However for practical engineering purposes, the localization is not important after the pulse has decayed to very low amplitude values. By using this argument, we proposed a novel and centrally well localized pulse shape for multi-carrier systems with unit density. We have named this novel pulse shape as UDALOP.

We also proposed using multiple Weyl-Heisenberg frames at the same time. By doing this, we increased the capacity of the multi-carrier systems significantly. We proposed multiple pulse shapes that are orthonormal to the time-frequency shifts of themselves and shifts of others in the group. Therefore, they can be used at the same time without introducing interference to one another. We investigated both half density and unit density cases. As a result, we have doubled the effective capacity of multi-carrier systems.

The results are also presented with their system wide effect on a typical wireless network deployment on a city wide scale employing real geographical data.

8.1 Future Work

There are various possible future works employing the architecture introduced in this thesis. The localized pulses can be employed in many different fields including physics, optics and different areas of wireless communication.

One interesting area is optical communications with intensity modulation. In the intensity modulated systems, the pulses must be non-negative. Therefore, the pulse shapes introduced in this dissertation are not directly applicable to the optical systems, since they include negative values as they are not intensity but voltage. On the other hand the methodology introduced can be employed with more constraints for acquiring pulse shapes for optical systems.

Another area would be using more than two orthogonal frames at the same time for increasing the capacity further. However, as it is mentioned in the dissertation, this would lead to a set of worse localized pulses. As a result, these pulse sets would be more suitable for systems working with AWGN channels but not fading channels. For these channels, more than two Weyl-Heisenberg frames can lead to further increased capacity.

Bibliography

[1] R. V. Nee and R. Prasad, *OFDM for Wireless Multimedia Communications*, Artech House, 2000.

[2] J. A. C. Bingham, "Multi-carrier modulation for data transmission: An idea whose time has come," *IEEE Communications Magazine*, vol. 28, pp. 5–14, May 1990.

[3] B. Le Floch, M. Alard, and C. Berrou, "Coded orthogonal frequency division multiple access," *Proc. IEEE*, vol. 83, pp. 982–996, June 1995.

[4] R. Haas and J-C. Belfiore, "Multiple carrier transmission with time-frequency well-localized impulses," in *IEEE Second Symposium on Communications and Vehicular Technology in the Benelux*, 1994, pp. 187–193.

[5] R. Balian, "Un principe d'incertitude fort en théorie du signal on mécanique quantique," *C. R. Acad. Sci. Paris*, vol. 292, no. série 2, pp. 5–14, 1981.

[6] I. Daubechies, "Ten lectures on wavelets," *SIAM*, 1992.

[7] T. Strohmer and S. Beaver, "Optimal OFDM design for time-frequency dispersive channels," *IEEE Transactions on Communications*, vol. 51, no. 7, pp. 1111–1122, July 2003.

[8] H. Bolcskei, P. Duhamel, and R. Hleiss, "Design of pulse shaping OFDM/OQAM systems for high data-rate transmission over wireless channels," in *IEEE International Conference on Communications*, 1999, vol. June, pp. 559–564.

[9] P. Beckmann, *Orthogonal polynomials for engineers and physicists*, Golem Press, 1973.

[10] Y. Eidelman, V. Milman, and A. Tsolomitis, *Functional Analysis - An Introduction*, American Mathematical Society, 2004.

[11] K. Gröchenig, *Foundations of Time-Frequency Analysis*, Birkhäuser, 2001.

[12] D. Slepian, "On bandwidth," in *Proceedings of the IEEE*, 1976, vol. 64, pp. 292–300.

[13] V. Bargmann, "On a Hilbert space of analytic functions and an associated integral transform," *Comm. Pure Applied Math.*, vol. 14, pp. 187–214, 1961.

[14] J. R. Klauder and B. S. Skagerstam, *Coherent States. Application in Physics and Mathematical Physics*, World Scientific Publishing Co., 1985.

[15] C. Corral et al., "Pulse spectrum optimization for ultra-wideband communication," *IEEE Conf. on Ultra Wideband Systems and Technologies, Baltimore, MA*, May 2002.

[16] L. B. Michael, M. Ghavami, and R. Kohno, "Multiple pulse generator for ultra-wideband communication using hermite polynomial based orthogonal pulses," *IEEE Conf. on Ultra Wideband Systems and Technologies, Baltimore, MA*, May 2002.

[17] G. Chunqing, "Characterization and transformation of astigmatic laser beams," *Berlin: Wissenschaft & Technik Verlag*, 1999.

[18] M. M. Rao, T. K. Sarkar, T. Anjali, and R. S. Adve, "Simultaneous extrapolation in time and frequency domains using hermite expansions," *IEEE Transactions on Antennas and Propagation*, vol. 47, no. 6, pp. 1108–1115, June 1999.

[19] R. Mizoguchi, K. Onda, S. S. Kano, and A. Wadaa, "Thinning-out in optimized pulse shaping method using genetic algorithm," *Review of Scientific Instruments*, vol. 74, no. 5, pp. 2670–2674, May 2003.

[20] T. A. C. M. Claasen and W. F. G. Mecklenbräuker, "The Wigner distribution- a tool for time frequency analysis. I. continuous time analysis," *Philips J. Res.*, vol. 35, no. 3, pp. 217–250, 1980.

[21] T. A. C. M. Claasen and W. F. G. Mecklenbräuker, "The Wigner distribution- a tool for time frequency analysis. II. discrete time analysis," *Philips J. Res.*, vol. 35, no. 4, pp. 276–300, 1980.

[22] T. A. C. M. Claasen and W. F. G. Mecklenbräuker, "The Wigner distribution- a tool for time frequency analysis. III. relations with other time-frequency signal transformations," *Philips J. Res.*, vol. 35, no. 6, pp. 372–389, 1980.

[23] D. Gabor, "Theory of communication," *J. Inst. Electrical Engineering*, vol. 93, no. 3, pp. 429–457, 1946.

[24] A.Ron and Z. Shen, "Weyl-Heisenberg frames and Riesz bases in $L_2(\Re^d)$," *Duke Mathematical Journal*, vol. 89, no. 2, pp. 237–282, 1997.

[25] K. G. Wilson, *Generalized Wannier Functions*, Cornell Univ., Ithaca, NY, 1987.

[26] I. Daubechies, S. Jaffard, and J. L. Journé, "Simple Wilson basis with exponential decay," *SIAM J. Math. Analysis*, vol. 22, no. 2, pp. 554–572, March 1991.

[27] G. Kutyniok and T. Strohmer, "Wilson bases for general time-frequency lattices," *SIAM J. Math. Analysis*, vol. 37, no. 3, pp. 685–711, November 2005.

[28] IEEE, *Information technology - telecommunications and information exchange between systems - local and metropolitan area networks - specific requirements. Part 1: wireless LAN Medium Access Control (MAC) and Physical Layer (PHY) specifications*, ISO/IEC 8802-11; ANSI/IEEE Std 802.11, 1999 edn, 1999.

[29] ETSI, *TS 101 475 V1.3.1 Broadband Radio Access Networks (BRAN)*, HIPERLAN Type 2; Physical (PHY) layer, 2002.

[30] IEEE, *IEEE Standard for Local and Metropolitan Area Networks Part 16: Air Interface for Fixed Broadband Wireless Access Systems*, IEEE Std 802.16-2004 (Revision of IEEE Std 802.16-2001), 2004.

[31] Wimax Forum, *http://www.wimaxforum.org*, , 2004.

[32] IEEE, *IEEE Standard for Local and Metropolitan Area Networks Part 16 Amendment E: Physical and Medium Access Control Layers for Combined Fixed and Mobile Operation in Licensed Bands*, IEEE Std 802.16e (Revision of IEEE Std 802.16-2004), 2006.

[33] Telecommunication Technology Association (TTA), *2.3 GHz portable internet service international standardization, progress and strategy report*, Technical Report TTAR-0021, Korea, 2004.

[34] IEEE, *Mobile Broadband Wireless Access (MBWA)*, IEEE Workgroup 802.20, 2006.

[35] I. Daubechies, "The wavelet transform, time-frequency localization and signal analysis," *IEEE Transactions on Information Theory*, vol. 36, no. 5, pp. 961–1005, September 1990.

[36] J. Zak, "Finite translations in solid state physics," *Physics Rev. Letters*, vol. 19, pp. 1385–1397, 1967.

[37] H. Bölcskei and F. Hlawatsch, "Discrete Zak transforms, polyphase transforms, and applications," *IEEE Transactions on Signal Processing*, vol. 45, no. 4, pp. 851–866, April 1997.

[38] W. Kozek and A. F. Molish, "Non-orthogonal pulse shapes for multicarrier communications in doubly dispersive channels," *IEEE Journal on Selected Areas in Communication*, vol. 16, no. 8, pp. 1579–1589, October 1998.

[39] C. H. Wilcox, "The synthesis problem for radar ambiguity functions," *The IMA Volumes in Mathematics and Applications*, vol. 32, no. 1, 1991.

[40] R. W. Chang, "Synthesis of band-limited orthogonal signals for multi-channel data transmission," *Bell Systems Technical Journal*, vol. 45, no. 1, pp. 1775–1796, December 1966.

[41] B. R. Saltzberg, "Performance of an efficient parallel transmission system," *IEEE Transactions on Communications*, vol. 15, no. 1, pp. 805–811, December 1967.

[42] B. Hirosaki, "An orthogonally multiplexed QAM system using the Fourier transform," *IEEE Transactions on Communications*, vol. 29, no. 1, pp. 982–989, July 1981.

[43] B. Hirosaki, S. Hasegawa, and A. Sabato, "Advanced group-band data modem using orthogonally multiplexed QAM technique," *IEEE Transactions on Communications*, vol. 34, no. 1, pp. 587–592, June 1986.

[44] R. J. Glauber, "The quantum theory of coherence," *Phys. Review*, vol. 130, pp. 2529–2539, 1963.

[45] J. R. Klauder and B. S. Skagerstam, *Coherent States*, World Scientific, 1985.

[46] E. W. Aslaksen and J. R. Klauder, "Unitary representations of the affine group," *Journal of Math. Physics*, vol. 9, pp. 206–211, 1968.

[47] R. Wang and S.-H. Cheng, "Performance of MC-CDMA based on wavelet packets in Rayleigh multipath fading channel," *IEE Electronics Letters*, vol. 36, no. 12, pp. 1070–1072, June 2000.

[48] J. P. Boyd, "Prolate spheroidal wavefunctions as an alternative to chebyshev and legendre polynomials for spectral element and pseudospectral algorithms," *Journal of Computational Physics*, vol. 199, pp. 688–716, 2004.

[49] D. Slepian, "Prolate spheroidal wave functions, Fourier analysis and uncertainty V-discrete case," *Bell System Technical Journal*, vol. 57, pp. 1317–1430, May 1978.

[50] D. M. Gruenbacher and D. R. Hummels, "A simple algorithm for generating dicrete prolate spheroidal sequences," *IEEE Transactions on Signal Processing*, vol. 42, no. 11, pp. 3276–3278, November 1994.

[51] D. M. Gruenbacher and D. R. Hummels, "N dimensional orthogonal QPSK signalling with discrete prolate spheroidal sequences," *IEEE Proceedings RAWCON*, pp. 63–66, 1998.

[52] X. Huang, J. Lu, J. Zheng, K. B. Letaief, and J. Gu, "Companding transform for reduction in peak-to-average power ratio of OFDM signals," *IEEE Transactions on Wireless Communications*, vol. 3, no. 6, pp. 2030–2039, November 2004.

[53] M. Sharif, M.Gharavi-Alkhansari, and B. H. Khalaj, "On the peak-to-average power of OFDM signals based on oversampling," *IEEE Transactions on Communications*, vol. 51, no. 1, pp. 72–78, January 2003.

[54] H. Ochiai and H. Imai, "On the distribution of the peak-to-average power ratio in OFDM signals," *IEEE Transactions on Communications*, vol. 49, no. 2, pp. 282–289, February 2001.

[55] H. Steendam, M. Moeneclaey, and H. Sari, "The effect of carrier phase jitter on the performance of orthogonal frequency-division multiple-access systems," *IEEE Transactions on Communications*, vol. 46, no. 4, pp. 456–459, April 1998.

[56] W. C. Y. Lee, *Mobile Communications Engineering*, McGraw Hill, 1998.

[57] J. G. Proakis, *Digital Communications*, McGraw Hill, 2001.

[58] Ericsson NetQual Inc., *http://www.ericsson.com/solutions/tems/*, 2006.

[59] T. E. Kolding, K. I. Pedersen, J. Wigard, Frederiksen, and P. E. Mogensen, "High speed downlink packet access: WCDMA evolution," *IEEE Vehicular Technology Society (VTS) News*, vol. 50, no. 1, pp. 4–10, February 2003.

[60] H. Holma and A. Toskala, *WCDMA for UMTS*, John Wiley and Sons, 2002.

[61] 3gpp.org, *Overview of 3GPP Release 5 - Summary of all Release 5 Features*, 3GPP, 2003.

[62] S. Parkvall, E. Englund, P. Malm, T. Hedberg, M. Persson, and J. Peisa, "WCDMA evolved - high-speed packet-data services," *Ericsson Review*, , no. 2, pp. 56–65, 2003.

[63] 3GPP R1-040223, *Selected Link Level Comparisons of WCDMA and OFDM Transmission*, Alcatel, 2004.

[64] R1-030519 3GPP, TSG RAN WG1, *System-Level Performance Evaluation Results for OFDM and WCDMA (Rake) in UTRAN*, Nortel Networks, 2003.

[65] R1-040571 3GPP, TSG RAN WG1, *Further Results on Link Level Comparisons of WCDMA and OFDM Transmission*, Alcatel, 2004.

[66] H. L. Van Trees, *Optimum Array Processing*, John Wiley and Sons, 2002.

[67] J. H. Whitteker, "Physical optics and field-strength predictions for wireless systems," *IEEE Journal on Selected Areas in Communications*, vol. 20, no. 3, pp. 515–522, April 2002.

[68] T. Kurt and H. Delic, "Space-frequency coding reduces the collision rate in FH-OFDMA," *IEEE Journal on Wireless Communications*, vol. 4, no. 5, pp. 2045–2050, September 2005.

[69] K. I.Pedersen, T. F. Lootsma, M. Stottrup, F. Frederiksen, T. E. Kolding, and P. E. Mogensen, "Network performance of mixed traffic on high speed downlink packet access and dedicated channels in WCDMA [cellular radio]," *IEEE Vehicular Technology Conference*, vol. 6, pp. 4496–4500, Fall 2004.

[70] G. Richter, G. Schmidt, M. Bossert, and E. Costa, "Performance of forward error correction for IEEE 802.16e," *10th International OFDM Workshop, Hamburg, Germany*, August 2005.

[71] D. J. C. MacKay, "Good error-correcting codes based on very sparse matrices," *IEEE Transactions on Information Theory*, vol. 45, no. 2, pp. 399–431, March 1999.

[72] T. Kurt, M. Siala, and A. Yongacoglu, "Increasing robustness to velocity by hermittian-based pulse shaping for OFDM systems," *13th European Signal Processing Conference, EUSIPCO*, September 2005.

[73] J. C. Lagarias, J. A. Reeds, M. H. Wright, and P. E. Wright, "Convergence properties of the nelder-mead simplex method in low dimensions," *SIAM Journal of Optimization*, vol. 9, no. 1, pp. 112–147, 1998.

[74] J. A. Nelder and R. Mead, "A simplex method for function minimization," *Computer Journal*, vol. 7, pp. 308–313, 1965.

[75] T. F. Coleman and Y. Li, "On the convergence of reflective newton methods for large-scale nonlinear minimization subject to bounds," *Mathematical Programming*, vol. 6, pp. 189–224, 1994.

[76] T. F. Coleman and Y. Li, "An interior, trust region approach for nonlinear minimization subject to bounds," *SIAM Journal on Optimization*, vol. 6, pp. 418–445, 1996.

[77] J. J. More and D. C. Sorensen, "Computing a trust region step," *SIAM Journal on Scientific and Statistical Computing*, vol. 3, pp. 553–572, 1983.